國立交通大學

光電工程研究所

博士論文

福衛三號大氣遙測星系效能及部署技術挑戰與展望

FORMOSAT-3 Constellation Performance, Deployment Challenges, and Prospect for Atmospheric Remote Sensing

研 究 生：方振洲

指導教授：祁　甡

中 華 民 國 九 十 八 年 三 月

福衛三號大氣遙測星系效能及部署技術挑戰與展望

FORMOSAT-3 Constellation Performance, Deployment Challenges, and Prospect for Atmospheric Remote Sensing

研 究 生：方振洲　　　Student：Chen-Joe Fong

指導教授：祁 甡　　　Advisor：Sien Chi

國 立 交 通 大 學

光 電 工 程 研 究 所

博 士 論 文

A Dissertation

Submitted to Institute of Electro-Optical Engineering

College of Electrical Engineering

National Chiao Tung University

in partial Fulfillment of the Requirements

for the Degree of

Doctor of Philosophy

in

Electro-Optical Engineering

March 2009

Hsinchu, Taiwan, Republic of China

中華民國九十八年三月

福衛三號大氣遙測星系效能及部署技術挑戰與展望

學生：方振洲 指導教授：祁 甡

國立交通大學光電工程研究所

摘 要

全球導航衛星系統(GNSS)無線電掩星(Radio Occultation，簡稱 RO)技術有別於傳統的衛星微波輻射計，是一個利用地球尺度的幾何光學折射原理用於大氣遙測的先進邊緣探空太空遙測技術。此技術主要係接收經過地球遮掩的 GNSS 衛星所傳送的電磁波折射信號，由電磁波訊號穿過電離層和大氣層時受電子密度、溫度、壓力、及水氣等影響而改變信號的時間延遲，反演推算行進路徑下的電離層和大氣層相關的資料。福爾摩沙衛星三號(FORMOSAT-3，簡稱福衛三號)任務，又名「氣象、電離層及氣候之衛星星系觀測系統」(Constellation Observing System for Meteorology, Ionosphere and Climate，簡稱 COSMIC)任務，係由六顆同型實驗微衛星組成，是世界上第一個進行全球氣象監測的近實時運作展示的 GPS RO 衛星星系觀測系統。福衛三號於 2006 年 4 月中旬，在美國加州的范登堡空軍基地發射升空到地表 516 公里的暫駐軌道上。六顆衛星本體完成入軌健康檢查之後，開始進行三個衛星酬載包括 GPS 氣象量測儀(簡稱 GOX)、小型電離層光度計及三頻段信標儀的一系列入軌儀器健康檢查、校正及實驗。隨後展開星系部署工作，前後共歷經 19 個月，近 500 次軌道轉換，每一顆衛星分別升軌到高度約 800 公里的全球均等分佈的六個軌道面上，福衛三號成為世界上第一個利用先進的地球進動理論進行星系部署的系統。微衛星的質量參數資料，將可供學術進行後續大地重力場量測及研究。目前每天觀測大約 1,800~2,200 個大氣層和電離層剖面資料點，提供給氣象操作中心和科學研究團隊進行氣象預報及分析用。經過全球氣象單位的資料評估及驗證，福衛三號對目前運作中的全球氣象預報模式及颱風及颶風軌跡路徑預測產生正面的影響，並可用以監測全球氣候變遷。利用先進的開迴路技術，福衛三號比之前的 CHAMP 任務所提供的 RO 資料，更深入穿透到對流層以下以探測大氣層的變化。由於福衛三號的優異科學成就，後續任務將進一步由實驗型轉換成作業型的任務，並計畫同時接收 GPS/GALILEO/GLONASS 系統的資料。本博士論文論述福衛三號星系任務的無線電掩星理論、星系部署原理、升軌操作技術、星系操作結果及所面臨的操作挑戰、及如何利用先進進動理論完成世界上第一個星系部署系統的寶貴操作經驗及成果，並敘述後續任務的任務分析及攜帶 GNSS RO 量測儀酬載的衛星概念設計。

FORMOSAT-3 Constellation Performance, Deployment Challenges, and Prospect for Atmospheric Remote Sensing

Student：Chen-Joe Fong Advisor：Sien Chi

Institute of Electro-Optical Engineering
National Chiao Tung University

ABSTRACT

The FORMOSAT-3/COSMIC (FORMOsa SATellite mission-3/Constellation Observing System for Meteorology, Ionosphere, and Climate) satellites were successfully launched in California on April 15, 2006 into a 516 km orbit plane. The FORMOSAT-3 mission consisting of six low-earth-orbiting satellites is the world's first demonstration of near real-time operational Global Positioning System (GPS) radio occultation (RO) mission for global weather monitoring. After six spacecraft bus in-orbit checkout activities were completed, the mission was started immediately at the parking orbit for in-orbit checkout, calibration, and experiment of three onboard payload instruments: GPS occultation receiver (GOX), Tiny Ionospheric Photometer (TIP), and Tri-Band Beacon (TBB). Individual spacecraft was then maneuvered into six separate orbit planes of ~800 km with evenly distributed global coverage. FORMOSAT-3 mission has verified a novel "proof-of-concept" way of performing constellation deployment by taking the advantage of nodal precession. The received RO data have been processed into 1,800 to 2,200 good atmospheric and ionospheric profiles per day, respectively. The processed atmospheric RO data have been assimilated into Numerical Weather Prediction (NWP) model for near real-time weather prediction and typhoon/hurricane/cyclone forecasting by global weather centers which have shown significant positive impact. With the advent of the open-loop technique, the quality, the accuracy and the lowest penetration altitude of the RO sounding profiles are better than CHAMP data. Due to the great success of this innovative FORMOST-3 mission, the goal of the follow-on mission is to transfer FORMOSAT-3 mission from research to operational with GPS, Galileo, and GLONASS tracking capabilities. In this dissertation we present the Global Navigation Satellite Systems (GNSS) RO theory, the constellation deployment theory, the constellation deployment results, the mission challenges, and the lessons learned. We also present the spacecraft system performance, the follow-on mission trade analysis results, and new spacecraft constellation system conceptual design with a next-generation GNSS RO receiver onboard.

誌　謝

(Acknowledgements)

在這本論文完稿之際，首先我必須感謝我的指導教授－祁甡老師，若不是他的悉心指導及論文建議方向，我想我不會走完最後這個階段。我也要謝謝溫盛發博士，曾經協助祁老師來指導我通過博士讀書計畫資格考。我也要謝謝國家太空中心的長官及指導並協助我以福衛三號的多項研究工作為方向一起完成研究的同事們，他們是李羅權前主任、陳紹興副主任、吳岸明副主任、陳正興副主任、陳正一前總計畫主持人、顏隆政總計畫主持人、劉說安主任、陳彥升組長、劉肩吾博士、朱崇惠、楊善國、蕭文宗、林辰宗、郭添全博士、黃成勇博士…等。福衛三號計畫是我國第三個衛星計畫，是建立全球大氣即時觀測網之先進技術發展計畫。它的成功發射，並且完成任務軌道部署，及提供了寶貴的衛星實時科學資料，建立了很多個世界第一。

令人高興及感到欣慰的是國家太空中心三號計畫團隊於 2008 年參加國家實驗研究院傑出科技貢獻獎的選拔，以「福爾摩沙衛星三號星系計畫的科技成效與成就」研究主題拿下科技服務類的秀姑巒山獎殊榮。更證實此計畫的成功背後是一個團隊合作的成功典範。2009 年 2 月所舉辦的「福衛三號成效評估報告暨後續計畫規劃」審查，更是獲得國研院審查委員的一致贊揚與好評。

我在完成所負責的華衛一號的整測及發射工作後，決定在十幾年前離開校園後，又回到校園去追求更高的學術研究，實在是我一個人生旅程的另一個轉捩點。整個論文研究從開始到更換題目到完成，證明了要在很短的時間內，我要能在事業工作、學業研究、家庭經營、小孩教育及身體健康上，都要能夠全部同時兼顧，是要我去完成一件不可能的任務。無論如何，這將是我人生歷程至生難忘的一段回憶。

我要感謝國家太空中心和國家科學委員會對本任務的資助。謝謝國科會、國研院及太空中心長官同事們對我的持續支持與關注。過去十年有很多人對福衛三號任務的貢獻，特別是對我的論文研究工作，還有太多人以至於我在此無法一一提及。我最後要謝謝我的家人及兩個可愛的小孩－俐婷及偉丞，謝謝 Jo 提供我一個寫作論文的寧靜環境地方，他們一步一步陪伴我走過這個艱辛的歷程。

Table of Contents

List of Tables

List of Figures

Nomenclature

α_1 = *Bending angle of L1 frequency*

α_2 = *Bending angle of L2 frequency*

$A_{C/A}$ = *Received power of the in-phase component of the L1 signal*

A_{P1} = *Received power of the quadrature component of the L2 signal*

A_{P2} = *Received power of the L2 signal*

a_{SMA} = *Semi-Major Axis of the Orbit Altitude in km*

Δa_{SMA} = *Maximal difference in SMA (in meter)*

b = *Impact Parameter*

$CA(t)$ = *Clear acquisition (C/A) code-modulating the in-phase component of L1 signal at a rate of 1.023 MHz*

E = *Eccentricity*

f = *Frequency of Global Positioning System Carrier Signal in Hz*

f_D = *Excess Doppler frequency shift measured by the GNSS receiver of LEO*

F = *Thrust force*

I = *Inclination*

I_{sp} = *Specific Impulse*

ΔL = *Maximal deviation Argument of Latitude in degree*

λ = *Wavelength of the harmonic wave*

$M(t)$ = *Amplitude modulation of L1 and L2 containing navigation data*

N = *Refractivity*

n = *Index of Refraction*

n_G = *Index of refraction at the occulted GNSS satellite*

n_L = *Index of refraction at the LEO satellite*

n_e = *Electron Density in Number of Electrons per Cubic Meter*

Ω = *Right Ascension Ascending Node (RAAN) in Degree*

$\Delta\Omega$ = *Drift of the RAAN after a deployment time*

$\Delta\varphi$ = *Phase delay*

P = *Pressure in hPa*

P_m = *Propellant Mass*

P_w = *Water Vapor Pressure in hPa*

$PY(t)$ = *Precision (P) code-modulating the in-phase component of L1 and L2 signals at a rate of 10.23 MHz*

r = *Position along the raypath*

r_G = *Geocentric position vector to the occulting GNSS satellite*

r_L = *Geocentric position vector to the LEO satellite*

r_{LG} = *Geometric straight line distance between the LEO satellite and the occulted GNSS satellite*

s = *Arc length along the ray path*

σ = *Standard Deviation*

T = *Temperature in Kelvin*

T_G = *Ray path tangent vectors of the occulted GNSS satellite*

T_L = *Ray path tangent vectors of the LEO satellite*

t = *Deployment Time Period in days*

V_G = *Velocity of the occulted GNSS satellite*

V_L = *Velocity of the LEO satellite*

$\Delta\rho$ = *Ray delay*

Chapter 1 Introduction

1.1 History of Occultation

The term "occultation" is widely used in astronomy when an object in the foreground occults (covers up) objects in the background, and it refers to a geometry involving the emitter, the planet and its atmosphere if any, and the receiver changes with times.[1] The first scientific application of the occultation technique was introduced in the eighteen century when it was used for timing astronomical events. By observing scintillations, refraction, and variations in stellar brightness and spectra when a star is occulted by a planet or moon, the spectral intensity fading could be used to approximate the scale height of planetary atmosphere by using the geometric ray optics theory [1].

Radio occultation (RO) is a remote sensing sounding technique in which a microwave emitted from a spacecraft passes through an intervening planetary atmosphere before arriving at the receiver, and is used to study the physical properties of planetary atmosphere in the early days of interplanetary mission [2]. The atmospheric radio RO observations represent a planetary-scale geometric optics experiment in which the atmosphere acts as a big optical lens and refracts the paths and propagation velocity of electromagnetic wave signals passing through it [3]. Mariner-4, the first spacecraft to Mars (in 1964), flew along a spacecraft trajectory that passed behind Mars when viewed from Earth [4]. When Mariner-4 spacecraft passed behind and emerged from the other site of Mars, the extra carrier phase delay and amplitude variation of the microwave signals were observed. These observed data provided a very first valuable atmospheric and ionospheric density information by using the inversion techniques derived from basic geometric ray optics theory, Fourier optics theory, and Maxwell's electromagnetic wave theory [5]. Mariner-4 opens an era of planetary RO

---

1 http://en.wikipedia.org/wiki/Occultation [cited 15 Dec. 2008].

experiments. Since then a series of planetary experimental missions were undertaken to study the atmospheres and ionospheres of the planets and their moons, as well as certain physical properties of planetary surfaces and planetary rings [6].

1.2 GNSS Radio Occultation

The limb sounding of the Earth's atmosphere and ionosphere using the RO technique can be performed with any two cooperating satellites before the United States' Global Positioning System (GPS), the first Global Navigation Satellite Systems (GNSS), becoming operational [7]. A few early RO experiments from a satellite-to-satellite tracking link had been conducted. These included the occulted radio link between ATS-6 and GEOS-3 [8] and between the Mir station and a geostationary satellite [9].

After GNSS becomes operational, substantial and significant progress has been made in the science and technology of ground-based and space-based GNSS atmospheric remote sensing over the past decade [10]. The ground-based GNSS atmospheric remote sensing with upward-looking observations arose in the 1980s from GNSS geodesy. As the rapid increase of the GNSS geodetic ground networks around the world, great quantity of atmospheric integrated perceptible water (PW) were used in numerical weather prediction (NWP) for weather and climate modeling [11]-[12]. However, one of the major limitations to the ground-based GNSS remote sensing is that it just only provides integrated PW with little useful vertical resolution, and it is restricted to land areas filled with GNSS networks. The space-based GNSS atmospheric limb sounding offers a complementary solution to these issues [13].

The space-based GNSS RO atmospheric remote sensing technique, which makes use of the radio signals transmitted by the GNSS satellites, has emerged as a powerful approach for sounding the global atmosphere in all weather over both lands and oceans [14]-[17]. Figure 1-1 shows a schematic diagram illustrating radio occultation of GNSS signals received by a low-earth-orbit satellite. The GPS/Meteorology (GPS/MET) experiment (1995-1997) showed that the GNSS RO technique offers great advantages over the traditional passive microwave measurement of the atmosphere by satellites and became the first space-based “proof-of-concept” demonstration of GNSS RO mission to Earth [18]-[23]. For a more complete history of GNSS RO see Melbourne et al. in [5] and Yunck et al. in [6].

The extraordinary success of GPS/MET mission had inspired a series of other RO missions, e.g., the Ørsted (in 1999), the SUNSAT (in 1999), the Satellite de Aplicaciones Cientificas-C (SAC-C) (in 2001), the Challenging Minisatellite Payload (CHAMP) (in 2001), and the twin Gravity Recovery and Climate Experiment (GRACE) missions (in 2002). The GPS RO sounding data have been shown to be of high accuracy and high vertical resolution. All these missions set the stage for the birth of the FORMOSA SATellite mission -3/Constellation Observing Systems for Meteorology, Ionosphere, and Climate mission, also known as FORMOSAT-3/COSMIC mission [19]-[24].[2]

1.3 FORMOSAT-3 Mission

The F3 mission is the world’s first demonstration of GPS radio occultation near real-time operational constellation mission for global weather monitoring. The primary scientific goal of the F3 mission is to demonstrate the value of near-real-time GPS RO observation in operational numerical weather prediction. With the ability of performing both rising and setting occultation, the F3 mission provides about 1,800 ~ 2,200 atmospheric and ionospheric soundings per day in near real-time that give vertical profiles of temperature, pressure, refractivity, and water vapor in neutral atmosphere, and electron density in the ionosphere with global coverage [25]-[33]. The mission results have shown that the RO data from F3 are of better quality than those from previous missions and penetrate much further down into the

[2] In this dissertation we refer to the FORMOSAT-3/COSMIC mission as F3 mission for simplicity.

troposphere, the mission results could be referenced to Cheng et al. in [28], Liou et al. in [29], Anthes et al. in [30], Fong et al. in [31] and [32], and Huang et al. in [33]. In the near future, other GNSS, such as the Russian Global Navigation Satellite System (GLONASS), and the planned European Galileo system, will be used to extend the region of applications by the use of GPS RO technique [32], [34]-[36].

Table 1-1 shows the F3 mission characteristics. The F3 mission was launched successfully from Vandenberg Air Force Base in California 1:40 UTC on April 15, 2006 into the same orbit plane of the designated 516 km circular parking orbit altitude. The F3 mission is jointly developed by Taiwan's National Space Organization (NSPO) and United State' University Corporation for Atmospheric Research (UCAR) in collaboration with Orbital Sciences Corporation (OSC or Orbital) for the satellites, NASA's Jet Propulsion Laboratory (JPL) and Naval Research Laboratory (NRL) for three onboard payloads including a GPS Occultation Receiver (GOX), a Tri-Band Beacon (TBB), and a Tiny Ionospheric Photometer (TIP). The TIP payload instrument is routinely collecting data at night, and observes the equatorial anomaly arcs and other density anomalies through measurements of 1356 Angstrom radiation. The nadir-pointing TBB enables observations of the line-of-sight total electron contents (TEC) and scintillations along the F3/COSMIC-TBB ground stations' radio links. The data from these two instruments complement the ionospheric observations from the GOX and are used to improve the retrieval of electron density profiles at night and over TBB ground stations. These data are also valuable for evaluation of ionospheric models and use in space weather data assimilation systems [30].

The retrieved RO weather data are being assimilated into the NWP models by many major weather forecast centers and research institutes for real-time weather predictions and cyclone/typhoon/hurricane forecasts [30], [37]. The great success of the F3 mission expected to operate through 2011, has initiated a new era for near real-time operational GNSS RO soundings [35]-[38].

1.4 F3 System

The F3 constellation system architecture consists of the six identical on-orbit micro-satellites, Spacecraft Operations Control Center (SOCC) in Taiwan, several TT&C (telemetry, tracking and command) Ground Stations, and two data receiving and processing centers, and the fiducial network. There are two TT&C local tracking stations (LTS), one located in Chungli and the other in Tainan of Taiwan, respectively. There are two remote tracking stations (RTS) to support the passes. Originally one is located at Fairbanks, Alaska and the other one is located at Kiruna, Sweden. After two years in orbit operation, the F3 program switches from these two ground stations to two new ground stations in Fairbanks (FBK), Alaska, and Tromso (TRO), Norway, plus a third RTS located in McMurdo, Antarctica. This McMurdo ground station is expected to reduce the data latency of some RO products. These three RTS are currently set as primary stations for the F3 mission. Figure 1-2 shows the F3 system architecture [32], [39],

The SOCC uses the real-time telemetry and the back orbit telemetry to monitor, control, and manage the spacecraft state-of-health (SOH). The downlinked science RO data is transmitted from the RTS via National Oceanic and Atmospheric Administration (NOAA) to the two Data Receiving and Processing Centers: (1) CDAAC (COSMIC Data Analysis and Archive Center) which is located at Boulder, Colorado, USA; and (2) TACC (Taiwan Analysis Center for COSMIC) located at Central Weather Bureau (CWB) in Taiwan. The fiducial GNSS data is combined with the occulted and referencing GNSS data from the GOX payload to remove the clock errors through double differencing. All collected science data is processed by CDAAC and then transferred to TACC and other facilities for science and data archival [40].

The processed results are then passed to the National Environmental Satellite, Data, and Information Service (NESDIS) at NOAA. These data are further routed to the weather centers in the world including the Joint Center for Satellite Data Assimilation (JSCDA), National Centers for Environment Prediction (NCEP), European Centre for Medium-range Weather Forecast (ECMWF), Taiwan CWB, UK Meteorological Office (UKMO), Japan Meteorological Agency (JMA), Air Force Weather Agency (AFWA), Canadian Meteorological Centre (Canada Met), Meteo France, etc. And they are made ready for assimilation into weather prediction models. The data is currently provided to weather centers within 90 minutes (data latency requirement is 180 minutes) after satellite on-orbit science data collection in order to be ingested by the operational weather forecast model [36].

1.5 F3 Follow-on Mission

As addressed in the Final Report of "Workshop on the Redesign and Optimization of the Space Based Global Observing System," the World Meteorological Organization (WMO) had recommended continuing RO observations operationally and the scientific community had urged continuation of the current mission and planning for a follow-on operational mission [41]. The proposed follow-on mission is a greatly improved operational and research mission with redundancy and robustness and consisting of a new constellation of 12 satellites. The need mission will seek to establish international standards so that future RO missions deployed by any country can be assimilated into the same systems. The primary payload of the follow-on satellite will be equipped with the GNSS RO receiver and will collect more soundings per receiver by adding European GALILEO system and Russian's Global Navigation Satellite System (GLONASS) tracking capability, which will produce a significantly higher spatial and temporal density of profiles. These will be much more useful for weather prediction models and also severe weather forecasting including typhoons and hurricane, as well as for a research [36].

In this dissertation we provide an overview of the radio occultation theory, new constellation deployment theory, the constellation spacecraft design, the constellation mission operations, the orbit-raising challenges, and the lessons learned during the orbit-raising operations. We also present the F3 satellite constellation system performance, and the prospect of a future follow-on mission with the performance enhancements we have accomplished.

TABLE 1-1 THE F3 MISSION CHARACTERISTICS

Number	Six identical satellites
Weight	~ 61 kg (with payload and fuel)
Shape	Disc-shape of 116 cm diameter, 18 cm in height
Orbit	800 km altitude, circular
Inclination Angle	72^{o}
Argument of latitude	52.5^{o} apart
Power	~ 81 W orbit average
Communication	S-band uplink (32 kbps) and downlink (2 Mbps)
Sounding	~2000 soundings per day
Data Latency	15 minutes to 3 hours
Design and Mission life	5 years
Launch date	15 April 2006

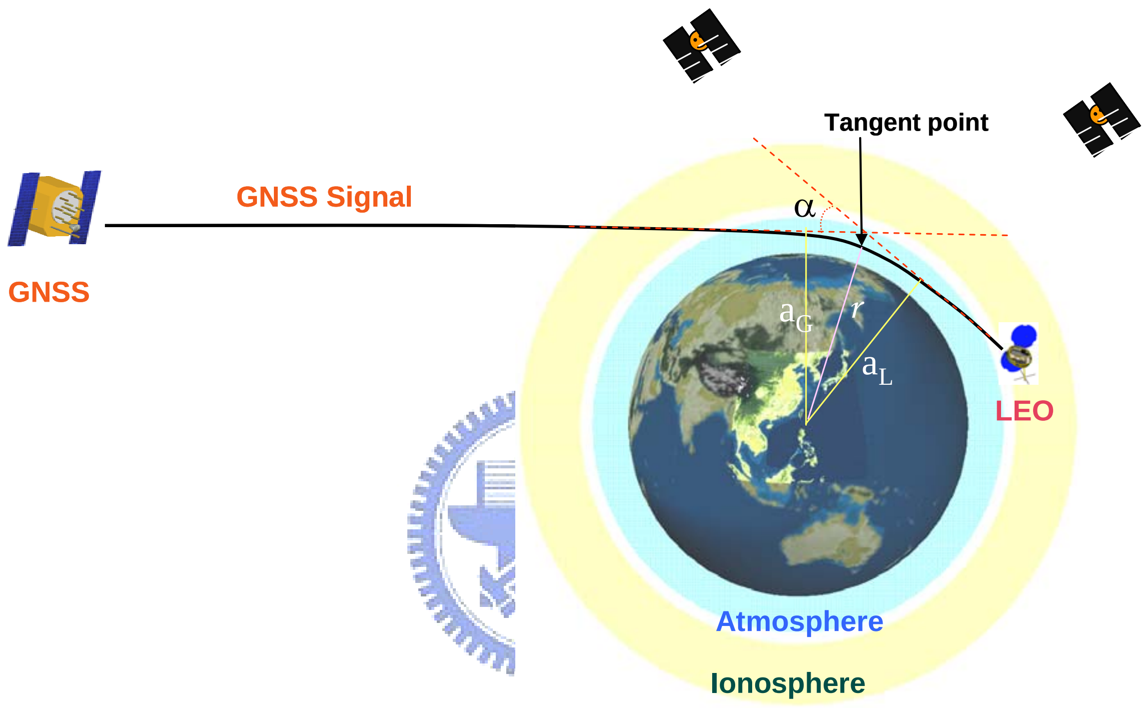

Figure 1-1. Schematic diagram illustrating radio occultation of GNSS signals.

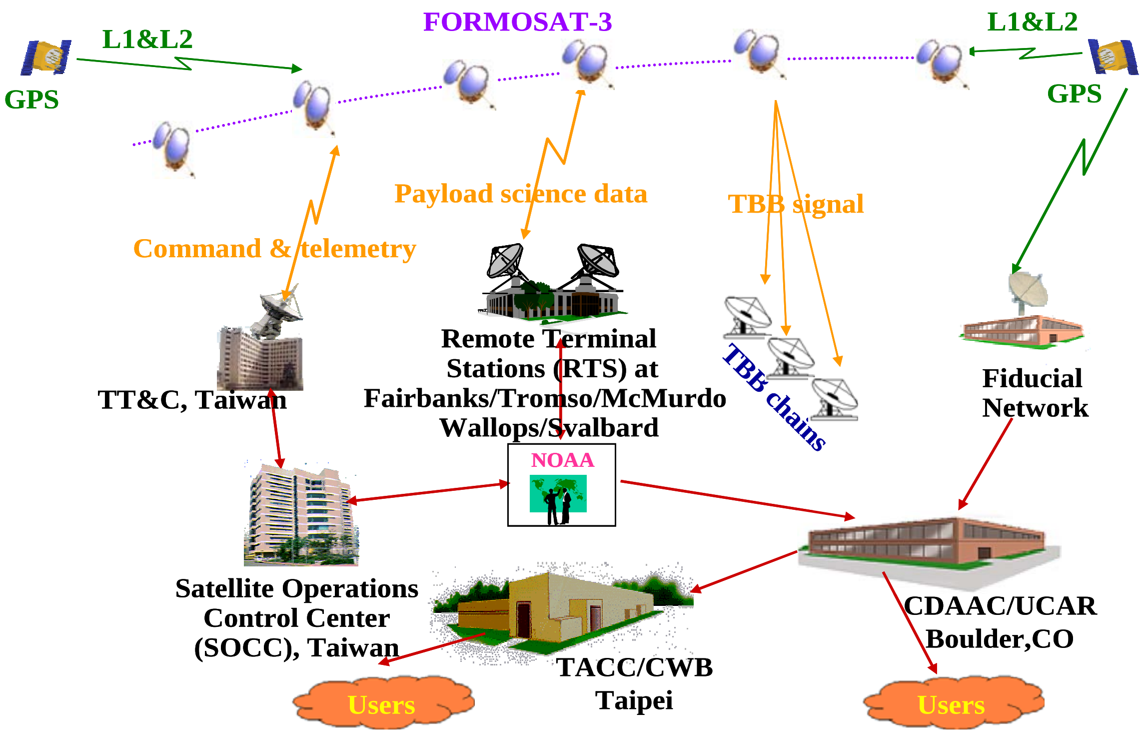

Figure 1-2. F3 system architecture.

Chapter 2 Radio Occultation Theory and Constellation Deployment Principle

2.1 Introduction

This Chapter begins with an overview of the GNSS radio occultation theory (in Section 2.2) and followed by the constellation deployment principle (in Section 2.3). In Section 2.2 we present the GNSS, GNSS radio occultation theory and operation concept; and radio occultation data retrieval theory. As for Section 2.3, we present earth oblateness right ascension ascending node phasing, argument of latitude, final phasing, contact conflict avoidance, and dispersion operation to maximize science data downloads, followed by the conclusion.

2.2 The GNSS Radio Occultation Theory

2.2.1 The Global Navigation Satellite System

The GPS developed by United States, is the only fully functional GNSS in the world. It consists of 24 satellites, with a few more satellites for backup, distributed in six circular orbit planes about the globe with an inclination angle of ~55^{o}, a period of 12 hours and an altitude of 20,200 km. Although originally designed as a navigation aid by the U.S. Air Forces, the ground-based and the space-based applications of the GNSS remote sensing have shown positive impacts on climate monitoring, global and regional weather prediction, ionospheric research, and space weather forecasting.

Each GPS satellite continuously transmits right-hand circularly polarized signals at L1 and L2 band frequencies. The L1 and L2 signals received from each GPS satellite can be written as [3]:

$$S_1(t) = \sqrt{2A_{p1}}M(t)P_Y(t)\cos(2\pi f_1 t + \theta_1) + \sqrt{2A_{C/A}}M(t)C_A(t)\sin(2\pi f_1 t + \theta_1), \qquad (1)$$

$$S_2(t) = \sqrt{2A_{p2}} M(t) P_Y(t) \cos(2\pi f_2 t + \theta_1) \,. \quad (2)$$

2.2.2 GNSS Radio Occultation Retrieval Theory

In Figure 2-1 a GNSS RO operation concept and data set for an occultation event are shown. By measuring the phase delay of radio waves from GNSS satellites as they are occulted by the Earth's atmosphere, accurate and precise vertical profiles of the bending angles of radio wave trajectories in the ionosphere, stratosphere and troposphere are obtained.

A complete GNSS RO data set for an RO event includes (1) Occultation data: signal from an occulting GNSS satellite to occulting LEO satellite with 20 msec data rate (see link 1 marked in Figure 2-1); (2) Referencing data: signal from a non-occulted GNSS satellite with 20 msec data rate (see link 2 marked in Figure 2-1); (3) Precision orbit determination (POD) data: signals from other three non-occulted GNSS satellites with 10 sec data rate; and (4) Fiducial IGS (International GNSS Service) data: GNSS navigation data from ground fiducial network sites with 1sec data rate from occulting GNSS satellite (see link 3 and link 4 marked in Figure 2-1) [39]-[40].

A basic GNSS RO measurements and processing flow is presented in Figure 2-2. We derive the single path GNSS RO theory in this Section. From the calculus of variation the ray path from the GNSS satellite to the LEO satellite, in a geometric optics context, is by definition a path of stationary path and satisfies Fermat's principle globally and Snell's law locally [5], [42]. Figure 2-2 we show a ray path geometry from a occulted GNSS satellite (point G) to a LEO satellite (point L) in the plane of propagation and illustrating radio occultation of GNSS signals. This ray must satisfy the requirement

$$\Delta\rho = \frac{\Delta\varphi}{k} = \int_G^L n(r)ds - |r_L - r_G| = \int_G^L n\sqrt{1+(r\theta')^2}\,dr - r_{LG} = \text{ a stationary value} \quad (3)$$

where $\Delta\rho$ is the ray delay, $\Delta\varphi$ is the phase delay, *n(r)* is the real part of the refractive index, *r* is the geocentric position vector of any point on the ray, *s* is the arc length along the ray path, r_L is the geocentric position vector to the LEO satellite, r_G is the geocentric position vector to the occulting GNSS satellite, and r_{LG} is the geometric straight line distance between the LEO satellite and the occulted GNSS satellite.

From Figure 2-2, the excess Doppler from the intervening medium can be derived as

$$\lambda f_D = n_L T_L \cdot V_L - n_G T_G \cdot V_G - \frac{(V_L - V_G)\cdot(r_L - r_G)}{r_{LG}} \qquad (4)$$

where $f_D = (d\varphi / dt)/2\pi$ is the excess Doppler frequency shift measured by the GNSS receiver of LEO; λ is the wavelength of the harmonic wave; n_L and n_G are the index of refraction at the LEO and occulted GNSS satellites and is equal to unity, respectively; T_L and T_G are the ray path tangent vectors of the LEO and occulted GNSS satellites, respectively; and V_L and V_G are the velocity of the LEO and occulted GNSS satellites, respectively. The triangle OLG defines the instantaneous plane of propagation of the ray from the occulted GNSS satellite to the LEO satellite. The interior angles of this triangle OLG and its sides are completely determined from the precision orbit determination (POD) information about the orbits of the LEO and occulted GNSS satellite. The refraction-related quantities, which are the bending angle $\alpha = \delta_L + \delta_G$, can be determined from the excess Doppler measurement of Eq. (4) by applying $a = n|r \times T| =$ constant, which is Bouguer's law, essentially a Snell's law for a spherical symmetric medium.

As the ionosphere is considered as a source of concentration of electrons and the frequency of electromagnetic wave, the L1 and L2 GNSS signals can be combined to significantly reduce the effect of the ionosphere. The atmospheric bending angle can be calculated using Eq. (5) below

$$\alpha(r) = \frac{f_1^2 \alpha_1(r) - f_2^2 \alpha_2(r)}{f_L^2 - f_2^2} \qquad (5)$$

where α_1 and α_2 are the bending angle of L1 and L2 frequency, respectively.

From the bending angles, profiles of atmospheric index of refraction are obtained through the equation of Abel transformation as [3], [42]:

$$n(a_p) = \exp\left[\frac{1}{\pi}\int_{a_p}^{\infty}\frac{\alpha(a)}{\sqrt{a^2 - a_p^2}}da\right], \tag{6}$$

where $n(a_p)$ is the refractive index at a_p, $a_p = nr_p$ is the impact parameter for the ray at perigee, and r_p is the altitude of perigee, $\alpha(a)$ is the bending angle at a.

In the atmosphere, the index of refraction, n, is very close to unity such that it is usually discussed in terms of the refractivity, N. By using Eq. (7) N is a function of temperature (T in K), pressure (P in hPa), water vapor pressure (P_w in hPa), electron density (n_e in number of electrons per cubic meter), and frequency of the GPS carrier signal (f in Hz) as

$$N = (n-1)\times 10^6 = 77.6\frac{P}{T} + 3.73\times 10^5\frac{P_w}{T^2} - 40.3\times 10^6\frac{n_e}{f^2}. \tag{7}$$

The refractivity profiles can be used to derive profiles of electron density in the ionosphere, temperature in the stratosphere, and temperature and water vapor in the troposphere by using Eq. (7).

For problems from multipath, there have been several data processing methods for RO data inversion to retrieve atmospheric parameters from a wave optics theory treatment [5], As for the F3 mission, Kuo et al. develop a RO data processing procedures used to obtain stratospheric and tropospheric bending angle and refractivity profiles from the raw phase and amplitude data [23], [37]. The Phase Lock Loop (PLL) technique employed in earlier RO missions was replaced by a novel open loop technique for the F3 mission [43]-[45]. There are other data processing procedures or algorithms developed by other methods [5], such as the geometrical optics method (GOM) [46]-[47], the back-propagation method (BPM) [48]-[49], the radio holographic method (RHM) [50]-[51], the amplitude-retrieval method (ARM) [52], the full-spectrum-inversion method (FSIM) [53], the canonical transformation method (CTM) [54], the sliding spectral (or radio optics) method (SSM) [44]-[45] and National Central University Radio Occultation (NCURO) algorithms [55]-[56].

The F3 RO processing includes four radio holographic algorithms: BPM, SSM, CTM, and FSIM. Detailed description and derivations of F3 RO data processing procedure could refer to Kuo et al. in [23]. The RO data processing procedure and steps currently used for F3 mission are listed as follows:

1. Input (Phase, amplitude, LEO/GPS position and velocity);

2. Open-loop data processing GNSS navigation data messages (NDM) removal and phase correction;

3 Detection of L1 phase locked loop tracking errors and truncation of the signal;

4: Filtering of raw L1 and L2 Doppler;

5. Estimation of the “occultation point”

6. Transfer of the reference frame to the local center of Earth’s curvature;

7. Calculation of L1 and L2 bending angles from the filtered Doppler;

8. Calculation of the bending angles from L1 raw complex signal;

9. Combining (sewing) L1 bending angle profiles from steps 7 and 8;

10. Ionospheric calibration of the bending angle;

11. Optimal estimation of the bending angle;

12. Retrieval of refractivity by Abel inversion;

13. Retrieval of pressure and temperature;

14. Output (bending angle, refractivity, pressure, temperature, moisture).

2.3 Constellation Deployment Principle

2.3.1 Earth Oblateness Right Ascension Ascending Node (RAAN) Phasing

The total mass of a F3 satellite is 61.05 kg, including the dry mass of 54.4 kg and the propellant mass of 6.65 kg. And the overall altitude increase from injection orbit to mission orbit is 285 km. The estimated total delta-V required is 147 m/s, and the estimated propellant required is 4.6 kg. Fuel margin is 2.05 kg [57]-[58].

Due to the oblateness of the Earth gravity, the RAAN (Ω) of a LEO satellite will drift away at a rate. The drift rate of RAAN (ΔΩ/Δt), also called "orbit precession rate," which is a function of the Semi-Major Axis (SMA), inclination, and eccentricity of the orbit. For the F3 near-circular orbit with an inclination of 72^o and eccentricity of 0, the orbit precession rate is modeled as an equation below [59]:

$$\Delta\Omega \cong -6.3804\times10^{13}\Delta({a_{SMA}}^{-7/2})\cdot\Delta t \quad (8)$$

where

$\Delta\Omega$ the drift of the RAAN after a deployment time of Δt;

a_{SMA} the SMA of the orbit altitude in km;

Δt the deployment time period in day.

The deployment strategy is to use the first raised spacecraft (FM5) as a reference point. The second spacecraft is then raised to its mission orbit when the difference of the RAAN between the first and the second spacecraft reaches the desired separation angle, and so forth.

2.3.2 Argument of Latitude (AOL) Final Phasing and Contact Conflict Avoidance

As one ground station can support one pass from elevation angle 10^o to 10^o, if there are two satellites flying over the same ground station at the same time frame, the ground station could support only one satellite unless there were special arrangements. Therefore, a 52.5^o phasing on AOL must be implemented to ensure that one orbit's worth of occultation science data are sent to the receiving stations. The maximal difference in SMA (Δa_{SMA} in meter) and the maximal deviation (ΔL in degree) of the AOL from its nominal value are deployed to fulfill the following equation

$$\Delta a_{SMA} + 5 * \Delta L < 50. \quad (9)$$

so that multiple contacts at the same ground station at the same time are avoided [57],[60].

The differentiation of the AOL of the other five satellites against the reference orbit is achieved by controlling the altitude deployment profile in the final stage of the “maneuvering window.” When the orbit altitude is different from the reference orbit (FM5), the AOL change rate is also different from the reference orbit. The different AOL change rate differentiates the AOL of the satellite against the reference orbit along with time. By manipulating the altitude deployment profile in the final stage, the AOL difference is targeted at the same time to maneuver the satellite into the mission orbit altitude. Then both the RAAN and AOL differences are frozen and kept constant simultaneously.

2.3.3 Dispersion Operation to Maximize Science Data Downloads

The dispersion operation is very similar to the AOL phasing. In order to increase the number of GOX data downlink, a spacecraft dispersion operation plan was executed to differentiate the AOL of FM4, FM3, FM1 and FM6 in parking orbits. These four satellites were maneuvered to the same altitude around 519 km with an AOL difference around 80^o so that they can contact a ground station in turn to increase GOX science data downlink with no contact conflicts [57]-[58].

2.4 Conclusion

In this Chapter we have given an overview of the GNSS radio occultation theory and the constellation deployment theory. The constellation deployment theory is used for unique F3 constellation deployment and the results are presented in Chapter 3.

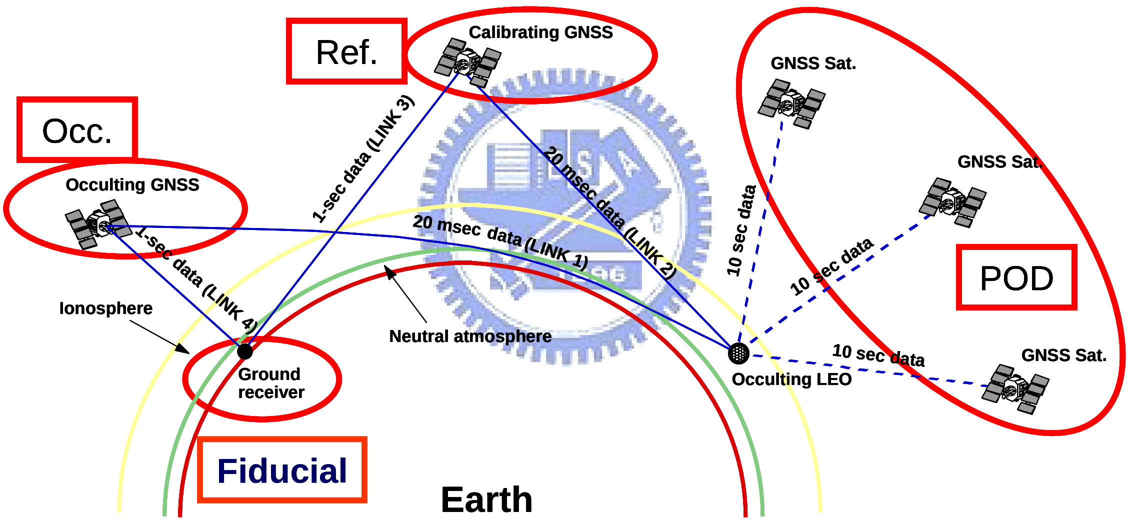

Figure 2-1. GNSS RO receiver operation concept.

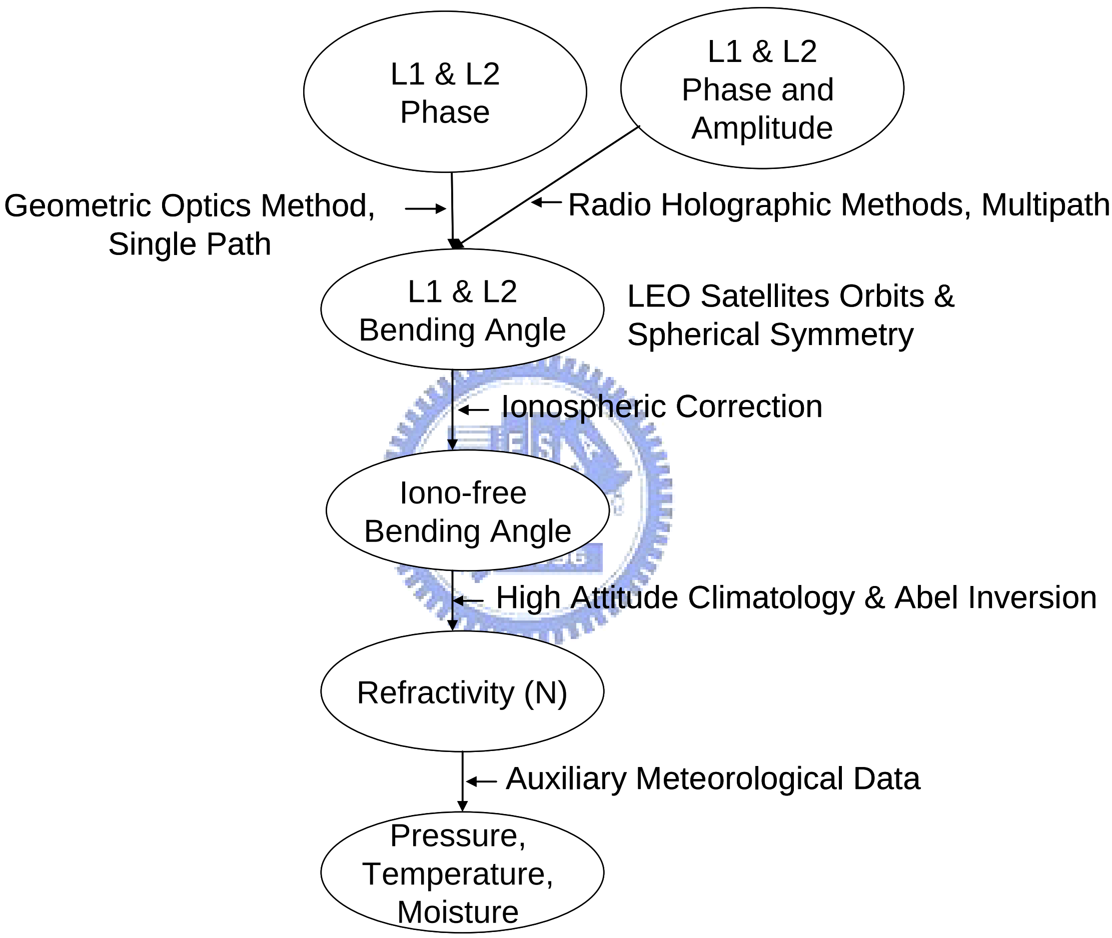

Figure 2-2. Basic GNSS RO measurements and processing flow.

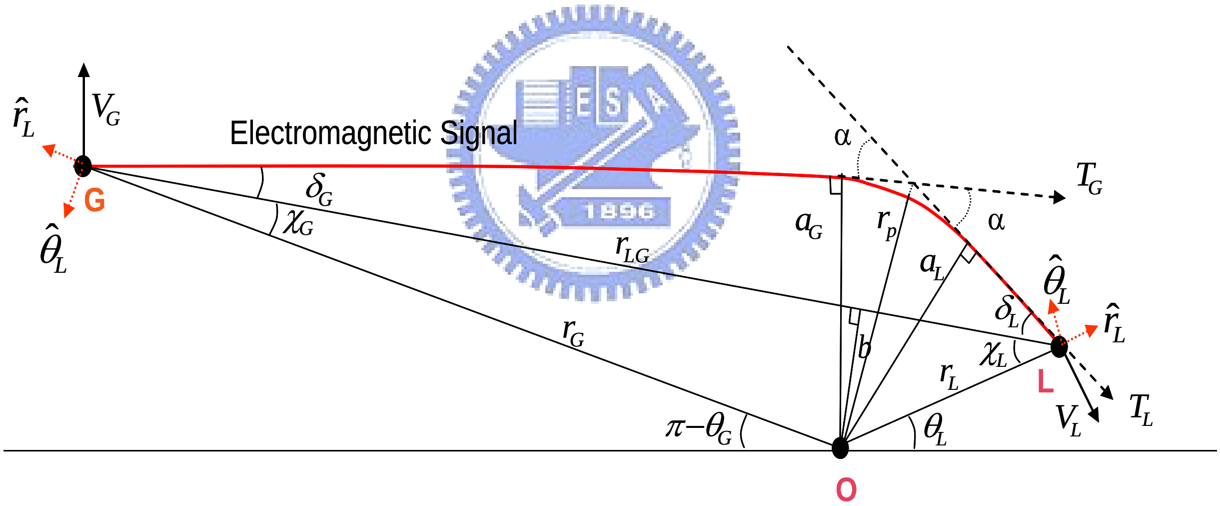

Figure 2-3. Ray path geometry from point G to point L in the plane of propagation. For a spherical symmetric medium $a = a_G = a_L$.

Chapter 3 Constellation Deployment

3.1 Introduction

The F3 mission operation concept is to launch the entire cluster of satellites by a single launch vehicle. All six satellites are delivered to the same injection orbit plane of a designated 516-km circular parking orbit altitude, and the six satellites are in a cluster formation fly configuration after separation from the launch vehicle. They are then deployed into six different orbit planes at specific time intervals using the constellation deployment principle[57]-[58], [61].

The F3 mission takes advantage of nodal precession to conduct orbit-raising maneuvers at the appropriate times so that the effect of different altitudes makes the orbital planes drift [62]. It is well-known that the nodal precession is a gravity phenomenon where the orbital plane drifts due to the Earth's oblateness. The approach using the natural physics of the Earth's oblateness, as well as time, allows the spacecraft to drift instead of requiring complex propulsion systems or even depending on individual launch vehicle to arrive at their orbit planes directly. Although this approach requires a lengthy orbit-deployment time, it significantly reduces the size of the propulsion subsystem design needed [31].

The F3 spacecraft systems for orbit raising and ground flight dynamics design are presented in Section 3.2 below. We present the evolution of the constellation plan in Section 3.3, the constellation deployment results in Section 3.4, and followed by the conclusion in Section 3.5.

3.2 Spacecraft System for Orbit Raising and Flight Dynamics

3.2.1 F3 Spacecraft System

Figure 3-1 illustrates the spacecraft in deployed configuration and its major components.

The major subsystem elements of the spacecraft system are Payload Subsystem, Structure and Mechanisms Subsystem (SMS), Thermal Control Subsystem (TCS), Electrical Power Subsystem (EPS), Command and Data Handling Subsystem (C&DH), Radio Frequency Subsystem (RFS), Reaction Control Subsystem (RCS), Attitude Control Subsystem (ACS) and Flight Software Subsystem (FSW). The spacecraft bus provides structure, RF power, electrical power, thermal control, attitude control, orbit raising, and data support to the instrument [32], [61]. Table 3-1 shows the F3 constellation spacecraft bus key design features.

3.2.2 Spacecraft Propulsion for Thrust Burn

The spacecraft propulsion subsystem (also named the RCS) is a blowdown monopropellant Hydrazine (N_2H_4) Propulsion Subsystem with gas-helium (GHe) as the pressurant. And the designed blowdown ratio is 5:1 with the MEOP (Maximum Expected Operating Pressure) of 400 psia at 50^{o}C. The initial tank pressure is pressurized to about 330 psia at 20^{o}C. We utilize the RCS to provide impulses for attitude control during orbit-raising and to transfer the satellite from the injection orbit to an intermediate orbit if required, and finally to the mission orbit of the constellation. Figure 3-2 shows the block diagram of the RCS. For F3 spacecraft system the RCS consists of a propellant tank, gaseous helium and Hydrazine service valves, a latching valve, a filter, an orifice, four thrusters, pressure transducer, and a set of pipelines. The spacecraft RCS characteristics are summarized as follows [57]-[58]:

- Thrust Force: 1.1 [Beginning of Life (BOL)]－0.2 N [End of Life (EOL)];
- Specific Impulse: 217－194 s;
- Propellant Mass: ~6.65 kg;
- Thrust Type: OFF pulsing (Duty Cycle ≦ 50%).

Figure 3-3 shows the locations of the four thrusters (R1, R2, R3, and R4) which are located in the four quadrants of the x-z plane of the satellites. These four thrusters are canted by 10° to enable three-axis control capability. By modulating the off-pulsing duration of the four thrusters, control torque is generated for the attitude control around X, Y, and Z axis of the satellite. The estimated thrust and specific impulse over the entire blowdown pressure range are shown in Figure 3-4.

3.2.3 Spacecraft Attitude Control for Orbit Raising

The function of the spacecraft ACS is to control the attitude of the satellite in the Safe Mode, the Stabilization Mode, the Nadir Mode, the Nadir-Yaw Mode, and the Thrust Mode. And the ACS sensors for attitude estimation include Earth horizon sensors, coarse sun sensors, and a magnetometer. The ACS actuators for attitude control include magnetic torquers, a reaction wheel and thrusters [57], [61].

Figure 3-5 shows the functional block diagram of the spacecraft ACS where FC stands for Flight Computer and ACE means the Attitude Control Electronics. In Figure 3-5 the Attitude Reference System (ARS) includes attitude and rate estimators using a Kalman filter algorithm with measurements from the sensors. The ACS Controller processes the attitude and rate estimation from ARS through the control gains/algorithm, and distributes the torque commands to the actuators. The ACS also receives the satellite position and velocity data from the bus GPS receiver (GPSR). Based on this information it then propagates and computes necessary information for the navigation purpose, the ARS and the commanded angles for the Solar Array Drive (SAD).

The Thrust Mode is dedicated to the orbit-raising operation. When the orbit-raising operation is performed, the satellite first maneuvers itself to a yaw angle of 90° to align the thrust direction with the velocity direction. Then, as soon as the ACS enters Thrust Mode the thruster ignition starts up, the attitude is controlled by thrusters while orbit-raising proceeds. When the operation is terminated or finished, the ACS enters the Nadir-Yaw

Mode and maneuvers itself to a pre-set yaw angle.

A proportional-integral-derivative (PID) controller is designed for the Thrust Mode to compute the desired 3-axis control torque. Four thrusters are commanded off-pulsing in each control cycle to provide both the impulse for orbit raising and the 3-axis control torque to diminish the attitude errors. Figure 3-6 shows the concept of the "off-pulsing" in each control cycle. In orbit-raising operations, the thrust turn-on time in each control cycle is either kept constant as the "InitialThurstPower" value, or increased by "AddThrustIncrement" seconds in every "AddThrustInterval" control cycles. The Thrust Mode control gains are adjusted in order to compensate for changes in thrust level during the RCS blowdown process.

The PID controller will minimize the attitude control error and improve the orbit-raising performance, but it suffers from the relative instability issue. This is because the control system may diverge with a large thruster turn on time when the PID integral terms are not yet converged to their steady-state values. Therefore, during orbit-raising operations, the PID controller requires a series of "calibration burns" in order to converge the attitude integral terms and to ramp up the thruster turn-on time to a larger value. Calibration burn is usually a smaller burn than the full-thrust burn. During the calibration process, the final values of the thrust turn on time and the integral terms of a previous burn are used as the initial values for the next burn. In this way, it takes about 6~8 calibration burns to reach the so-called full-thrust burn.

3.2.4 Flight Dynamics and Orbit Dynamics

The main function of ground-based Flight Dynamics Facility (FDF) is to conduct various orbit dynamics analyses including orbit determination, orbit-ephemeris propagation, orbit-maneuver planning, orbit-parameter trending, and orbit-event prediction. In the F3 mission, we use the commercial off-the-shelf software package called "Orbit Analysis System

(OASYS)" in FDF for orbit analysis. The OASYS database includes the thrusting model of the onboard RCS and ACS, such as the thruster number, location and direction; propellant mass and pressure; pressurant mass; blowdown curves for thrust and specific impulse; and thrust type, thruster duty cycle and efficiency [57], [61].

The blowdown curves for thrust force (F) and specific impulse (I_{sp}) as shown in Figure 3-4 are modeled as the equations:

$F = (0.001141+0.0006*P)* 4.448221$ (in newtons). (1)

$I_{sp} = 222.84 - 2268.4/P_m$ (in seconds). (2)

where

F the thrust force;

I_{sp} the specific impulse;

P_m the Propellant Mass.

and used in the OASYS database for F3 orbit raising. Both equations are functions of the propellant tank pressure in the unit of psia.

The thrust power in each ACS control cycle is modeled as the duty cycle of the thruster and listed as *Duty Cycle = Thrust Power/Control Cycle.* In full-thrust orbit-raising burns, the thrust power in each control cycle is kept constant, as the duty cycle is in the OASYS model. However, in calibration burns, the thrust power in each control cycle is linearly ramped up to the end of the burn. In other words, the duty cycle in each control cycle also increases in the same way as the thrust power does. Unfortunately, there is no way in OASYS to correctly model the calibration burns with increasing thrust powers. Instead, an averaged thrust power (duty cycle) using the initial and final thrust powers of the burn is used in the OASYS database to model the thrusting of a calibration burn.

The OASYS is also used to conduct an orbit determination to compare the actual post-burn orbit and the OASYS-planned post-burn orbit after a thrust-burn is completed. Based on the actual and OASYS-planned orbit altitude, a thrusting efficiency is recalculated, which in turn provides another input for the next orbit-raising planning.

3.3 Constellation Deployment Plan Evolution

3.3.1 Original Constellation Deployment Plan

The F3 mission operation plan changes as time passes following launch. Originally the F3 constellation deployment plan included a tandem flight design during the deployment phase. The tandem flight satellites would maintain an along-track distance of 200~400 km. Two pairs (FM1&FM2, FM3&FM4) of satellites would fly in tandem in an intermediate orbit altitude (525km and 576 km) for the geodesy research. However, spacecraft FM3 and FM4 have been very close together since launch of the satellites. The data from April to October were able to provide adequate data for geodesy research at the parking orbit of 516 km. The constellation plan was thus changed to meet the need for more science dumps for Intensive Operation Period (IOP) campaign and tropical cyclone (typhoon and hurricane, etc.) prediction forecast studies [29], [31].

The constellation plan at an 800-km orbit with 24^{o} separation planes was for a shorter deployment time consideration (13 months after launch) and based on the assumption that spacecraft attitude control performance in lower altitude is worse than that in the mission orbit. However, this plan is not favorable for the ionospheric monitoring and climate seasonal variability studies, due to non-uniform coverage globally. Shorter duration to complete the constellation deployment has become less of a concern since the spacecraft attitude performance is better than expected and the data of the early phase (mostly at lower orbit) are much better than anticipated [61].

3.3.2 New Constellation Deployment Plan

Scientists from Taiwan and the US coherently favor 30^{o} separation with ~6 months longer constellation deployment duration over 24^{o} separation for global uniform coverage in local solar time (LST). The original constellation mission operation plan was revised, manpower was reallocated, and the orbit-raising schedule was rearranged to accommodate the science team's request. This change in new constellation plan reflects integral teamwork among the operations team and data users and leads to greater mission success. The constellation deployment plan change from the 24^{o} separation to 30^{o} separation was made in September 2006 after the completion of FM5 orbit transfer and during FM2 orbit raising. The decision was made to put the FM2 orbit transfer on hold in October 2006 and to allow its separation from FM5 further. The decision postponed the completion of the final constellation to December 2007 [29],[57],[61].

3.4 Constellation Deployment Results

3.4.1 As-Burn Constellation Results

The current constellation configuration as of December 2007 is five satellites (FM5, FM2, FM6, FM4, and FM1) successfully reaching the 800-km mission orbits. On August 3, 2007 FM3 encountered the solar array drive mechanism malfunction when reaching the 711 km orbit. This anomaly blocks the FM3 thrust burn activity to be deployed at the 800 km mission orbit. The reasons for this anomaly are still under investigation. The constellation deployment status as-of- December 2007 is shown in Figure 3-7. The dash line is the newly planned schedule and the dots recorded the execution results of the thrusting. The relative orbital separation angle, the relative AOL, and the relative altitudes of these four satellites are shown in Table 3-2 [57].

3.4.2 Spacecraft Thrust-Burn Performance Statistics

Figure 3-8 and Table 3-3 show the spacecraft thrust-burn performance statistic results in strip chart and table formats, respectively [57]. Starting from FM4 orbit transfer, the NSPO operations team uses the autopilot scheme to increase the burn success rate and reduce the burn working days. The data show that the FM5 burn working days number 39. However, it takes 75 calendar days to complete the burn activities. The operations team scheduled seven burns per day for FM4 and FM1 compared to three burns per day for FM5 as deployed earlier. The better spacecraft burn performance indicates that more successful rate has been achieved. The operations team has decreased the planned burn duration from 456 minutes for FM5 to 382.8 minutes for FM1 and also decreased the executed burn duration from 326.1 minutes for FM5 to 329.8 minutes for FM1. These results show that the thrust-burn success rate (= executed burn/planned burn) has been increased by the operations team from 71.5% for FM5 to 86.2% for FM1. Total burn number has increased from 53 times in FM5 to 71 times in FM1. From Table 3-3 it can be seen that the average orbit transfer height per burn has decreased from 5.4 km/burn for FM5 to 3.4 km/burn for FM1. Additionally, the average burn duration per burn has decreased from 369.4 sec/burn for FM5 to 238.4 sec/burn for FM1.

3.4.3 Spacecraft Mass Property and Moment of Inertia Results

We found that the propellant mass remains in the propellant tank are about 2.0 kg after the orbit-transfer operations are completed for each satellite. It is also expected that the spacecraft mass property (weight and center of gravity) and moment of inertia (MOI) are changed accordingly when propellant mass is changed. It was observed that the spacecraft center of gravity (CG) has a change of -0.7 cm shift in Z-axis before and after orbit-transfer activities, and has a CG shift in -Y and -X axes too. These changes will have a significant impact on the geodesy and earth gravity research [63]-[64]. Table 3-4 shows the spacecraft mass property and moment of inertia results of the six satellites. The spacecraft remaining propellant mass was estimated and provided by Propulsion subsystem. The error of the mass was estimated in the range of ±0.1 kg. Based on computation results, a very minor impact on MOI and CG results was observed due to this error range [57].

In the F3 satellites case, the TBB Boom and the Solar Panels are two portions that are deployed after satellite separation from the launch vehicle. The propellant fuel is also changed after orbit transfer. For the MOI computation, we assume the SAD is at 0^o position.

The CG is valid for any SAD position, and therefore applies to the ACS Nadir and Nadir-Yaw Modes. The MOI and CG for six spacecraft were re-computed based on the above propellant mass.

3.5 Conclusion

We have presented a new fundamental operation concept for the F3 spacecraft constellation deployment, orbit-raising results, operations challenges and lessons learned. With five satellites (FM5, FM2, FM6, FM4, and FM1) successfully reaching the 800-km mission orbits as of December 2007, the F3 mission has verified the "proof-of-concept" of a novel way of performing constellation deployment by taking the advantage of nodal precession. This novel approach has dramatically reduced the spacecraft propellant mass and the complexity of the spacecraft RCS and ACS subsystem design. The success of the constellation deployment of the F3 mission has also provided a powerful demonstration of RO scheme in particular and for the remote-sensing applications of micro-satellite constellations in general. All these technical principles have paved the way for the design of future GNSS RO remote-sensing systems

TABLE 3-1 F3 CONSTELLATION SPACECRAFT BUS KEY DESIGN

Mass	~ 54 kg (Dry Weight)
Power:	~ 81 Watts (bus and payload)
Shape	Disc-shape of 116cm diameter, 18cm in height
Science Data Storage	128 MB
Distributed Architecture	Motorola 68302 Microprocessor
Attitude Control	Magnetic 3-axis Control Pointing Control = 5° Roll & Yaw, 2 ° Pitch
Propulsion	Hydrazine Propulsion Subsystem
S-Band Communications	HDLC Command Uplink (32 kbps) CCSDS Telemetry Downlink (2 Mbps)
Single String Bus	Constellation Redundancy

TABLE 3-2 CONSTELLATION DEPLOYMENT STATUS WITH FIVE SATELLITES (FM5, F M2, FM6, FM4, AND FM1) AT FINAL ORBITS AS-OF-2 DEC, 2007

Items / SC No.	SMA (km)	Eccentricity	Inclination (deg)	RAAN (Ωi/5) (deg)	AOL (Li/5) (deg)
FM5	799.475	0.0046	71.973	0	0
FM2	799.449	0.0041	72.037	29.9	50.7
FM6	799.444	0.0051	71.982	62.0	104.4
FM4	799.471	0.0072	72.009	90.0	158.2
FM3*	711.047	0.0054	72.012	129.9	Time Variant
FM1	799.475	0.0046	71.973	145.9	262.53

*Note: On 3 Aug. 2007 the FM3 encountered solar array drive mechanism malfunction when reached 711 km orbit.

TABLE 3-3 SPACECRAFT THRUST-BURN PERFORMANCE STATISTICS

Items / SC No.	Total Burn Days (Days)	Total Burn Number (no.)	Planned Burn (Minutes)	Executed Burn (Minutes)	Successful Rate (%)	Total Fuel Used (kg)	Total Fuel Mass (kg)	Average SMA/burn (km/burn)	Average Duration/burn (sec/burn)
FM5	39	53	456	326.1	71.5	4.634	6.671	5.4	369.4
FM2	50	80	646.5	321.7	49.8	4.686	6.651	3.6	241
FM6	36	65	390	294.7	75.6	4.332	6.635	4.4	279.9
FM4	41	90	390.5	307.8	78.8	4.644	6.627	3.2	205.4
FM3	39	74	265.7	190.3	71.6	3.345	6.665	2.7	154.3
FM1	40	71	382.8	329.8	86.2	4.993	6.697	3.4	238.4

Table 3-4 Spacecraft Mass Property and Moment of Inertia for Six Satellites as-of-2 Dec, 2007

Items / SC No.	Total Mass (Full Tank) (kg)	Remaining SC Total Mass (kg)	Remaining Propellant +/- 0.1 kg (kg)	Center of Gravity (CG) (m)	Moment of Inertia (MOI) Assume SAD = 0 deg kg m^2		
FM1	61.097	56.104	1.704 (94 psi/ 13.2 ^oC)	x= 0.0035084 y=-0.0043757 z=-0.0334029	Ixx= 7.1677273 Iyx= 0.0288131 Izx=-0.0071984	Ixy= 0.0288131 Iyy=10.0887230 Izy=-0.4359628	Ixz=-0.0071984 Iyz=-0.4359628 Izz= 5.2806052
FM2	61.295	56.609	1.965 (100 psi/ 12.68 ^oC)	x=-0.0034182 y=-0.0041841 z=-0.0364667	Ixx= 6.9711402 Iyx= 0.0292363 Izx=-0.0096030	Ixy= 0.0292363 Iyy= 9.8405863 Izy=-0.4376625	Ixz=-0.0096030 Iyz=-0.4376625 Izz= 5.2101918
FM3	61.295	57.950	3.320 (129 psi/ 27.86 ^oC)	x= -0.0015454 y=-0.0070990 z=-0.0367495	Ixx= 7.0538797 Iyx= 0.3262446 Izx= 0.1441285	Ixy= 0.3262446 Iyy= 9.8458681 Izy= -0.2834290	Ixz= 0.1441285 Iyz= -0.2834290 Izz= 5.1711034
FM4	61.020	56.376	1.983 (105 psi / 29.10 ^oC)	x = -0.0037843 y = -0.0073189 z = -0.0371947	Ixx= 6.8193710 Iyx= 0.0317362 Izx= 0.0744942	Ixy= 0.0317362 Iyy= 9.7484668 Izy=-0.4389625	Ixz= 0.0744942 Iyz=-0.4389625 Izz= 4.8734748
FM5	61.167	56.533	2.037 (98 psi/ 13.68 ^oC)	x=-0.0036067 y=-0.0045262 z=-0.037113	Ixx= 6.9437632 Iyx= 0.0275360 Izx=-0.0087138	Ixy= 0.0275360 Iyy= 9.8007081 Izy=-0.4379625	Ixz=-0.0087138 Iyz=-0.4379625 Izz= 5.2086237
FM6	61.315	56.983	2.303 (106 psi/ 18.40 ^oC)	x = -0.0032281 y = -0.0044101 z = -0.0360353	Ixx= 6.9827399 Iyx= 0.0289346 Izx=-0.0115537	Ixy= 0.0289346 Iyy= 9.8596525 Izy=-0.4397625	Ixz=-0.0115537 Iyz=-0.4397625 Izz= 5.2408835

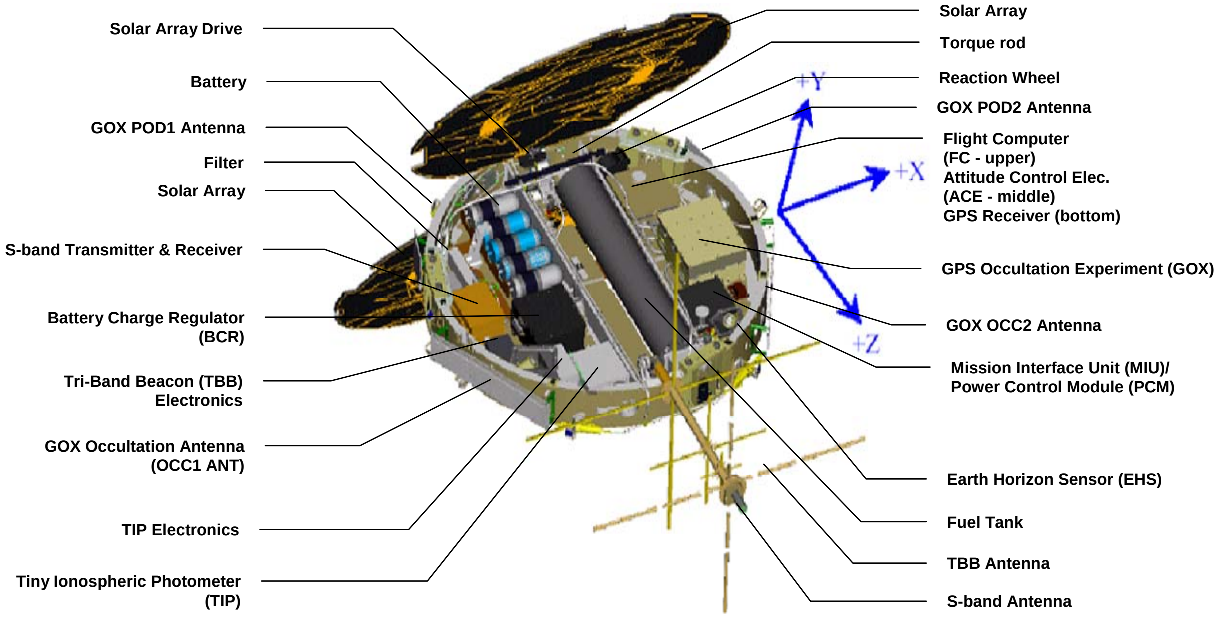

Figure 3-1. F3 spacecraft in deployed configuration and its major components.

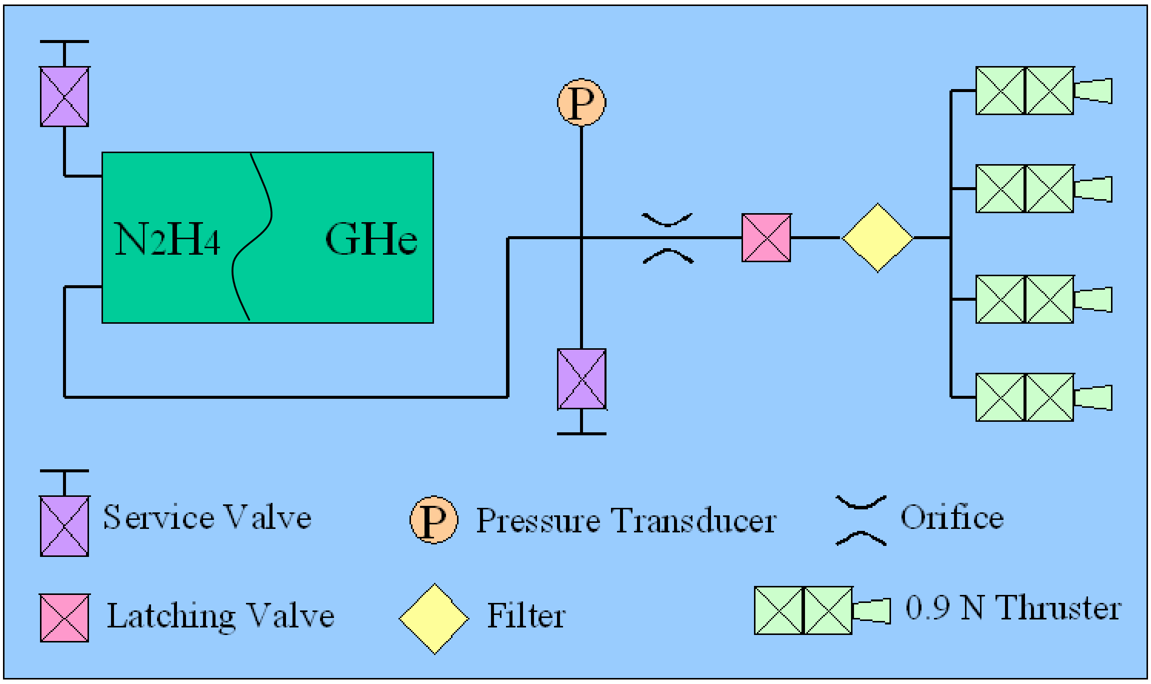

Figure 3-2. Spacecraft Reaction Control Subsystem block diagram.

Thruster Geometry

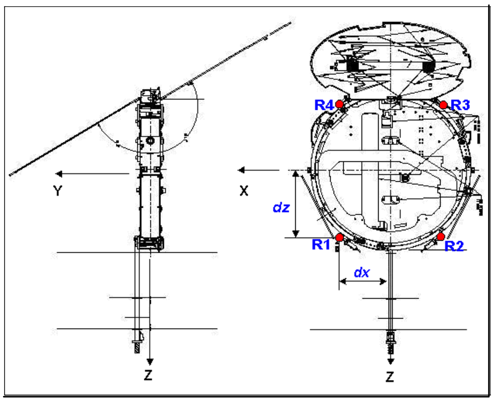

Cant (10°) Enables 3-Axis Control

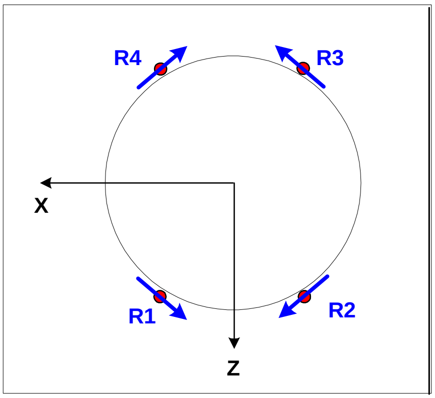

Torque Generation

Torque Direction	Thruster Combination
+X	R3 & R4
-X	R1 & R2
+Y	R2 & R4
-Y	R1 & R3
+Z	R1 & R4
-Z	R2 & R3

Flight Configuration

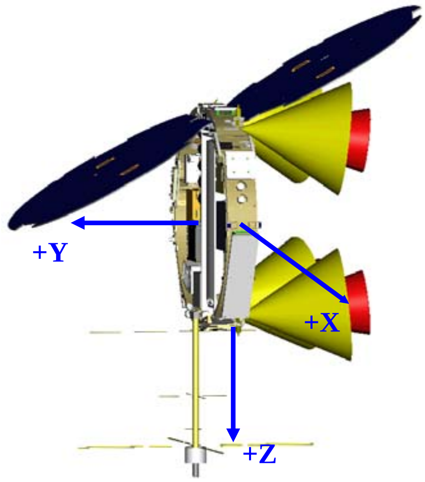

Thruster Data:

- **15 msec min. Turn-On time**
- **0.2 lbf (BOL), 5:1 Blowdown**

Figure 3-3. Reaction Control Subsystem thruster geometry and torque.

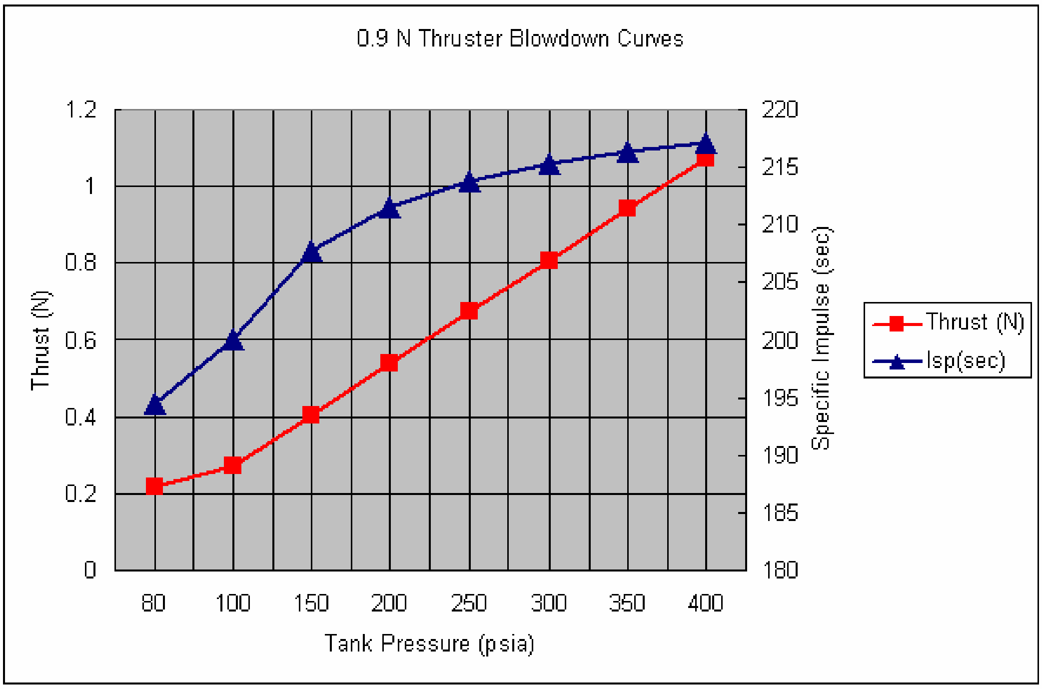

Figure 3-4. Reaction Control Subsystem blowdown curve.

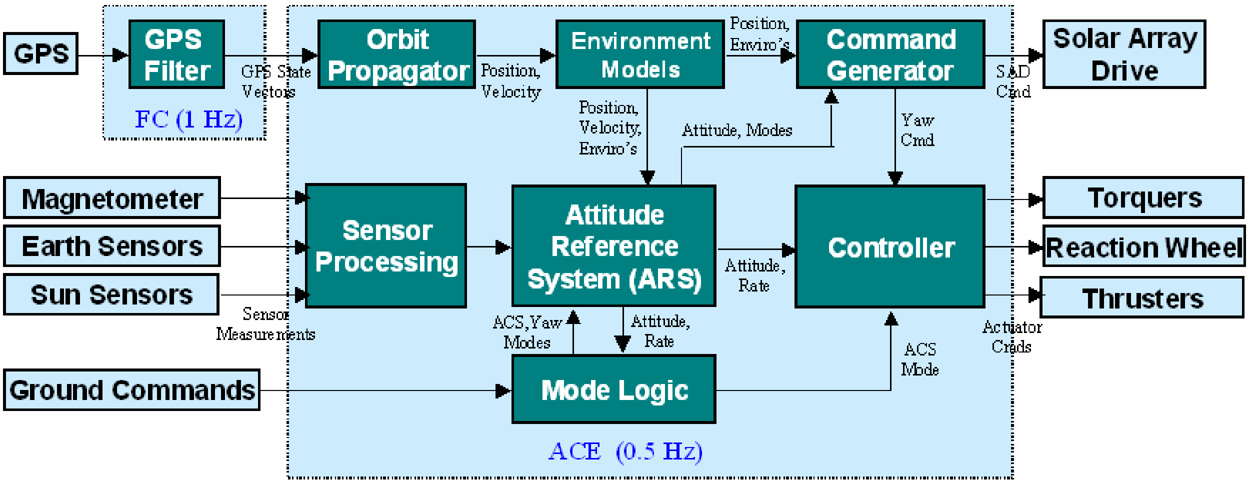

Figure 3-5. Functional block diagram of the spacecraft attitude control subsystem.

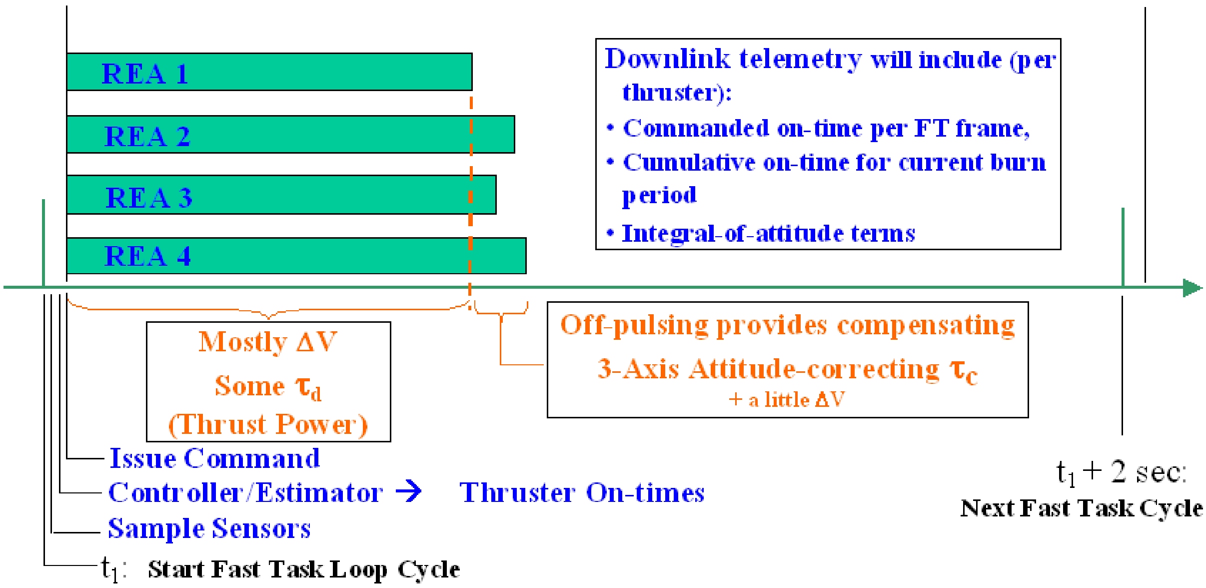

Figure 3-6. Off-pulsing concept of ACS thrust mode.

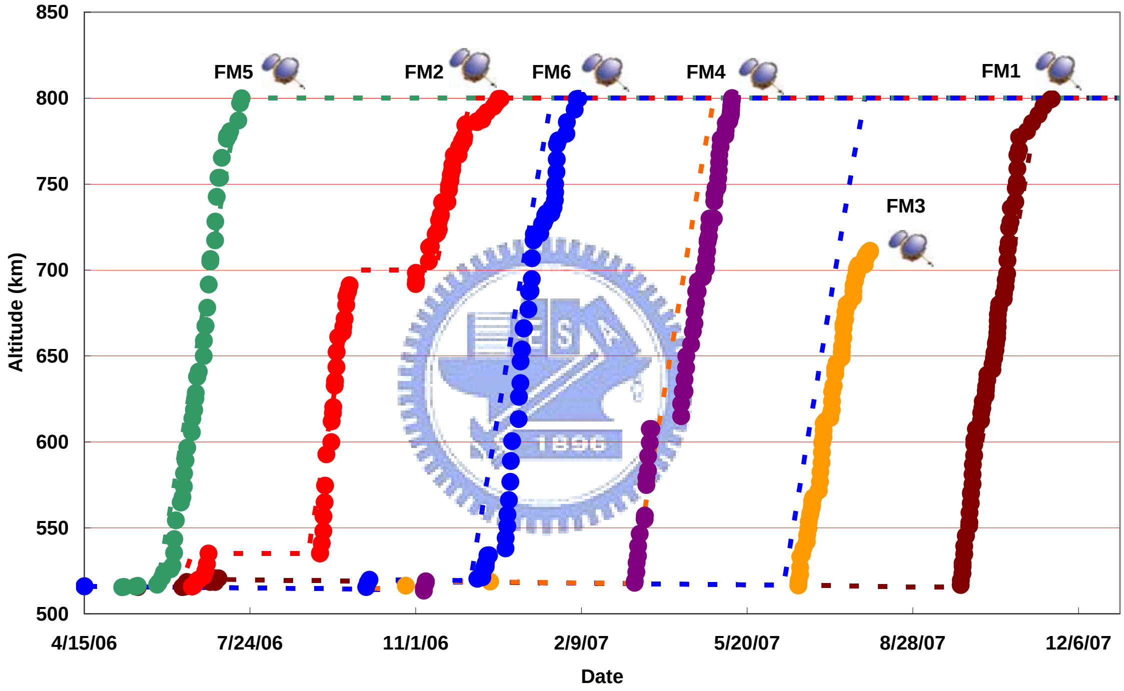

Figure 3-7. F3 as-is burn history and deployment timeline.

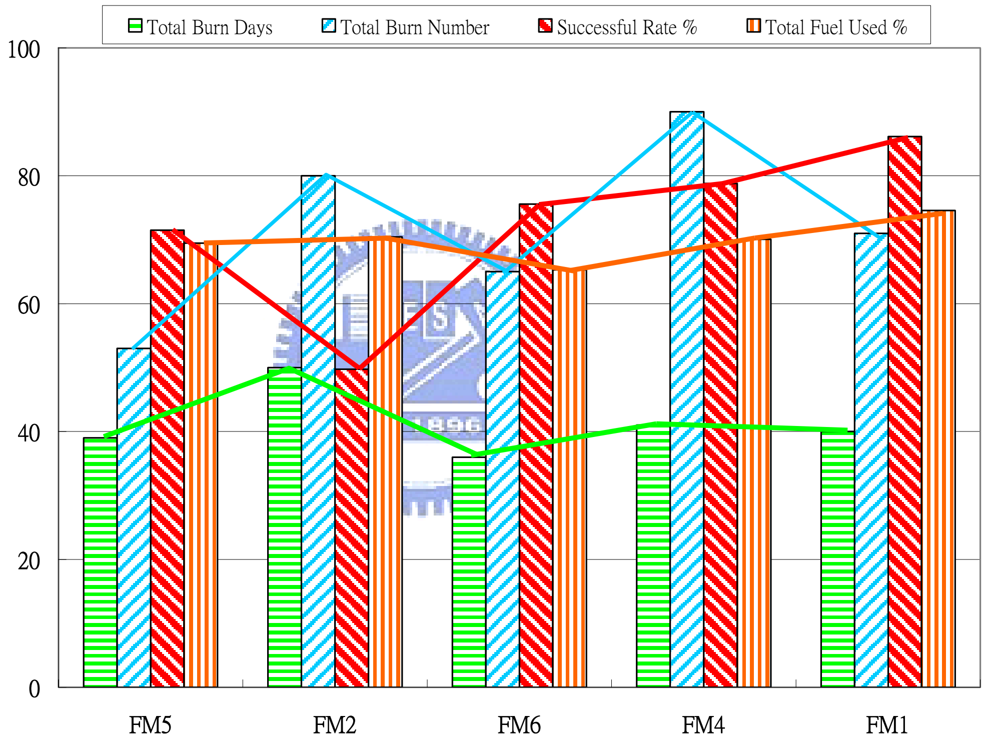

Figure 3-7. Spacecraft thrust-burn performance statistics.

Chapter 4 Challenges of Constellation Mission Operations and

4.1 Introduction

The F3 constellation mission operations are divided into four phases: phase I is the Launch and Early Orbit (L&EO) phase; phase II is the constellation deployment phase; phase III is the final constellation phase; and phase IV is the extended mission phase. The phase I includes launch, separation, ground initial acquisition, spacecraft bus checkout, and payload checkout. During phase II the spacecraft are raised to the final mission orbit heights by means of nodal precession. The science mission is already started during phase II when there is no thrust-burn. All spacecraft should reach their final orbits with the designed RAAN and AOL at phase III, and all science experiments are conducted continuously when there is no burn activity. After the completion of Phase III, it is the commencement of phase IV for a duration of three years [61].

4.2 Constellation Mission Operation

4.2.1 Launch and Orbit Injection

After successful launch the F3 constellation has the following orbit characteristics [57], [61]:

- SMA: 6893 km;
- Eccentricity (E): 0.00323;
- Inclination (I): 71.992^{o};
- Right Ascension Ascending Node (RAAN, Ω): 301.158^{o}.

The six identical satellites are deployed into six mission orbits with the following orbit characteristics for i=1~6:

- SMAi: 7178 km;
- Eccentricity (Ei): < 0.014;
- Inclination (Ii): 71.992°;
- RAAN (Ωi): Ω5, (Ω5 - 30°), (Ω5 - 60°), (Ω5 - 90°), (Ω5 - 120°), (Ω5 - 150°) ±5°;
- (AOL, L_i): L_5, (L_5 - 52.5°), (L_5 - 105°), (L_5 - 157.5°), (L_5 - 210°), (L_5 - 262.5°) ± 8°

4.2.2 Collision Avoidance

The separations of F3 spacecraft from the final stage of the launch vehicle relied on the separation mechanism built into the structure of each spacecraft. All the six satellites were injected heading along the velocity direction. The separation of each spacecraft from the spacecraft stack and the final stage of the launch vehicle obey the conservation laws of momentum and energy. As a result of calculation, the velocity after separation should be $V_{FM1} > V_{FM2} > V_{FM3} > V_{FM4} > V_{FM5} > V_{FM6}$ [57], [61].

We conclude that the spacecraft will not collide with each other because the velocity of spacecraft N is always faster than the velocity of spacecraft N+1. When taking into account the variance and the accuracy of measurement, there may be approximately 12.5% variance in the energy of the spring in F3's case. To avoid collisions, the compressions of the sets of springs for each spacecraft are different: $x_{FM1} > x_{FM2} > x_{FM3} > x_{FM4} > x_{FM5} > x_{FM6}$. The resulting separation simulation results are illustrated in Figure 4-2. The separation intervals are set at 60 seconds. The higher dashed line represents +12.5% of specified spring energy, and the lower dashed line represents -12.5%. In Figure 4-2 Distance = 0 represents an imaginary object which is the non-separated final stage and spacecraft suite. And the different slopes correspond to different velocities. If the lines do not intersect each other, no collision is expected to happen.

4.2.3 Separation Sequence

Ten days before launch, NSPO was informed that there is unexpected residual thrust in the final stage of the launch vehicle as the first separation is triggered. Additional simulation analyses were performed and the results indicated that the relative positions with respect to the six satellites and final stage are adequate to avoid collision. However, the effect of residual thrust did result in changes to the spacecraft sequence. The expected spacecraft sequence should be FM6->FM5->FM4->FM3->FM2->FM1 based on the designed installation of a separation spring without the 4^{th} stage residual thrust. The satellite cluster sequence with the anticipated 4^{th} stage residual thrust after launch became FM6->FM1->FM5->FM4->FM3->FM2. FM1 has lagged behind as expected in the cluster sequence since it has the least effect due to the 4^{th} stage residual thrust. This sequence change has no practical impact on flight operations or mission operations [57], [61].

4.2.4 Beacon Mode Exit

Each of the satellites flew in a cluster after launch and all beacon modes of the satellites worked well for the first and second orbit. However, problems were encountered when not receiving telemetry from spacecraft at the third and the fourth orbit after launch. The exit-beacon-mode-flag uplink command was sent to all six satellites and verified the downlink signals of all satellites at the fifth orbit. It was later determined that the reason for the erroneous telemetry reception on orbits three and four was that the onboard bus GPSRs aboard FM3, FM4, and FM6 were unable to lock onto the GPS signals for proper time synchronization for the beacon mode [32].

4.2.5 Spacecraft and Payload Checkout

The spacecraft checkout starts when the satellite exits the beacon mode after the initial spacecraft acquisition. The flight software configurations were checked and confirmed as normal on all six satellites, initially, and later the navigation anomalies that were attributed to the erroneous GPSR behaviors appeared at Launch plus three (L+3) days. It was not possible to isolate the root cause of these erroneous GPS behaviors. However, an alternative resolution of feeding the known state vector to each spacecraft via uplink commands regularly was able to stop the GPS-related navigation anomalies. All six satellites were ready to be powered on the payload at L+6 days. The GOX payload of each spacecraft was powered on first at L+6 days, the TIP payload on at L+8 days, and TBB payload on at L+13 days respectively, according to the operation in-orbit checkout plan [32].

4.2.6 Constellation Deployment

During the L&EO phase the satellites were separated one by one into the same injection orbit with the same RAAN and RAAN drift rate. The strategy to differentiate the RAANs among the six orbits is to maneuver the six satellites into the mission orbit altitude of 800 km at different "maneuvering windows" (typically 45 days) in the year in order to get into the designated separate orbital planes through nodal precession. All satellites will reach their final orbits with each designed RAAN and AOL at this phase [32], [57].

4.2.7 Final Constellation and Extended Mission

The final constellation of F3 has six orbit planes as shown in Figure 4-3. Each orbit is at an altitude of 800 km with an inclination angle of 72^{o}. The separation angle among orbit planes is 30^{o} and the AOL separation between satellites in adjacent orbit planes is of 52.5^{o}. The final constellation allows the six satellites to collect 1,800 to 2,200 atmospheric sounding data on an average per day worldwide.

4.3 Constellation Operations Challenges

4.3.1 Spacecraft Bus GPS Receiver Non-Fixed Issue

The spacecraft bus GPSR of FM1, FM3, FM4, and FM6 could not reliably acquire and lock onto the signals from the GPS constellation, as shown in Figure 4-4 and 4-5. The bus GPSR sometimes provides erroneous data, causing problems in the TIP payload time stamping, ACS navigation processing, and the onboard timing system. These data problems cause the navigation to output erroneous data and result in erratic attitude excursions behaviors on the spacecraft. The issue has been resolved by inhibiting any state vector solution from the bus GPSR and then commanding four known state vectors daily to each corresponding spacecraft from SOCC. The state vector is obtained from the GOX payload. FM5 and FM2 were chosen as the first two spacecraft to be raised from their parking orbit, since their bus GPSRs were behaving nominally. This allowed the team to perform orbit determination using the data from the spacecraft bus GPSR. As for the other four spacecraft (FM1, FM3, FM4 and FM6), NSPO has modified the thrusting procedure to include GOX operations as part of burn activities [31]-[32], [61].

4.3.2 High Beta Angle Effect

There were thermal anomalies related to orbital high beta angles. At high beta angles, the spacecraft were in constant sunlight. This causes the earth horizon sensor (EHS) temperature to become higher than expected. Additionally the battery pressures rose higher and closer to the specified limit during this time period. To solve this issue, TIP and TBB were turned off when the beta angle was higher than 60^{o}. To resolve the battery pressure issue, the charge rate was fine-tuned to maintain the battery within the normal pressure limit through frequent monitoring and commanding. The power control flight software was subsequently modified to include a new battery overpressure protection function and this was successfully uploaded early in 2007. Currently the battery pressure is being maintained at nominal condition autonomously [31]-[32], [61].

4.3.3 Spacecraft Computers Reset/Reboot

A total of 87 out of 102 recorded spacecraft resets and reboots events including Flight Computer (FC), Battery Charge Regulator (BCR) and Attitude Control Electronics (ACE) have been observed after two years in orbit since launch. Figure 4-6 shows the projected geographic locations of these reset/reboot events on the Earth after two years in orbit.. .

Further investigation shows that most of the time and geo-locations the spacecraft anomalies occurred are closely correlated to the space radiation environment. Single Event Effects in the South Atlantic Anomaly (SAA) region and the polar region are identified as the most probable root cause. The spacecraft will recovers from system level Failure Detection & Correction (FDC) strategies after resets and reboots events occurred, and no spacecraft performance has been degraded by these anomalies [31]-[32], [61].

4.3.4 Spacecraft FM2 Power Shortage

As shown in Figure 4-7, generally the average solar power falls into 140~150W with a 200W solar array power capacity in design. Actual flight experience shows that battery capacity is greater than specified value in typical normal operation. The maximum battery capacity or SOC can be as high as 15Ah after being charged. The peak power-tracking scheme can maintain the solar array at its maximum power output, but it is restricted by maximum battery charge current as well. On March 1, 2007 the operations team observed that the maximum power capacity of the solar arrays had been reduced from 200 W to 100 W by about 50%. FM2 had experienced a sudden solar array power shortage. The effect was deemed to be mechanical and resulted in a permanent power failure from one solar array. An investigation of this power shortage anomaly resulted in a recovery plan to operate the GOX at a reduced-duty cycle. Currently FM2 is supporting the GOX at ~70% duty cycles with the secondary payloads remaining off at all times [31]-[32], [61].

4.3.5 Spacecraft FM3 Solar Array Lockout

On August 3, 2007 FM3 encountered the solar array drive mechanism malfunction when it reached a 711 km orbit. The stuck solar array effects were two-folded, one was to block the thrusting to continue to 800 km mission orbit, and the other one was the lost sun tracking capability of solar array for the spacecraft. Currently FM3 is able to operate the GOX at a ~50% duty cycle with TBB and TIP payloads turned off at all times. The reasons for this anomaly are still under investigation [32], [61].

4.3.6 Spacecraft FM6 67-Days Outage

Spacecraft flight model number 6 (FM6) lost its communication on 8 Sep. 2007 [65]. There was no warning that indicated a spacecraft problem prior to the FM6 outage event. Many emergency recovery attempts were tried by the operations team, without success. However, after 67 days the FM6 resumed contact and recovered back on its own after a computer master reset event occurred over the SAA region. The FM6 transmitter's RF spectrum looked normal with no sign of degradation and all the spacecraft subsystems were found to be in good health status. The FM6 started to provide data again on next day. After analysis two possible root causes were identified: (1) an intermittent hardware failure of the Field Programmable Gate Array (FPGA) inside the Mission Interface Unit (MIU), or (2) an intermittent short circuitry of the Pin Grid Array (PGA) matrix related to thermal effects. Science data from FM6 are looking good and are provided to users from CDAAC/TACC [36], [65].

4.4 Payload Operation Challenges

4.4.1 Payload Power On/Off Statistics

The payload powered-off statistics shown in Figure 4-8 were analyzed from Day 2006-175 to Day 2007-105. Before Day 2006-175, the 8^o off angle in earth sensors haven't been fixed and the GOX has not been ON for continuous 24 hour. We also excluded the action events done by the operations team such as flight software and common spacecraft database upload, and some processors reset by the team, etc. The events for payload off reduce the science data volume. The goal of the statistics is to realize the causes of payload off. During the one year operation, the causes of payload off are categorized to: (i) processor reboot, (ii) entrance to stabilized/safehold mode, (iii) stabilized mode after thrust burns, (iv) nadir mode after thrust burns so that spacecraft entering into power contingency, (v) power contingency due to staying nadir mode too long, (vi) dMdC (Derivative of Battery Molecular to Charge) anomaly, (vii) FM2 power shortage, and (viii) Power Control Module (PCM) DC off anomaly [31]-[32], [61].

4.4.2 GOX Payload Reboot Loop

Two kinds of reboot loop anomaly events were observed, one is the GOX instrument will automatically reboot itself when there is no navigation solution for 15 minutes. This happened on FM1 and FM6 in the past. The other kind of reboot anomaly is that consecutive reboots occurred every 15 minutes. When GOX has this kind of anomaly, GOX instrument still could be automatically recovered by power cycle command. FM6 had the later kind of reboot anomaly occurred in February and April of 2007 recently, however, FM6 didn't recover by itself. The root cause was preliminary identified as low signal-to-noise ratio (SNR) of the navigation antenna when the spacecraft was entered into beta angle between 0 and -30^{o}. A new firmware (FB 4.4) was loaded in June to enable to selection of the other healthy antenna as the navigation antenna. The reboot loop stopped since then. [31]-[32], [61]

4.4.3 Solid State Recorder (SSR) Data Overflow

The SSR data storage only allocated 32 Mbytes (MB) for GOX-B out of 128 MB total memory. During the constellation deployment phase it was always possible to accumulate GOX data more than 32 MB before dumping the data to the ground. When the data overflow took place, it always came along with the data wrapping (disorder) because the 32 MB was not an integer numbers of the science data packet size, and the write pointer of the SSR would pass over the read pointer when data overflow occurred. To resolve this issue, the operations team narrowed the GOX field of view to control the data volume. When the spacecraft orbit planes separated and the availability of ground pass became better, the team opened up the GOX's field of view and scheduled the dump to prevent the occurrence of SSR data overflow. The auto-scheduling tool was generated to optimize the ground station utilization so as to minimize data dumped. After all spacecraft reach the final constellation with the orbit phasing under control, the loss of data due to SSR overflow no longer occurred [32], [61].

4.4.4 Maximizing Science Data Downloads

A total of 84 data dumps per day can be realized when all six spacecraft reach the final mission constellation. In the early phase of the mission, only a total of 12 data dumps (2 per each spacecraft) in a day could be executed, primarily due to the cluster formation during the constellation deployment phase. The GOX firmware was upgraded to improve the quality and the quantity of the science data as the satellite constellation configuration (such as altitudes, field of views, etc.) changed. In parallel, optimization efforts were implemented to the spacecraft operations processes, the ground software, the ground control auto scripts, and the spacecraft flying formation, etc. to maximize the number of science data dumps per day. Currently there are around 66 dumps on average per day, a dramatic increase from the 12 dumps a day as originally planned [32], [61].

4.4.5 GOX Data Gapping Issue

The GOX data gapping problem is that 29% of RO science data has gapping issues. After investigating questionable raw data, we found that a similar data dropout pattern has been observed in the ground End-To-End (ETE) tests. However, the on-orbit gapping issue is much worse than that found in the ETE tests. Through several analysis and tests, it was concluded that when dumping the stored spacecraft data and science data simultaneously the data dropouts are the worst. The operations team made these two data dumps separately to recover the data dropout issue, and rescued 70% of the lost data. Even when the science data is downloaded alone, the data dropouts still cause 8% of data gapping. A typical dump has a very small amount of data dropouts (~0.04%), but it actually causes 8% of RO data gapping.

The remedy for reducing data gapping is to dump the same science data twice. Eventually, these two dumps will not drop the same data packets, so we can make up any dropout. The saved data from double dumps is only about 0.04% of the whole data volume, but the RO data will increase 8%. Hence, even though double dumps increase local data storage and double the data transfer time from ground station to the data analysis center, they are still worthwhile [32], [61].

4.5 Constellation Deployment Challenges

4.5.1 Thrust Burn Failures and Challenges

NSPO experienced numerous thrust-burn failures during spacecraft constellation deployment of FM5 [44]. By analyzing the spacecraft back-orbit data and using the animation result of the dynamic EDU (Engineering Development Unit) simulator with real telemetry data, we observed and summarized that the thrust-burn failure was attributed to the incorrect thrust-burn modeling, the incorrect spacecraft mass properties data and the incorrect moment of inertia data. The thrust gain factor in the spacecraft model is designed to be adjustable by the spacecraft ground command. By adjusting the thrust PID gain "factor" for roll and yaw, the reduction factor for the thrust torque (R x F), and the ACS common spacecraft database (CSD) parameters, the thrust-burn activity was continued and performed successfully. The major impact of the thrust-burn failure is that the operations team could not perform the full burn (turn ON thruster 0.8 seconds in 2-second control cycle) by routine process as planned. This caused a significant schedule slip in the first orbit-transfer activities for FM5 [32], [58].

4.5.2 Spacecraft Attitude Excursion Challenges

Another lesson learned from the follow-on FM2 and FM6 thrust-burn activities comes from the spacecraft attitude excursion challenge. From the thrust-burn history statistics it was observed that the orbit-transfer activities were performed very successfully with a 100%

success rate when the thrust-burn activity was planned during the spacecraft eclipse time period. But it was also observed that the orbit-transfer activities were performed unsuccessfully with around a 50% success rate when thrust-burn activity was planned during the spacecraft daytime period. The source of this attitude excursion problem for daytime thrust-burn activity is the fact that the sensor-processing algorithm used for the spacecraft ARS to perform attitude control will sometimes generate incorrect sun vector solutions depending upon numbers of Cosine Sun Sensors (CSSs). As soon as the algorithm generates an unreliable sun vector output solution to the ARS, the ARS and the ACS will immediately generate a large attitude transient incident when responding to the error [32], [58].

4.5.3 Automation of Ground Operations Procedure

It usually takes two station contacts for a thrust-burn: one contact to upload the burn commands and the other to check out the burn results. This constrains the thrust operation to two burns per day. To increase the number of burns per day, the operation team developed a Satellite Test and Operations Language (STOL) procedure to generate the burn command sequence. After checking out the burn results during a station contact, the STOL procedure could extract the post-burn data of tank pressure, thrust power and control integral terms from the telemetry. The tank pressure was used to calculate the thrust force level. The thrust power and integral terms were used as the initial conditions of the next thrusting. With these data from the telemetry, the STOL procedure could generate and upload the time-tag commands for the next burn during the same station contact. The STOL procedure increased the operation efficiency to one burn per orbit. Three burns or more (seven burns were achieved at once) are planned per day to increase the operation flexibility and efficiency [32], [58].

4.5.4 Remote Tracking Station (RTS) Ground Support Limitation

The operations team needs to observe the results of the thrust-burn from the real-time telemetry and then estimate the corresponding two line elements as the inputs to ground antenna pointing. During UTC time 00:00:00~06:00:00, Kiruna RTS is not staffed so that they can not support the update of the NORAD (North American Aerospace Defense Command) two-line elements. This constraint impacted the thrusting operations to be conducted after UTC 06:00:00 if the post-burn contact station is Kiruna [32], [58].

4.6 Conclusion

We have summarized the satellite constellation system performance after one year in orbit. All six spacecraft are in good condition after six satellite years of operation, and were on their way toward the final constellation. With the development and application of the open loop tracking technique by JPL and UCAR, the quality, accuracy and lowest penetration altitude of the RO sounding profiles have been improved in comparison to previous RO missions. As of April 15, 2007 about 1800 high-quality soundings were being retrieved daily on a global basis. The constellation spacecraft system on-orbit performance will be constantly monitored, tracked, evaluated and enhanced by NSPO's operations team in the future. It is anticipated that an increasing number of global operational centers will use F3 data operationally for the years to come.

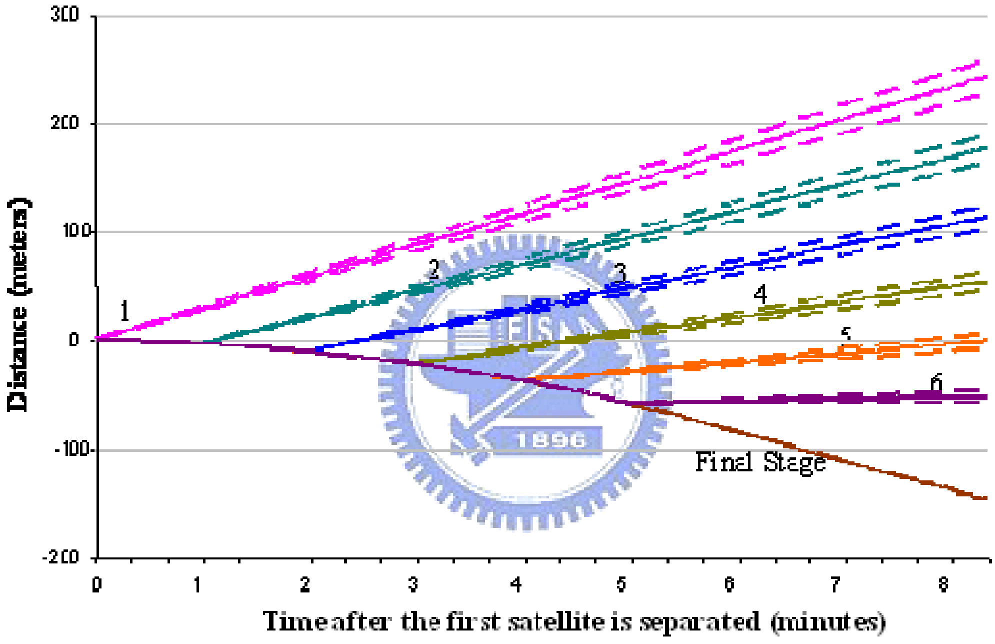

Figure 4-2. Six spacecraft separation simulation result.

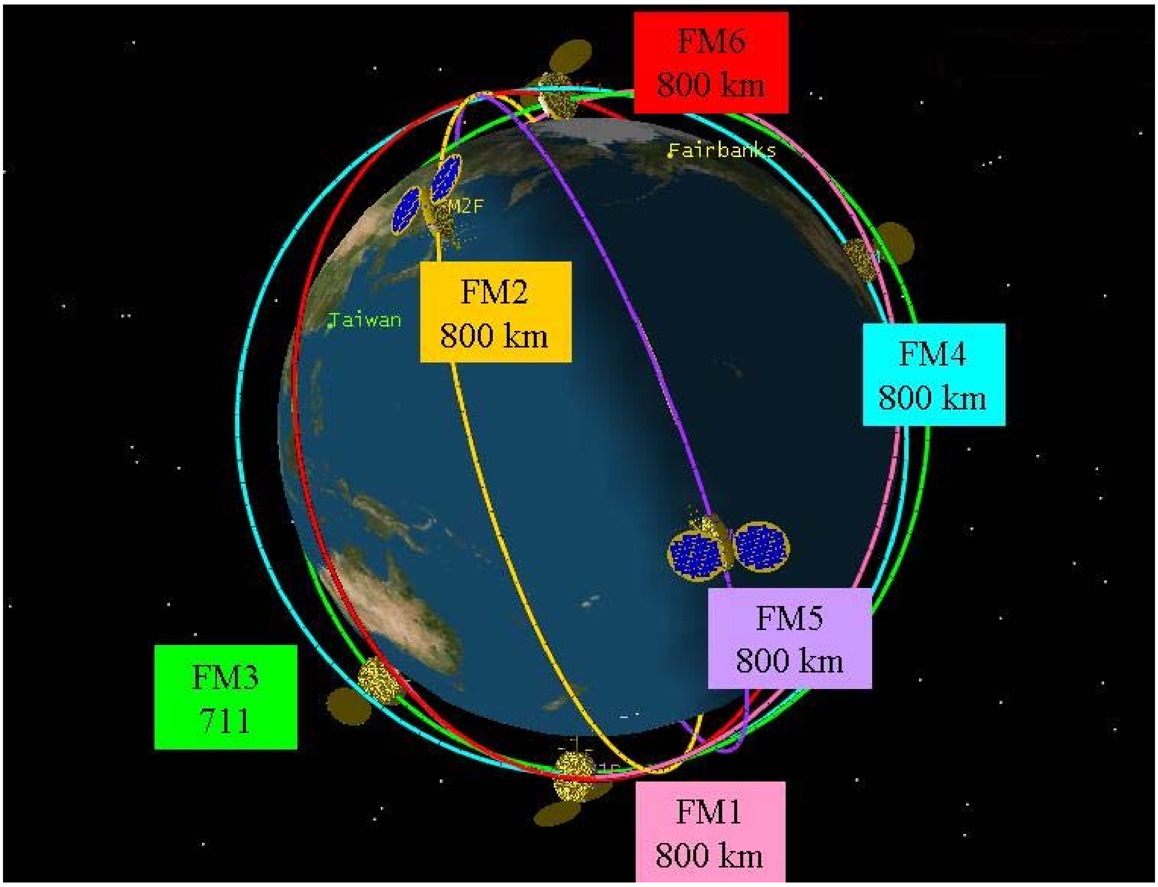

Figure 4-3. F3 final constellation.

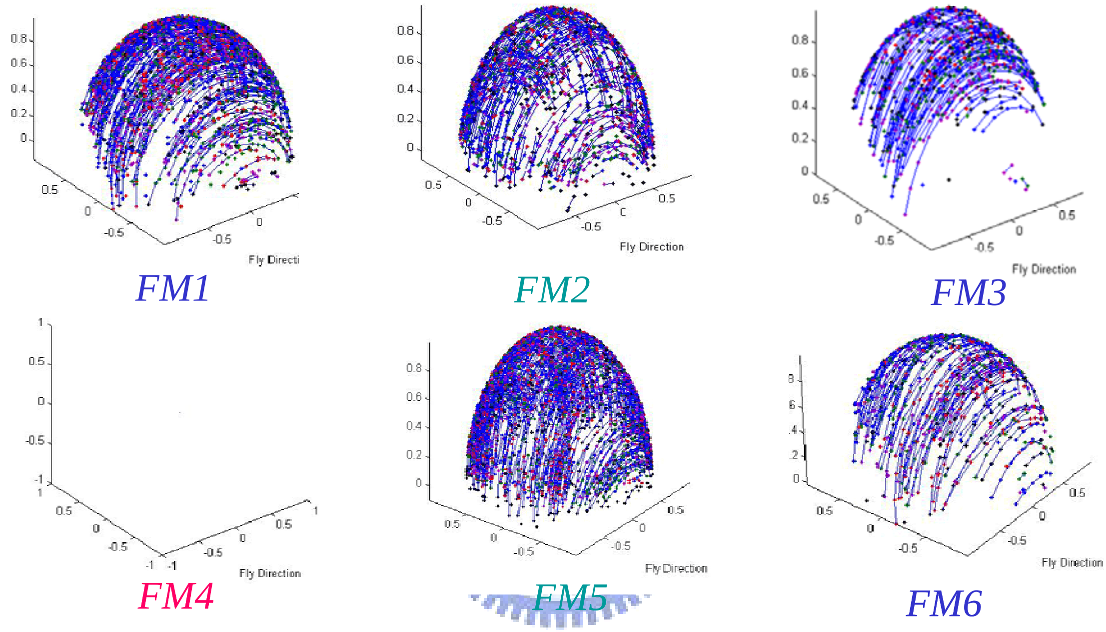

Figure 4-4. GPS three-dimensional (3D) tracking coverage of all six spacecraft Bus GPSR

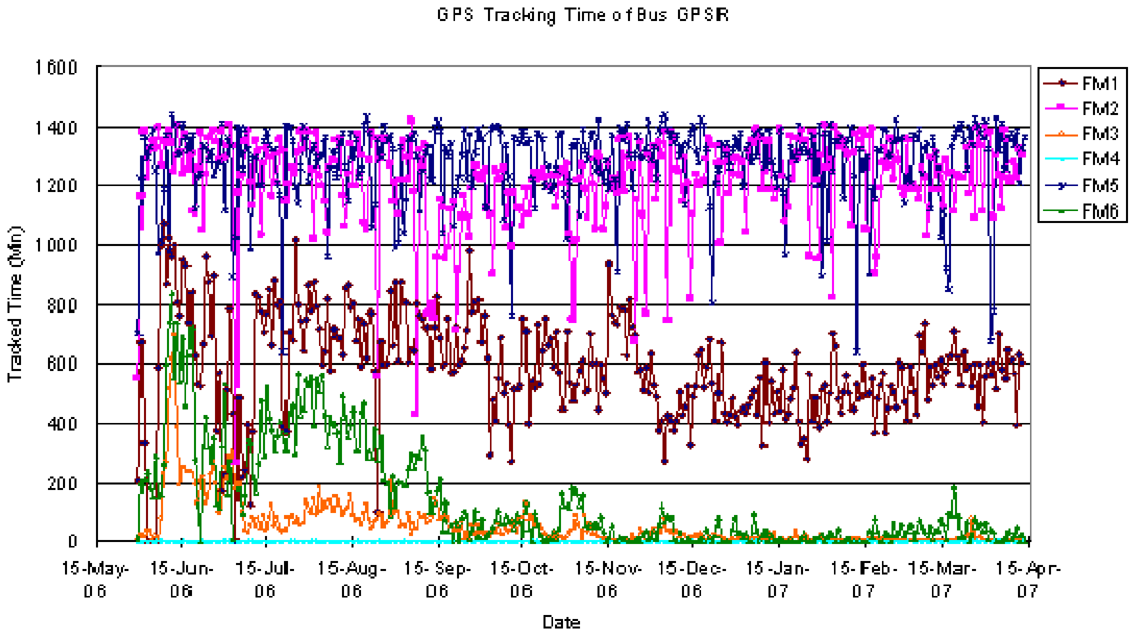

Figure 4-5. Number of GPS satellite vehicle tracked statistics for all six spacecraft bus GPSRs of one-year data after launch.

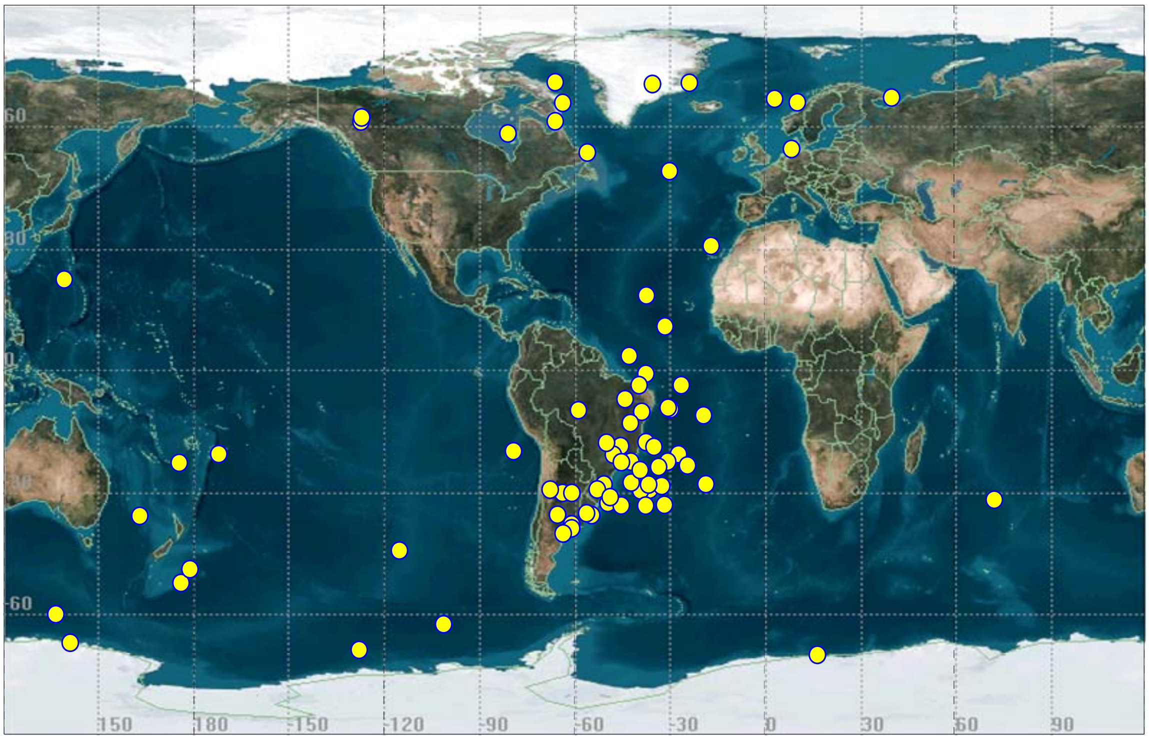

Figure 4-6. Geographic location of the spacecraft resets/reboots events two years since launch.

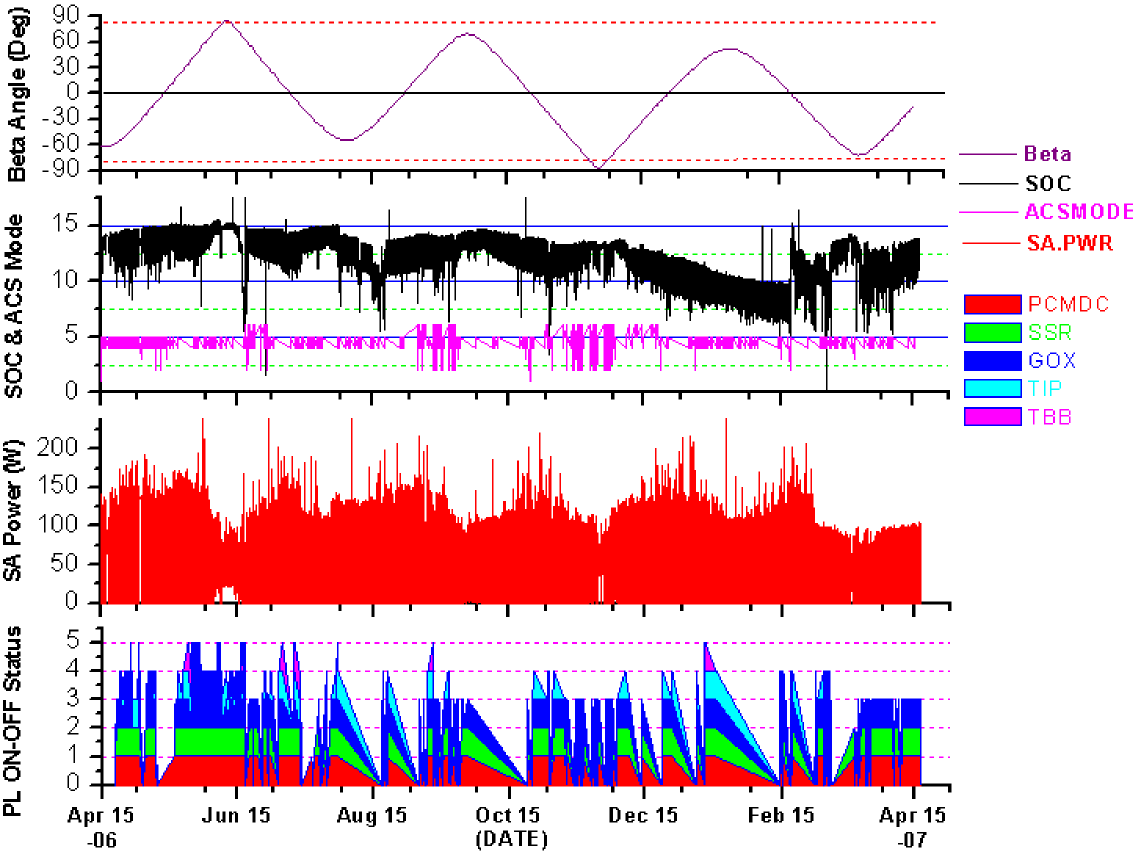

Figure 4-7. One-Year Trend of Solar Power and Battery SOC, ACS Mode, and Payload On-Off Status on Spacecraft FM2.

	FM1	FM2	FM3	FM4	FM5	FM6	Total	Percentage
Nadir	21	1	10	13	6	6	57	35.6 %
Burn to Stabilized		23	1	1	4	11	40	25.0 %
Processor Reboot	3	11		1	7	6	28	17.5 %
Stabilized/Safehold	4	3	3	1		1	12	7.5 %
Power Shortage		9					9	5.6 %
dMdC		3	1		1	1	6	3.8 %
Burn to Nadir				1	1	2	4	2.5 %
PCM DC Off		4					4	2.5 %

(Unit is number of event)

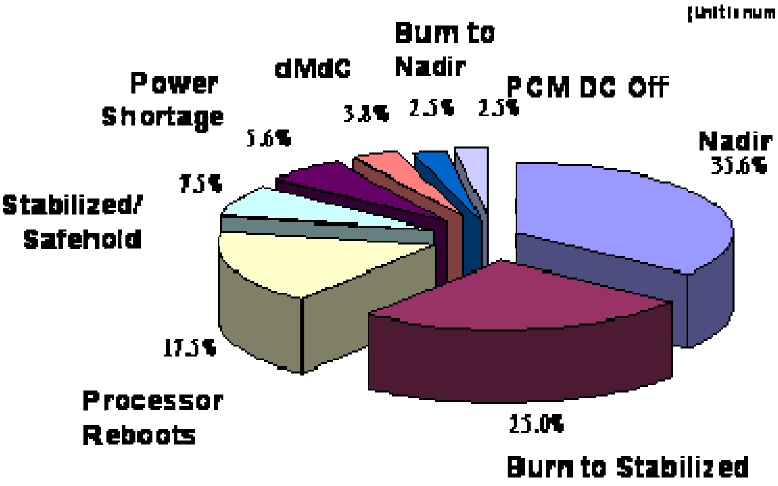

Figure 4-8. Payload (GOX/TBB/TIP) power-on/off Statistics.

Chapter 5 Constellation Spacecraft System Performance

5.1 Introduction

The F3 spacecraft subsystems and the state of spacecraft health are summarized in this Chapter Unlike a single spacecraft mission, the F3 satellite constellation provides a unique opportunity to assess the performance of multiple spacecraft at the same time [32], [61]. The Chapter begins with spacecraft bus performance summary (in Section 5.2) and followed by spacecraft subsystem on-orbit performance (in Section 5.3). In Section 5.4 we will show the GOX payload science performance results, and followed by the conclusion (in Section 5.5).

5.2 Constellation Spacecraft System Performance Summary

Table 5-1 shows the constellation spacecraft performance summary after two years in orbit. And Table 5-2 shows the operational status of each subsystem in all six spacecraft after two years in orbit. All six F3 satellites except spacecraft flight model number 2 and 3 (FM2 & FM3) are currently in a satisfactory state-of-health at 700~800-km final orbit. FM2 has a power shortage issue with only one working solar panel and FM3 currently remains at an orbit of 711 km due to a stuck solar array drive. Five out of six satellites have reached their final mission orbit of 800 km since the end of November 2007. The FM2, FM3 power shortage issue is presented in Section 4.3.4 and 4.3.5, respectively. The FM6 lost its ground communication issue is presented in Section 4.3.6. As for the primary payload, four GOX are operated at a duty cycle of 100% and two other GOX (FM2 and FM3) are operated based on sun beta angle due to power shortage and stuck solar array drive..

5.3 Spacecraft Subsystem On-Orbit Performance Summary

The spacecraft subsystem performance and its major functions are shown in Table 5-3. All the radio frequency (RF) uplink and downlink trend data show that the spacecraft meet the specified RF subsystem requirements. Suspected space weather disturbances, which are correlated to the spacecraft onboard computer reboot and spacecraft reset events, had no performance impact on the C&DH subsystem and spacecraft system. The FSW status of all six satellites is normal and the spacecraft are recovered automatically as expected by design from abnormal reboot/reset conditions. Under normal FSW conditions, the error count is less than 10 per day. The thermal control subsystem is behaving nominally across the range of solar beta angles. There was an issue concerning excessive Earth Horizon Sensor (EHS) temperature increases at high beta angles, which has been resolved by an operations solution of turning off the secondary payloads during these periods [32], [61].

The principal contributors to the ACS pointing error are the orbital position, solar beta angle effect, hardware, and hardware configuration. The spacecraft's magnetically controlled ACS performed correct mode transition as designed, and all six spacecraft performed their on-orbit ACS functions as expected. However, ACS experienced excursions from the required $\pm 5^{\circ}$ pointing accuracy in roll, pitch and yaw, which sometimes has an impact on GOX sciences data. Figure 5-1 shows all the six spacecraft attitudes on-orbit performance with respect to the sun beta angle for two years in orbit data since launch. FM5 is the first spacecraft for orbit transfer on May 7 (Day 127), 2006 and arrived at mission orbit on July 19 (Day 200), 2006. From the spacecraft trend data, we observed no major pointing performance improvement when FM5 arrived at its mission orbit. This seems to be the same for the other five satellites. As for pointing knowledge performance, all six spacecraft meet the requirements of both roll and pitch axes. Each spacecraft is equipped with two Earth horizon sensors to provide roll and pitch attitude information. The Earth horizon sensor is relatively precise compared to coarse sun sensor and Magnetometer, and can provide attitude information to meet the pointing knowledge requirement. While the attitude information for the yaw axis relies on the coarse attitude sensors, it is difficult to meet the pointing knowledge requirement when attitude excursion occurs [31]-[32], [61].

The spacecraft bus GPSR is designed to be the main source of ACS navigation information. However, for six spacecraft, some of the GPSRs rarely work well. For the spacecraft with poorly performed GPSR, the navigation information is externally fed by daily uploaded Position/Velocity/Time (PVT) information from the ground, such that the ACS FSW could propagate the correct PVT and perform the navigation function. As shown in Figure 4-4, the GPS 3D on-orbit tracking coverage of all six spacecraft bus GPSR was reconstructed on the ground around October and November 2006, for two to three days of tracking data depending on the number of GPS satellite vehicle tracked status. Figure 4-5 shows the duration of the tracked GPS satellite statistics for all six spacecraft bus GPSRs for one year. It is shown that FM2 and FM5 are fully functional, and any degradation is not shown, unlike FM1, FM3, and FM6, which are only partially functional and have suffered performance degradation since launch. FM4's GPSR has tracked almost no GPS signals from the beginning [32], [61].

The RCS is designed for providing the required thrust to transfer the satellites from their parking orbits to the higher-altitude mission orbits. The plots in Figure 5-2 illustrate the trend of tank pressure and tank temperature for FM2, FM4, FM5, and FM6. When the satellite orbit is in high beta angle situations, direct solar heating will cause a higher temperature level in the satellite and it also influences the tank temperatures and pressures. During the delta-V burns periods, the tank pressure decreases from 320 psi to around 100 psi.

There is a 40% power margin on average for each spacecraft observed, based on the one-year trend data. There is also no sensible degradation in the power system on any of the satellites except FM2 and FM3, which is suffering from an additional 20% power shortage when the 40% original margin is taken into account. It is observed that the FM2 maximum power capacity of the solar arrays had been reduced by about 50% starting on March 1, 2007. In Figure 4-7 we show the one-year trend of solar power and battery state of charge (SOC), ACS mode, and payload on-off status for FM2. As for FM3, currently FM3 is able to operate the GOX at a ~50% duty cycle with TBB and TIP payloads turned off at all times [31]-[32], [61].

5.4 GOX Payload Science Performance Results

5.4.1 GOX Payload On-Orbit Performance

Table 5-4 shows the GOX firmware build (FB) change history since launch. Figure 5-3 shows the RF Signal-to-Noise Ratio (SNR) performances of four GOX antennas (POD1, POD2, OCC1, and OCC2) on each GOX payload instrument in all six spacecraft after one year in orbit. In these figures, only data received after July 13 (Day 194), 2006, where FB4.2.1 was uploaded, are shown. The definition of the daily SNR value shown in Figs. 6 (A) to 6 (B) is the bottom limit of the top 90% SNR value of all the tracked GPS satellites' signal SNR values received by that particular antenna either in Coarse/Acquisition or Precision (P2) signal code. Following the uploading of FB version 4.3 (FB4.3) of the GOX payload to all the six spacecraft, from December 2006 onward, the trends of the GOX payload's SNR data did not show any sign of degradation at all from the available GPS RO science data. The SNR value of OCC1 on spacecraft FM3 shown in Figure 5-3(C) did show a decreasing tendency; the value drops very rapidly when the spacecraft is at a high beta angle. We observe that the SNR value returns to its normal value when GOX temperature is below 40^{o}C and spacecraft FM3 leaves the high beta angle. The decreasing of GOX SNR on FM6 as shown in Figure 5-3(F) is related to the reboot loop issue and will be addressed later [6]. The FB version 4.4 (FB 4.4) was provided to fix GOX reboot loop issue (see Section 4.4.2) even only the fore navigation antenna (POD) is working and to improved L2 tracking and produced the tracking data of the new L2C GPS signal.

5.4.2 GPS RO Profile Statistics

In Figure 5-4 we show the number of daily atmospheric profiles (atmprf) and ionospheric profiles (ionprf) retrieved for two years since launch. The term "atmphs" in the figure indicates the number of excess phase files that are generated and also represent the atmospheric RO profiles that can be observed by F3 satellites in the neutral atmosphere (stratosphere and troposphere). The "ionphs" in the figure indicates ionosphere. The new open loop FB version 4.2.1 (FB4.2.1) was uploaded to the GOX payload in July 2006, which caused a large jump in the daily RO profile numbers for August 2006. From Figure 5-4 it is clear that ~37% of the total events cannot be retrieved to neutral vertical atmosphere profiles. This is true for ~25% of ionospheric profiles. It also shows that the F3 mission has processed 1800 to 2200 high-quality neutral and ionospheric atmospheric sounding profiles per day, which is more than the total number of worldwide radiosondes launched (~900 mostly over land) per day [31]-[32], [61].

5.4.3 Lowest Altitude Penetration of GPS RO Retrievals

We studied the global distribution statistics of the lowest height of the retrieved profiles for F3 and CHAMP satellites for the period from January 1 to May 10, 2007 [31], [33]. Figure 5-6 shows the comparison of the lowest altitude penetration of RO profiles versus latitude for F3 and CHAMP mission. The solid lines above and below the median value are respectively the 75% and 25% statistical average value of the distributed data for F3. The bold dashed line is the median value of the lowest altitude penetration for CHAMP. The dashed lines above and below the median value are the 75% and 25% statistical average value of the distributed data for F3. The gray area plot is the water vapor specific humidity distribution with respect to altitude and latitude. The specific humidity data are obtained from a NCEP (National Centers for Environmental Prediction) analysis averaged from March 1968 to 1996

[31], [33].

We observe that the lowest height of the tangent point of the RO signals is limited by high terrain. The retrieved profiles were separated into two groups: one over the ocean and the other over the land. The lowest heights reached by the profiles of the land group for F3 and CHAMP were analyzed. It was noted that they are mostly below 0.5 km over the surface in the southern polar region. In most other land regions, the lowest heights reached are all below 1 km. Those with lowest heights reached above 1 km are mostly located in the mountainous areas such as Himalaya mountains, the Tibetan plateau, and the Andes Mountain because high mountains prevent RO signals with lower tangent point heights from being tracked [31], [33].

5.5 Conclusion

We have summarized the satellite constellation system performance after two years in orbit. With the development and application of the open loop tracking technique by JPL and UCAR, the quality, accuracy and lowest penetration altitude of the RO sounding profiles have been improved in comparison to previous RO missions. After two years in orbit about 1800 to 2200 high-quality soundings were being retrieved daily on a global basis. It is anticipated that an increasing number of global operational centers will use F3 data operationally for the years to come.

TABLE 5-1 CONSTELLATION SPACECRAFT PERFORMANCE SUMMARY (AFTER TWO YEARS IN ORBIT)

SC ID	Summary
FM1	☐ Bus GPSR GPS Non-Fixed -> Operation Solution ☐ GOX Reboot Loop -> Auto Recovery
FM2	☐ Stay in Phoenix -> Operation Solution ☐ GOX Reboot Loop -> Auto Recovery ☐ Solar Array Power Shortage -> Reduced GOX Operation ☐ BCR dMdC Charge Algorithm Issue-> FSW Update ☐ Battery Pressure Difference Anomaly -> FSW Update ☐ PCM DC Converter Abnormally Off -> TBB & TIP Off
FM3	☐ Lost of Communication -> Auto Recovery ☐ Solar Array Driver Lockout -> Reduced GOX operation ☐ Bus GPSR GPS Non-Fixed -> Operation Solution ☐ OCC2 (ANT03) SNR Decreasing -> Recovery after High Beta Angle
FM4	☐ Bus GPSR GPS Non-Fixed -> Operation Solution
FM5	☐ GOX Reboot Loop -> Auto Recovery ☐ GOX RF1 Lower SNR -> Auto Recovery
FM6	☐ Lost of Communication -> Auto Recovery ☐ GOX Reboot Loop -> GOX FB 4.4 Update ☐ Bus GPSR GPS Non-Fixed -> Operation Solution

TABLE 5-2 SPACECRAFT OPERATION STATUS OF EACH SUBSYSTEM IN ALL SIX SPACECRAFT (AFTER 2 YEARS IN ORBIT)

Spacecraft	**Operational Mode**	**SC State**	**ACS Mode**	**EPS Mode**	**C&DH Mode**	**GOX**	**TIP**	**TBB**
FM1	Normal	Normal	Fixed-Yaw	Normal	High Rate	Operating	Operating	Plan IX
FM2	Normal	Normal (Power Shortage)	Fixed-Yaw	Variable Power	High Rate	Reduced Operating	Off	Off
FM3	Normal	SAD Abnormal (Power Shortage)	Fixed-Yaw	Variable Power	High Rate	Reduced Operating	Off	Off
FM4	Normal	Normal	Fixed-Yaw	Normal	High Rate	Operating	Operating	Plan IX
FM5	Normal	Normal	Fixed-Yaw	Normal	High Rate	Operating	Operating	Plan IX
FM6	Normal	Normal (Resume Contact)	Fixed-Yaw	Normal	High Rate	Operating	Operating	Plan IX

TABLE 5-3 SPACECRAFT SUBSYSTEM PERFORMANCE (AFTER 2 YEARS IN ORBIT)

Unit	Major Function	Two-Year Performance
☐ Payload (PL)	☐ GPS RO primary mission	☐ Trends on low SNR data on FM3, FM5 and FM6 after FB4.3 uploaded did not show any sign of degradation at all from the available data. ☐ FM1, FM3, FM5 and FM6 had reboot loop issues. ☐ TBB & TIP are functioning OK.
☐ Radio Frequency Subsystem (RFS)	☐ RF uplink and downlink	☐ No RF degradation observed from FM1 to FM6. ☐ All RF trending data meet specified criteria.
☐ Command and Data Handling Subsystem (C&DH)	☐ Command handling and telemetry gathering, health and maintenance, GPSR management	☐ The GPS Non-fixed on FM1, FM3, FM4 & FM6 Bus GPSRs impacted onboard time maintenance, ACS performance and TIP payload time stamping. Operation Solution by upload State vector using GOX PVT data was performed to eliminate all impacts. ☐ The suspected space weather correlated onboard computer reboot and spacecraft reset events have no performance impact on C&DH and Spacecraft
☐ Flight Software Subsystem (FSW)	☐ FC/ACS/BCR Flight software, software upload, payload, launch vehicle interface	☐ FSW status on all satellites is normal; SC is automatically recovered from abnormal conditions. ☐ Under normal FSW condition, the error count increased rate is smaller than 10/day.
☐ Attitude Control Subsystem (ACS)	☐ Control of nadir pointing and sun pointing, GPS data processing	☐ Correct ACS mode transition was observed. ☐ All six spacecraft performed their ACS functions on orbit as expected.
☐ Reaction Control Subsystem (RCS)	☐ Orbital transfer and raising	☐ FM2, FM5, FM6 and FM4 have arrived at the mission orbits, and the remaining propellant masses for these three satellites are around 2.0 kg (~30% of full capacity) ☐ RCS functions are all healthy and ready for any planned orbit maneuvers in the future.
☐ Thermal Control Subsystem (TCS)	☐ Maintain avionics and battery at operating temperatures	☐ Thermal behavior of all six satellites is normal and in good shape.
☐ Electrical Power Subsystem (EPS)	☐ Solar array and battery charge control, power switching, deployment sequence	☐ No sensible degradation on all six satellites except FM2 and FM3. ☐ Solar power reduced on FM2 & FM3and Reduced GOX operation plan was modified. ☐ Pressure difference on FM1~FM4 reduced to safe range (<650 psi) and stable now. ☐ Power margin is estimated at 40% on solar power except FM2. ☐ Battery High Pressure Sensors on FM2 is fixed by FSW 6.2

TABLE 5-4 GOX FIRMWARE BUILD (FB) CHANGE HISTORY SINCE LAUNCH

Version	Upload date	Objective
FB4.1	5/18/2006	An improved atmospheric model for open loop tracking.
FB4.2	5/30/2006	1. Double precision P2 Phase. 2. To facilitate ionospheric occultation. 3. Bookkeeping.
FB4.2.1	6/29/200	1. To avoid logging unnecessary data and to get more occultation events. 2. To make sure that occulting satellites do not get used in the Navigation solution.
FB4.3	12/27/2006	1. Fix bugs such as: azimuth window, rising occultation to end earlier than at the commanded height, integer cycle slips during transition from open to closed loop tracking of rising occultation, halt acquisition and tracking of a particular PRN 2. Insertion of S4 scintillation parameter for ionosphere study.
FB4.4	6/2007	1. Fixed GOX reboot loop issue even only the fore navigation antenna (POD) is working 2. Improved L2 tracking and produced the tracking data of the new L2C GPS signal

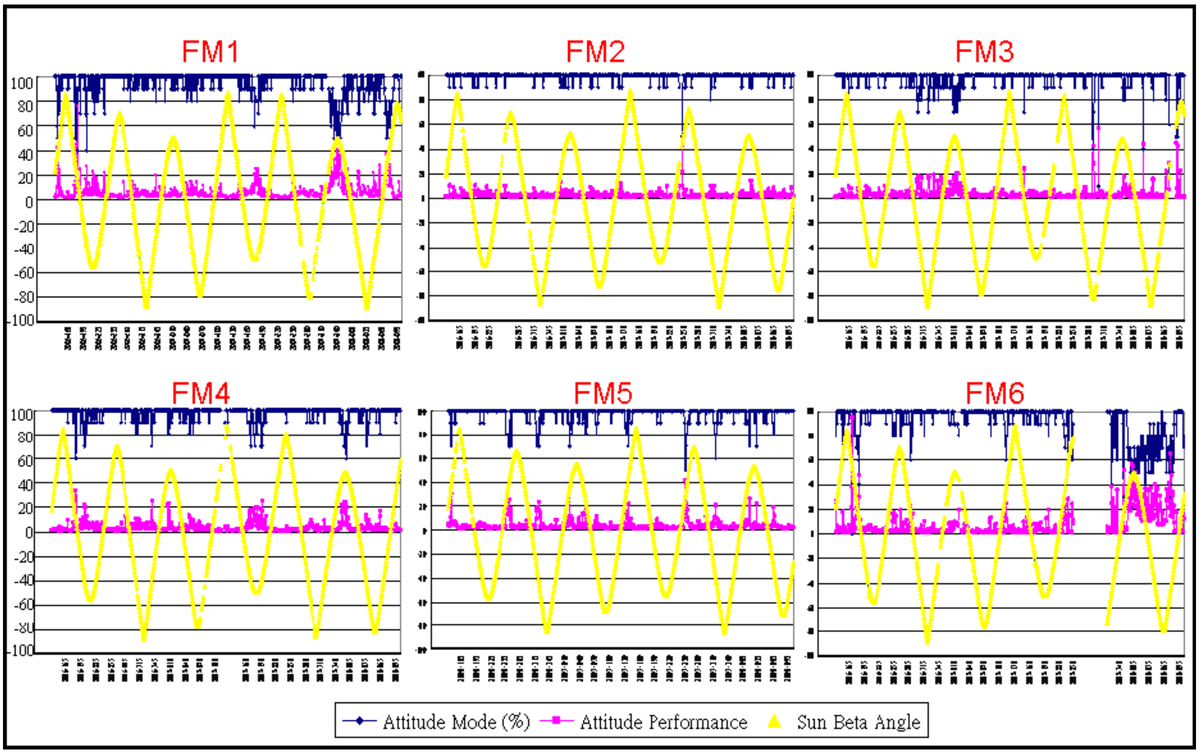

Figure 5-1. The six satellites attitude on-orbit performance with respect to the sun beta angle for one-year data since launch.

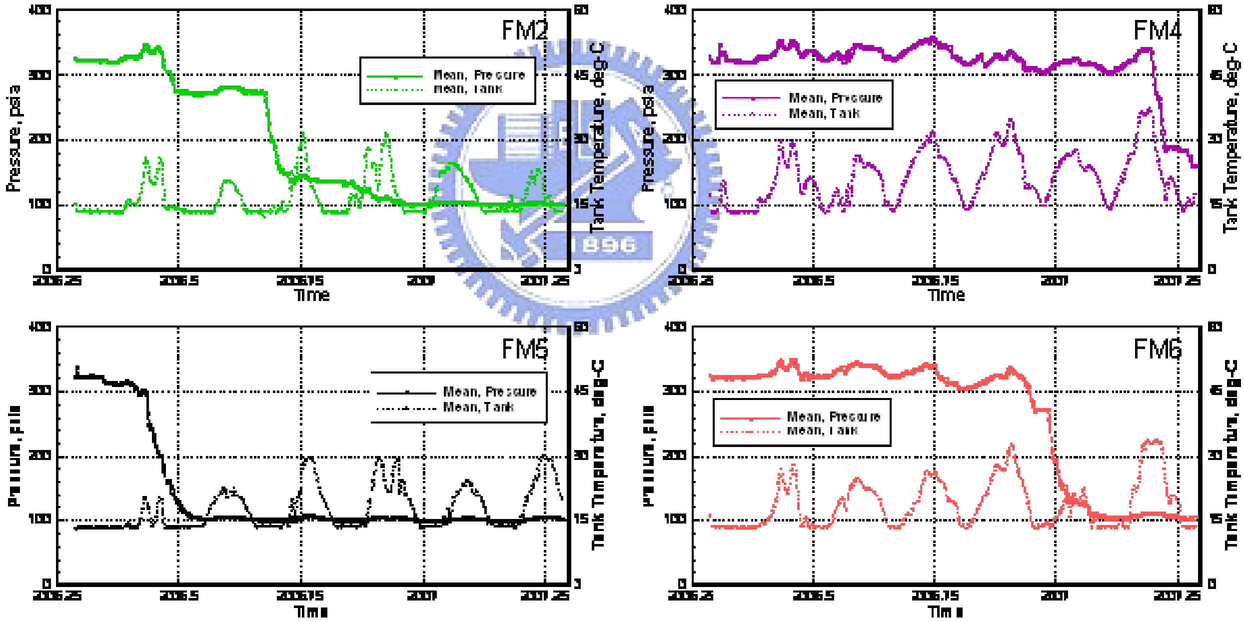

Figure 5-2. Trending plots of the tank pressures and temperatures for FM2, FM4, FM5, and FM6 (from 15 April 2006 to 15 April 2007)

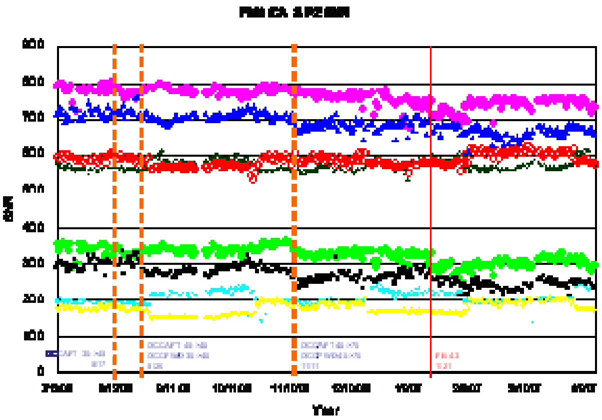

(A)FM1

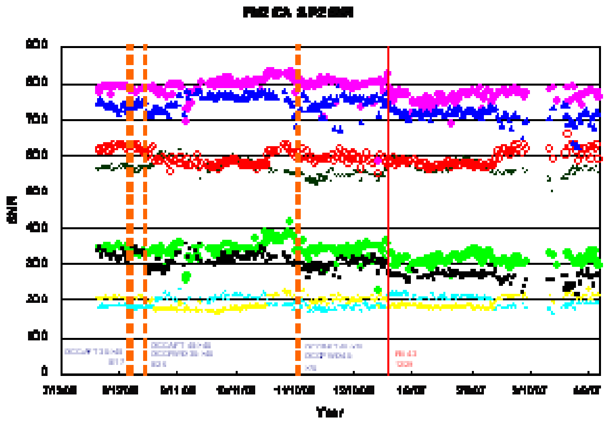

(B)FM2

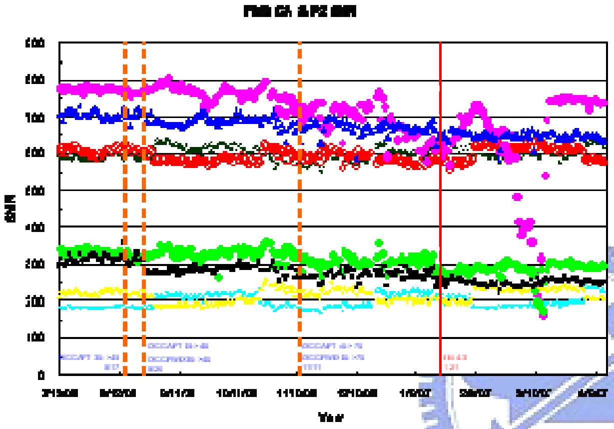

(C)FM3

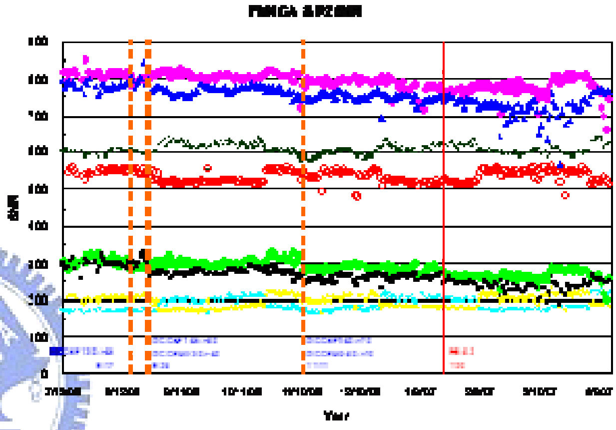

(D)FM4

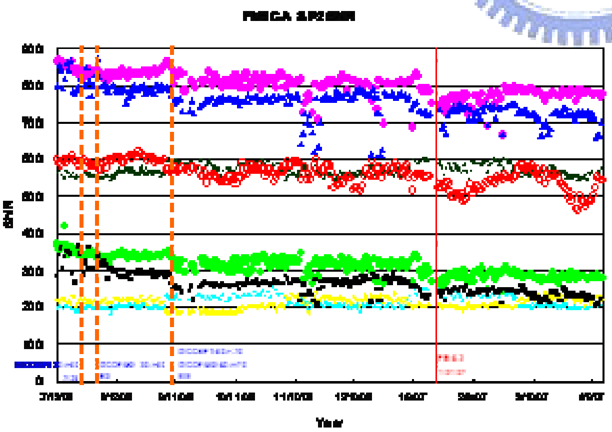

(E)FM5

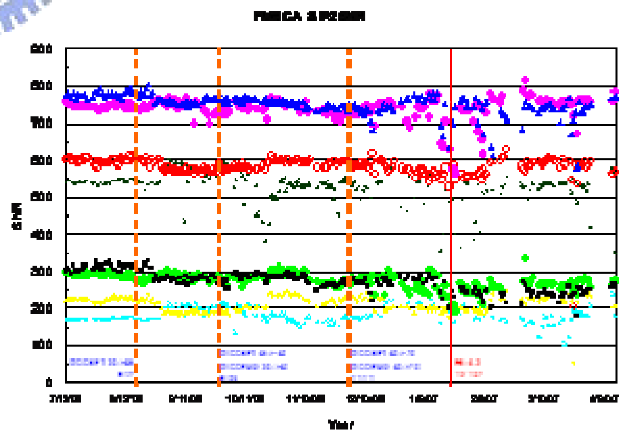

(F)FM6

● OCC1 CASNR ▲ OCC2 CASNR ✱ POD1 CASNR ○ POD 2 CASNR ● OCC1 P2SNR ■ OCC@ P2SNR × POD1 P2SNR + POD2 P2SNR

Figure 5-3. F3 Payload POD & OCC CA and P2 SNR for all six spacecraft.

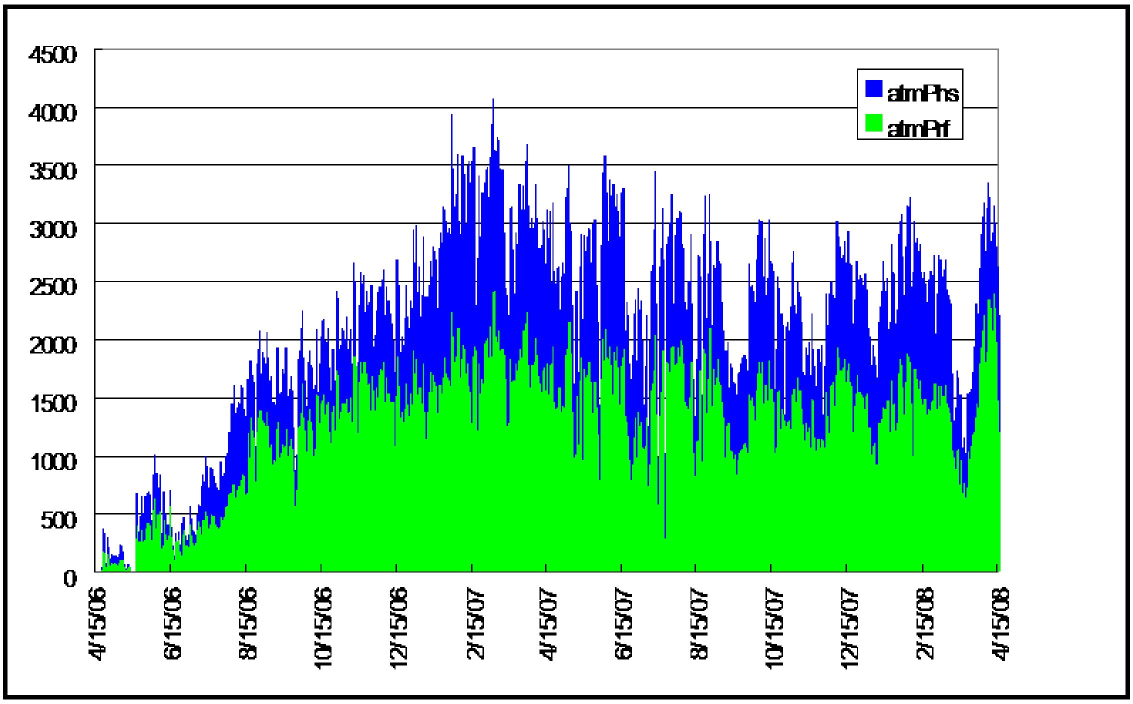

Figure 5-4. Two Years Statistics of the Number of Daily Occultation Events for Atmosphere Profiles since Launch.

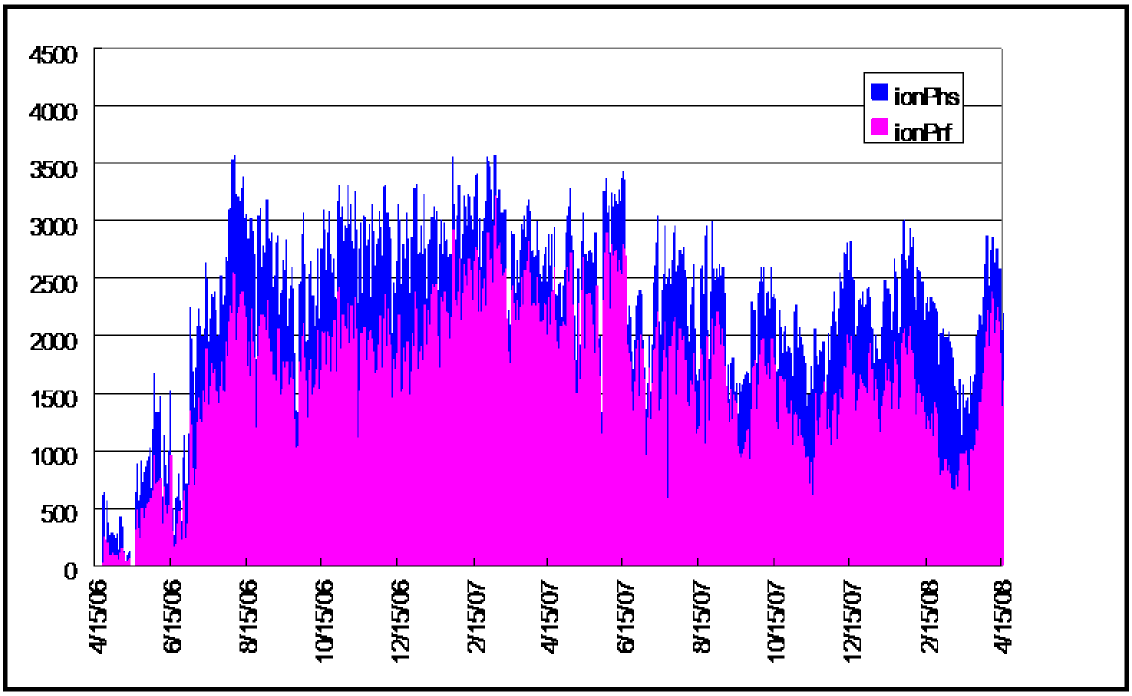

Figure 5-5. Two Years Statistics of the Number of Daily Occultation Events for Ionosphere Profiles of Electron Density since Launch.

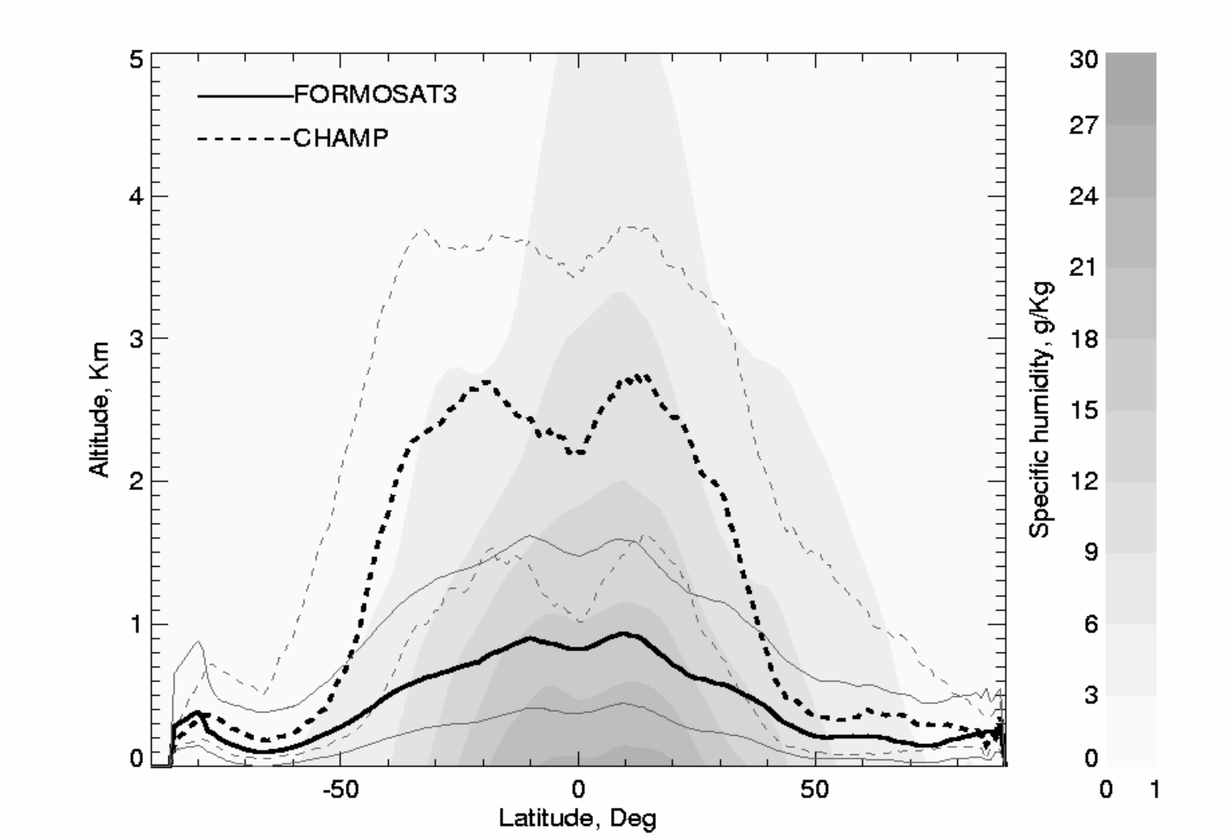

Figure 5-6. Comparison of the lowest altitude penetration of RO event versus latitude for F3/COSMIC and CHAMP.

Chapter 6 Follow-On Mission Trade Analysis and Design

6.1 Introduction

The success of the F3 mission has initiated a new era for operational GPS RO soundings [30], [36]. As addressed in the Final Report of “Workshop on the Redesign and Optimization of the Space based Global Observing System,” [41] the World Meteorological Organization (WMO) has recommended continuing RO observations operationally and the scientific community had urged continuation of the current mission and planning for a follow-on operational mission. The proposed follow-on mission is a greatly improved operational and research mission with redundancy and robustness and consisting of a new constellation of 12 satellites. The new mission will establish the international standards so that future RO missions deployed by any country can be assimilated into the same systems. The primary payload of the satellite will be equipped with the advanced GNSS RO receiver and will collect more soundings per receiver by adding Galileo and GLONASS tracking capability, which will produce a significantly higher spatial and temporal density of profiles. These will be much more useful for weather prediction models and severe weather forecasting including typhoons and hurricane, as well as for a research. In this Chapter the F3 follow-on mission definition trade analysis results is presented in Section 6.2, its system architecture and system design are presented in Section 6.3, and followed by the conclusion.

6.2 Follow-On Mission Definition Trade Analysis Results

In this Section we discuss follow-on mission major trade analysis results performed during the advanced study mission definition phase. The major trade analysis results include the mission orbit properties, the orbit inclination angle, the sounding data distribution, the proposed follow-on constellation spacecraft configuration, and the number and density of occultation data points. Then we discuss the data latency analysis that will impact to the overall space system architecture design and ground communication network. At the end we show the follow-on mission system architecture and preliminary spacecraft conceptual design [32], [36], [67].

6.2.1 Mission Orbit Properties

The follow-on mission requires the satellite at low-Earth-orbit from 500 km to 900 km. The engineering consideration on the altitude is mainly for the constellation deployment period. Constellation deployment period is a function of inclination angle, eccentricity, and difference of the parking orbit altitude. If the altitude difference of parking orbit and mission orbit is larger, it will be sooner for the mission to achieve its final constellation. Therefore, we propose 500 km as the parking altitude and 800 km as the mission altitude.

As for the shape of the orbit, a circular orbit is preferred for simplification. The optimal performance of the radio occultation payload is to have highest gain pointing to the Earth surface. However, if there is a requirement from scientific payload, it is probably feasible to have one satellite with an elliptical orbit with the difference of apogee and perigee less than 150 km, which is the capability of GOX on F3.

6.2.2 Orbit Inclination Angle

The following four important factors depend on the orbit inclination angle:

(1) Number of ground stations: general speaking, if the satellite is at high inclination angle orbit, it requires fewer ground receiving stations to achieve the full data dumps per revolution.

(2) Constellation period: the constellation period depends on the cosine the inclination angle. Therefore the inclination angle can not be too close to 90^{o}.

(3) Total occultation number: the relationship between total occultation number and

inclination angle is as shown in Figure 6-1. It is understandable that the number of occultation is higher if the inclination angle is higher since the GNSS system is orbiting at a higher inclination angle.

(4) Data distribution and spatial density: the topic will be analyzed further since the mission requires the data to be distributed homogeneously over the globe.

The analysis of inclination angle vs. measurement distribution has been studied and published by authors [32], [36], [67]. It is realized the inclination angle of 72^o of F3 will make the measurements in low latitudes a little bit sparse. Therefore, there will be a need to add some satellites at a low inclination orbit.

6.2.3 Sounding Data Distribution and Spatial Density

We define the "equivalent area covered by one occultation" or "horizontal spatial density" as the average area in square km associated with a single sounding, e.g., one sounding per N km (x N km). As we take a closer look at the dependence of data distribution and density with inclination angle, a high inclination angle favors the data collection at high latitudes and a low inclination angle favors the data distribution at low latitudes. Taking a 72^o inclination as an example (see Figure 6-2), the data distribution at low latitudes is sparser than at high latitudes. Within the latitude zone of -10^o to $+10^o$, there is one sounding per 1530 km x 1530 km and within the latitude zone of 80^o to 90^o (northern and southern hemisphere), there is one sounding per 800 km x 800 km .

Figure 6-3 shows our analysis for inclination angles of 0^o, 12^o, 24^o, 60^o, 72^o, 90^o and 98.6^o. 98.6^o is corresponds to a 800 km sun-synchronous orbit. One can see the trend for 72^o, 90^o, and 98.6^o are similar and the trend for 0^o, 12^o, and 24^o are similar. Therefore, the approaches for global distribution homogenously are (1) to pick the inclination in the middle; (2) to choose a satellite constellation combined with high inclination and low inclination. For this project, we start with the latter approach because F3 is a constellation with 72^o

inclination angle and it is running well in terms of payload, spacecraft, and data centers.

6.2.4 Follow-on Spacecraft Constellation

We propose the following constellation of 12 satellites (Figure 6-4 shows 12 satellites constellation) as follows: 8 of them will be at high inclination angle (72^{o} for this analysis) and 4 of them will be at low inclination angle (24^{o} for this analysis). The satellites at high inclination angle will be stacked in one (or two) launch vehicle(s) and be placed to the parking orbit. The operations team will then perform the thrust burns so that their orbital plane can be separated through the differential precession rate with the differential orbit altitude. The satellite at low inclination angle will go through the similar launch and constellation deployment process. The final constellation of 12 satellites constellation would be 8 high-inclination-angle satellites at 8 orbital planes which are marked as pick lines in Figure 6-4, and 4 low-inclination-angle satellites at 4 orbital planes which are marked as blue lines in Figure 6-4.

6.2.5 Occultation Points

With the various uncertainties on the follow-on project, we also calculate the number of occultation points with 12 satellites in the constellation. They are listed in Table 6-1. Figure 6-5 shows the daily occultation point distribution with 12-satellite constellation for the F3 follow-on mission. The calculation is based on 28 GPS satellites, 27 GALILEO satellites, and 21 GLONASS satellites with the assumption of 350 effective atmospheric profiles per LEO per day if the satellites perform similarly to the F3 satellites. Please note that the estimation is based on the following ideal conditions: no spacecraft emergency, no anomaly on ground segment, and no errors from operation segment.

6.2.6 Data Latency

The data latency depends on the number and locations of the available ground stations in the world. In the analysis, the ground stations, which are located at Fairbanks, Tromso, and McMurdo, used for F3 are assumed to receive the data from the high-inclination-angle satellites of the follow-on mission. For the low-inclination-angle satellite, we tentatively use TT&C stations located in Taiwan, Banglore, and Mauritius for the RO number calculation and latency analysis. These three low-latitude ground stations can also to support data dumps from the high-inclination-angle satellites. To maximize the use of the ground stations, the argument of latitude of the orbit needs to be phased properly to avoid more than one spacecraft flying over the same ground station at the same time. For a constellation of 12 satellites, the data latency due to storage and dumping is about 36 minutes on the average. If we assume ground network and processing take about another 14 minutes, the total average data latency is about 50 minutes.

6.2.7 Effective Coverage Area

Currently, the F3 constellation can collect about 2500 measurements per day when all six GOX are at 100% duty cycle. After the data are processed, the number of good atmospheric soundings is about 70% of the total measurements. In other words, there are approximately 1600-2200 good soundings per day depending on the GOX duty cycles. For this number of soundings the spatial data density is about one sounding per 550 km x 550 km. It should be noted that the horizontal scale of a tropical cyclone is about several hundred square kilometers. Therefore F3 may take only one measurement in the area of highest interest. Therefore, the follow-on mission should have significantly more soundings distributed more or less homogeneously over the globe to make the system a significant improvement over F3. The effective spatial data density in the contemplated 12 satellites constellation of the follow-on mission with GNSS capable of receiving GPS, GALILEO and GLONASS signals can be reduced to one soundings per 250 km x 250 km.

6.3 Follow-On Mission System Architecture and System Design

6.3.1 Follow-On Mission System Architecture

The advanced program team at NSPO is currently at the stage of mission definition design phase. We show here some of the planned mission and spacecraft design features for the follow-on mission. Figure 6-6 shows the proposed F3 follow-on mission system architecture with constellation of 12 satellites that requires three launches. The primary payload of the follow-on satellite will be equipped with next-generation GNSS RO receiver to collect more soundings per receiver by adding Galileo and GLONASS tracking capability.

6.3.2 Spacecraft Bus Design

Based on the F3 satellites design lessons learned, integration and test lessons learned, and the mission operation experiences, the follow-on spacecraft will be a high reliable and robustness satellite and will improve the payload performance by using the next generation Tri-G RO Receiver. The follow-on satellite will be neither a perfect satellite nor a multi-purpose satellite. The follow-on satellite will be designed to provide better attitude performance to reduce the spacecraft recovery time and payload down time.

The proposed spacecraft bus design will be accommodate up to one GNSS RO payload plus two optional additional science payloads. The team will use standard modular design approach for the payload suites. For each science payload suite 5 kg of mass and 5W of power will allocated. And the memory margins will be designed to support additional payload capacity. As for communications subsystem design, identical to F3 Ground System Interface, the team will use S-Band Uplink/Downlink (CCSDS) 2Mbps Downlink and 32Kbps Uplink, respectively. For C&DH subsystem design, the team will use centralized integrated avionic unit with radiation hardness chip and with 1 Gigabytes of SDRAM. For the ACS, pointing performance will be greatly improved over F3 performance based on the lessons learned from the F3 mission operation experiences, the pointing accuracy will be designed to within ±0.2 deg. (3σ) in Roll/Yaw/Pitch axes, respectively. And the pointing knowledge will be designed to within ±0.2 deg. (3σ) in Roll/Yaw/Pitch axes, respectively. For EPS Subsystem, the team will use lithium ion battery to improve the battery lessons learned of the current F3 mission. The control algorithm will be a voltage-based algorithm, and the power margins support additional payload capacity. And the aluminum structure will be used for the follow-on mission.

The follow-on spacecraft bus design vs. current F3 design is shown in Table 6-2. Figure 6-7 shows the proposed F3 follow-on mission spacecraft configuration. The benefit and improvement for the follow-on spacecraft will improve payload performance, better attitude performance, simplified operation, simplified orbit transfer, increased data storage, and modular design for and additional science payloads (optional) and launch vehicle interface.

6.3.3 GNSS Payload Design

GNSS RO instrument is the primary payload for the follow-on mission. The manufacturer of the GNSS RO payloads except the GRAS instrument in METOPS-A, are most from the Blackjack technology, which developed by JPL/NASA then transferred to Broad Reach Engineering, such as the following space mission: GPS/MET, SUNSAT, ORSTAD, CHAMP, SAC-C, JASON-1, GRACE (x2), F3 (x6), TERRASAR-X, TCSAT, TanDEM-X, KOMPSAT-5, and IOX.

The GNSS will include 29 operational United States' GPS satellites, several Russia's GLONASS (planning to have 18 satellites), and European GALILEO system (plan to have 30 GNSS satellites by 2013). The GNSS RO payload in the follow-on mission will utilize the advanced requirements to be able to receive the US GPS L1/L2/L5 signals, also to receive the GALILEO E1/E5/E6 signals, and to receive Russia's L1/L2/L5 signals as well. The other advanced requirements for the next generation RO payload are major on the performance improvement from the current GOX payload in F3 in order to achieve more soundings.

The advanced GNSS RO payload should be able to have robust software upload design for modifying the GNSS RO application. The software for the other specific GNSS application or experiment can also be uploaded from ground to GNSS RO payload. JPL's Tri-G is now currently under development for such requirements and will be available for test flight on 2010.

6.4 Conclusion

The success of the F3 mission has initiated a new age for operational GPS RO soundings and is the world's first demonstration of the impact of near real-time GPS RO observations in operational global weather forecasting. We provide the proposed follow-on mission definition trade analysis results, especially the system architecture and spacecraft bus and GNSS RO payload design. The follow-on spacecraft design will have robustness design and improve the payload performance by using the next generation GNSS RO payload and provide better attitude performance to reduce the spacecraft recovery time and payload down time. The follow-on mission is expected to have a significantly improved impact on global weather prediction. And its promise for weather and climate research and space weather monitoring is equally far-reaching.

Table 6-1 Expected Atmospheric Profiles vs. Different Constellation and Different Receiver Capability.

Satellites in constellation	GPS	GALILEO	GLONASS	GPS+ GALILEO	GPS+GALILEO +GLONASS
High Inc. @72^o	500	480	390	980	1,370
Low Inc. @24^o	500	470	330	970	1,300
12(=8+4)	6,000	5,720	4,440	11,720	16,160

TABLE 6-2 PROPOSED FOLLOW-ON MISSION SPACECRAFT BUS DESIGN VS. F3 DESIGN.

Function	Follow-On Design	F3 Design	Benefit
Weight	<50 kg	61 kg (w/ Propellant)	Stacked or Single Launch Piggy-Back Launch
Attitude Control Performance	3-axis linear control Roll/Yaw:+/-0.2^{o} (3σ) Pitch: +/- 0.2^{o} (3σ) 3-Axis Gyro, 3-axis MAG, RWA x 3, Torque x 3, GNSS PL x 1	3-axis nonlinear control Roll/Yaw: +/-5o (1σ) Pitch: +/- 2o (1σ) Earth Sensor x 2, CSSA x 8, RWA x 1, Torque x 3, Bus GPSR PL x 1	Improved PL Performance Better Attitude Performance Simplified Operation Simplified Orbit Transfer
Science Data Storage	>1.5 G	128 M	Increased Data Storage Simplified Operations
Avionics Architecture	Centralized Architecture Radiation - Hardness	Distributed Architecture (Multiple Avionics Boxes)	Simplified Integration Harnessing & Mass Reduced
Electrical Power	Lithium Ion Battery Voltage Based Algorithm	Ni-H2 Battery dM/dC Charging Algorithm	Reduced Mass & Volume Simplified Operations
Structure	Aluminum	Metal Matrix (AlBeMet)	Cost Reduced
Payload Interface	Main PL: GNSS RO Rcvr 2 Science PL (Optional)	Primary PL: GOX Secondary PL: TIP, TBB	Modular Design Cost Reduced

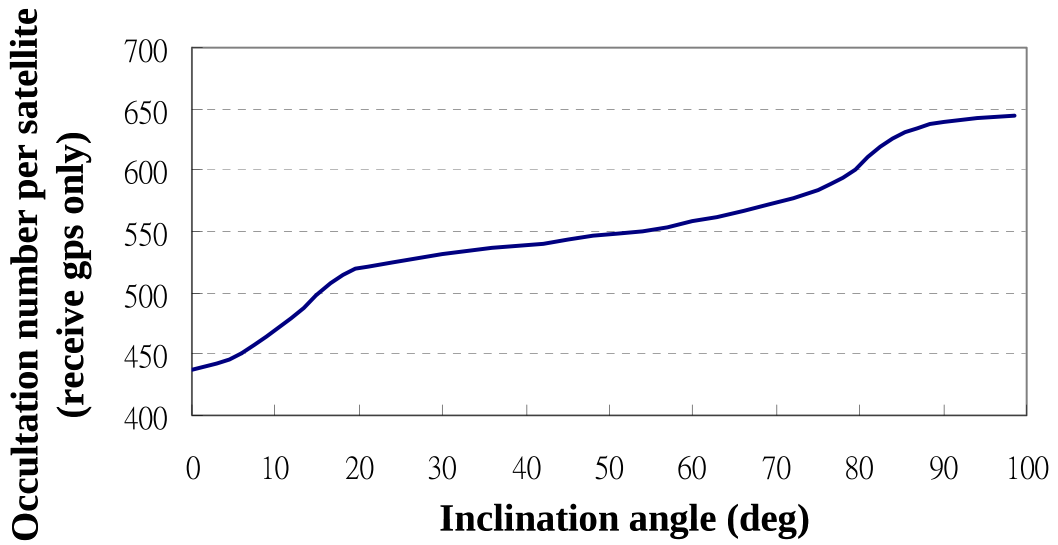

Figure 6-1. The relationship between total occultation number and inclination angle for one satellite receiving GPS only.

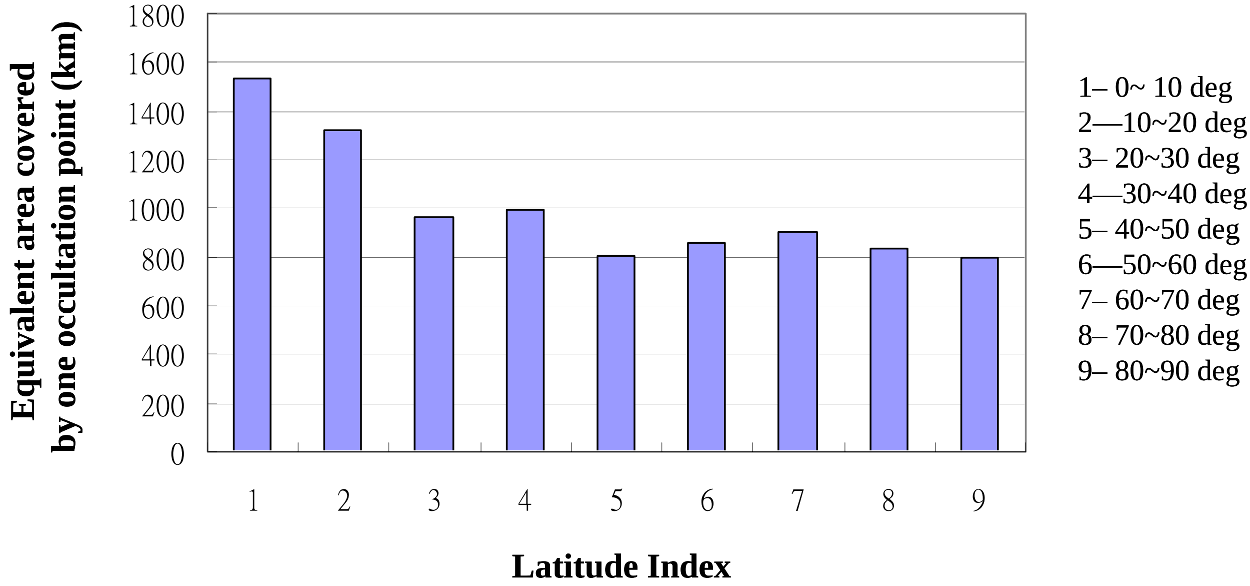

Figure 6-2. The dependence of data distribution vs. latitude for a 72o inclination angle. The "equivalent area covered by one occultation" is defined as the average area in square km associated with a single sounding. e.g., one sounding per N km (x N km).

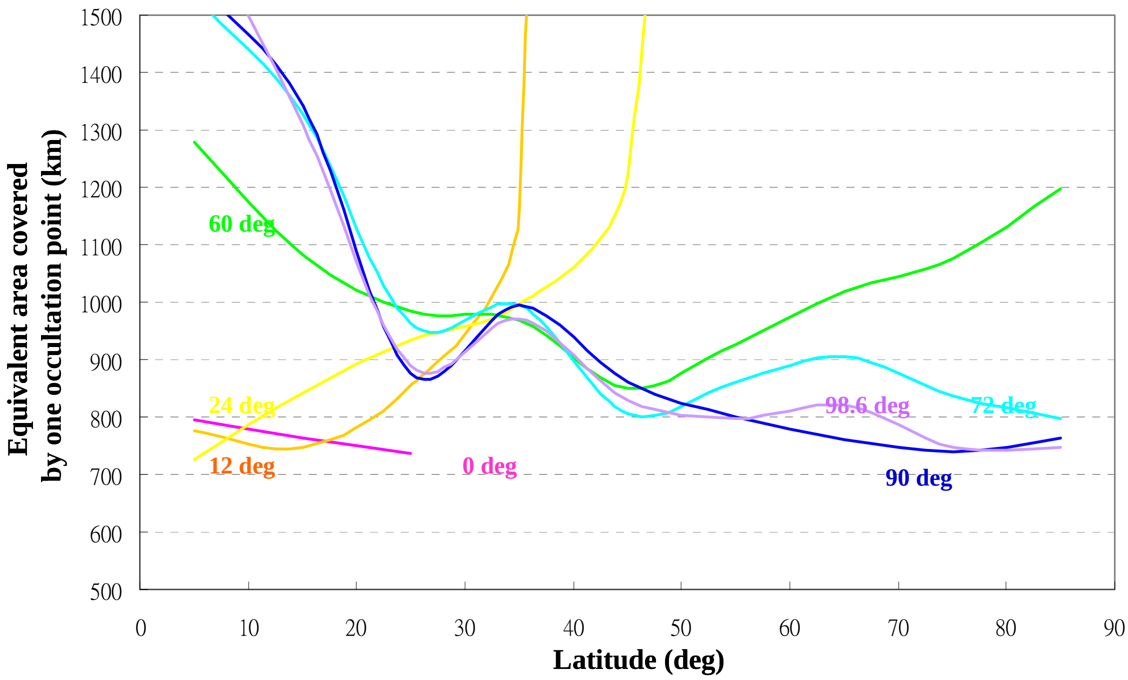

Figure 6-3. The dependence of data distribution with inclination angle. The "equivalent area covered by one occultation" is defined as the average area in square km associated with a single sounding. e.g., one sounding per N km (x N km).

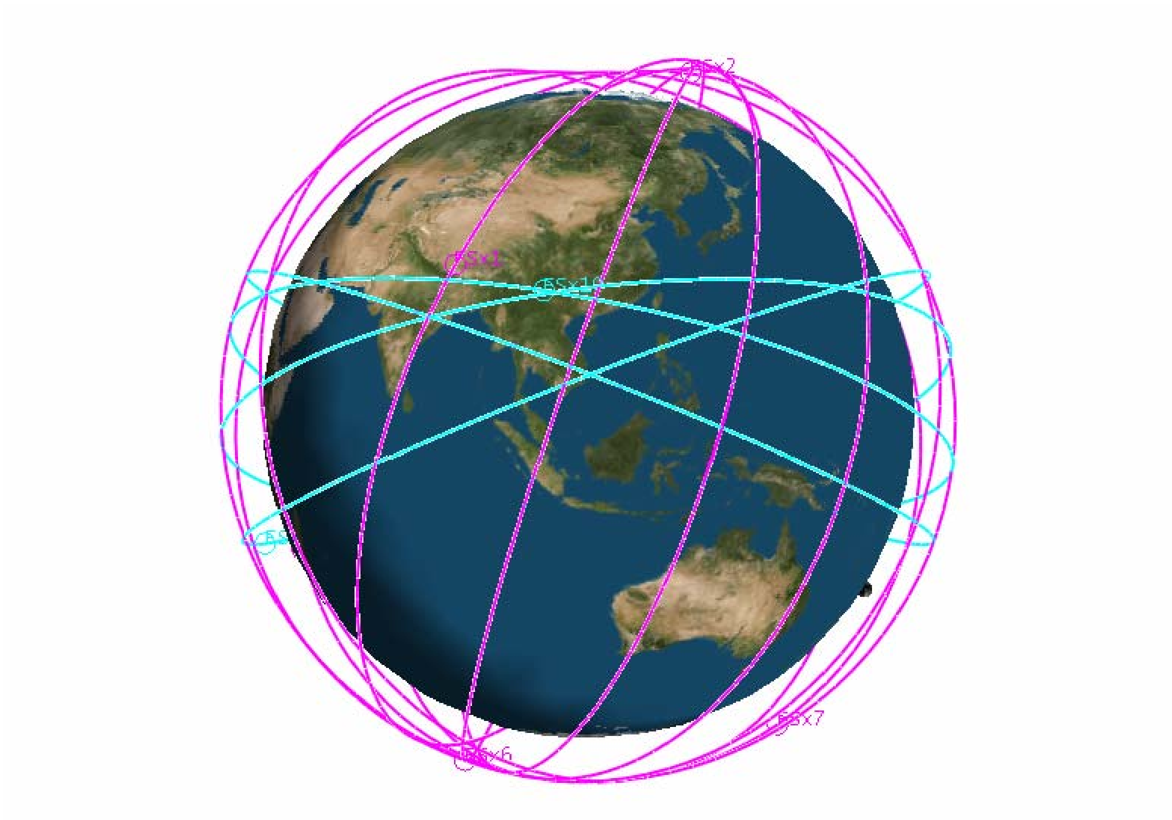

Figure 6-4. The F3 follow-on constellation with 12 satellites.

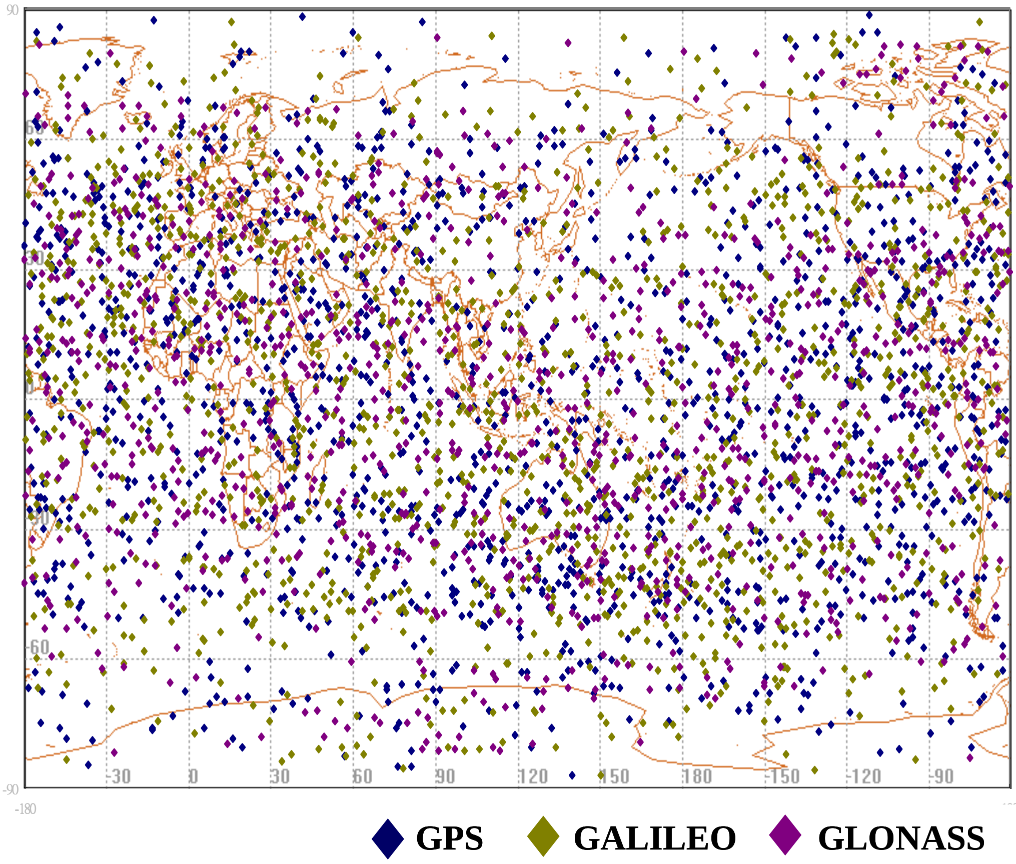

Figure.6-5. 6-hr Occultation Distribution with 12-satellite constellation for the F3 follow-on mission (the blue dots are from GPS, the green dots are from GALILEO, and the purple dots are from GLONASS)

Figure 6-6. The F3 follow-on mission system architecture with constellation of 12 satellites.

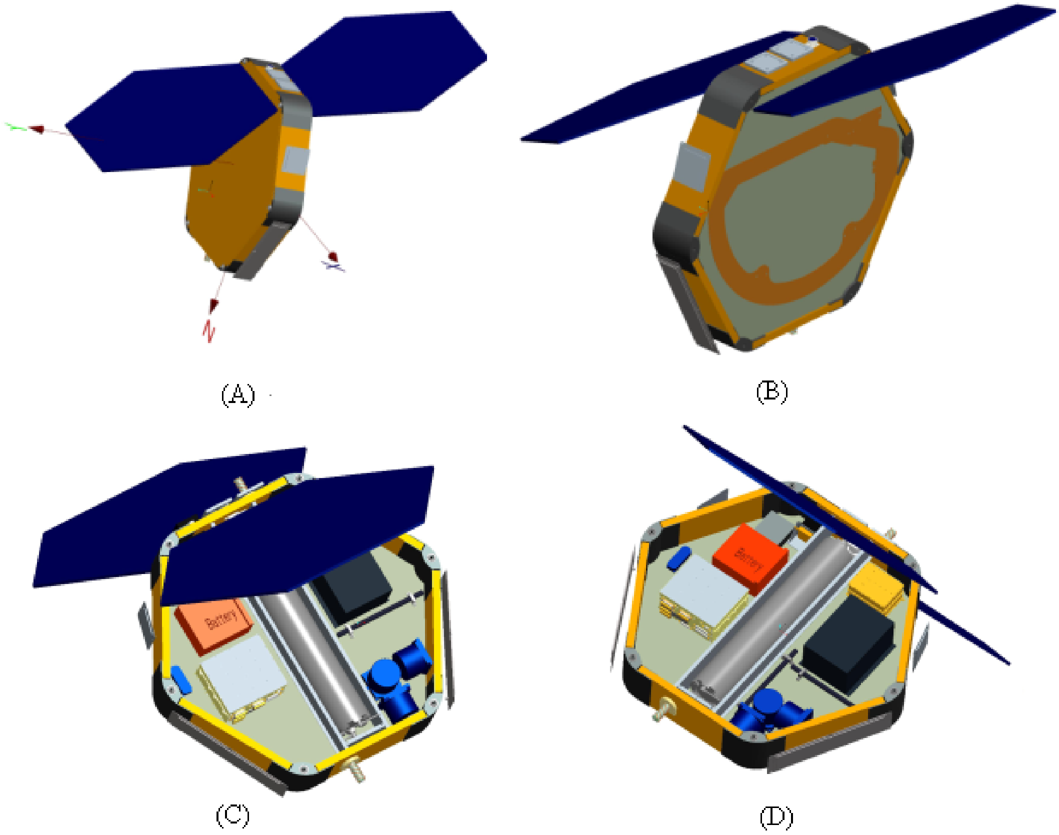

Figure 6-7. The proposed F3 follow-on mission spacecraft configuration.

Chapter 7 Conclusions

In this dissertation we have presented an overview of the new constellation deployment theory, constellation spacecraft design, constellation mission operations, orbit-raising challenges, and lessons learned during the 19 month's constellation deployment. We have also presented the constellation system performance, and the follow-on mission trade analysis results, and a proposed new spacecraft constellation system conceptual design with next-generation RO receiver onboard.

The F3 mission is the world's first demonstration of near real-time operational GPS RO mission for global weather monitoring and we also verified a novel "proof-of-concept" way of performing constellation deployment by taking the advantage of Earth nodal precession principle. This advanced approach has dramatically reduced the spacecraft propellant mass and the complexity of the spacecraft propulsion and attitude control subsystem design.

Due to the great success of the innovative F3 mission, the goal of the follow-on mission is to transfer the mission from research to real-time operational with GPS/Galileo/GLONASS system tracking capabilities, a greatly improved constellation that would have significant impacts on future operational numerical weather prediction and research in the areas of weather, climate and space weather.

References

1. W. G. Melbourne, E. S. Davis, C. B. Duncan, G. A. Hajj, K. R. Hardy, E. R. Kursinski, T. K. Meehan, L. E. Young, and T. P. Yunck, “The application of spaceborne GPS to atmospheric limb sounding and global change monitoring,” Jet Propulsion Laboratory, Pasadena, CA, JPL Publication 94-18, Apr. 1994.
2. G. Fjeldbo and V. R. Eshleman, “The bistatic radar-occultation method for the study of planetary atmospheres,” J. Geophys. Res., vol. 70, pp. 3217-3225, 1965.
3. E. R. Kursinski, G. A. Hajj, S. S. Leroy, and B. Herman, “The GPS occultation technique,” Terrestrial, Atmospheric and Oceanic Sciences (TAO), vol. 11, no. 1, pp. 53-114, Mar. 2000.
4. A. J. Kliore, D. L. Cain, G. S. Levy, V. R. Eschleman, G. Fjeldbo, and F. D. Drake, “Occultation experiment: results of the first direct measurement of Mars’ atmosphere and ionosphere,” *Science*, vol. 149, no. 3689, pp. 1243-1248, Sep. 1965.
5. W. G. Melbourne, Radio Occultation Using Earth Satellites: A Wave Theory Treatment, John Wiley & Sons, Inc., ISBN 0-471-71222-1, 2005.
6. T. P. Yunck, C. H. Liu and R. Ware, “A history of GPS sounding,” Terrestrial, Atmospheric and Oceanic Sciences (TAO), vol. 11, no. 1, pp. 1-20, Mar. 2000.
7. B. Lusignan, G. Modrell, A. Morrison, J. Pomalaza, and S. G. Ungar, “Sensing the Earth's atmosphere with occultation satellites,” Proc. IEEE, vol. 57, no. 4, pp. 458-467, Apr. 1969.
8. A. S. Liu, “On the determination and investigation of the terrestrial ionospheric refractive indices using GEOS-3/ATS-6 satellite-to-satellite tracking data,” Jet Propulsion Laboratory, Pasadena, CA, NASA-CR-156848, Nov. 1978.
9. O. Yakovlev, I. Matyugov, and I. A. Vilkov, “Radio-wave phase and frequency fluctuations as observed in radio occultation experiments on the satellite-to-satellite

link," Journal of Communications Technology and Electronics, vol. 41, no. 11, pp. 993-998, Nov. 1996.

10. J. L. Davis, T. A. Herring, I. I. Shapiro, A. E. E. Rogers, and G. Elgered, "Geodesy by radio interferometery: Effects of atmospheric modeling errors on estimates of baseline length," Radio Sci., vol. 20, no. 6, pp. 1593-1607, 1985.

11. G. Elgered, B. Stoew, L. Gradinarsky, and H. Bouma, "Analysis of atmospheric parameters derived from ground-based GPS observations," Proc. Int. Workshop on GPS Meterology, Tsukuba, Japan, 14-17 Jan. 2003.

12. S.-Y. Ha, Y.-H. Kuo, and G.-H. Lim, Assimilation of GPS slant wet delay data and its impact on the short-range NWP, Proc. Int. Workshop on GPS Meterology, Tsukuba, Japan, 14-17 Jan. 2003.

13. T. P. Yunck and G. A. Hajj, "Global navigation satellite sounding of the atmosphere and GNSS altimetry: prospects for geosciences," IUGG General Assembly, Sapporo, Japan, 8-11 Jul. 2003.

14. ——, W. G. Melbourne, and C. L. Thornton, "GPS-based satellite tracking system for precise positioning," IEEE Trans. Geosci. Remote Sens., vol. GE-23, no. 4, pp. 450-457, Jul. 1985.

15. ——, G. F. Lindal, and C. H. Liu, "The role of GPS in precise Earth observations," in Proc. IEEE: Position Location and Navigation Symposium, 1988. Record. 'Navigation into the 21st Century'. IEEE PLANS '88, 29 Nov.-2 Dec. 1988.

16. ——, S. C. Wu, J. T. Wu, and C. L. Thornton, "Precise tracking of remote sensing satellites with the global positioning system" IEEE Trans. Geosci. Remote Sens., vol. 28, no.1, pp. 108-116, Jan. 1990.

17. S. C. Wu and W. G. Melbourne, "An optimal GPS data processing technique for precise positioning," IEEE Trans. Geosci. Remote Sens., vol. 31, no. 1, pp. 146-152, Jan. 1993.

18. R. Ware, C. Rocken, F. Solheim, M. Exner, W. Schreiner, R. Anthes, D. Feng, B. Herman, M. Gorbunov, S. Sokolovskiy, K. Hardy, Y. Kuo, X. Zou, K. Trenberth, T. Meehan, W. Melbourne, and S. Businger, "GPS sounding of the atmosphere from low earth orbit: Preliminary results," Bulletin of the American Meteorological Society (BAMS), vol. 77, no. 1, pp. 19-40, Jan. 1996.

19. E. R. Kursinski, G. A. Hajj, W. I. Bertiger, S. S. Leroy, T. K. Meehan, L. J. Romans, J. T. Schofield, D. J. McCleese, W. G. Melbourne, C. L. Thornton, T. P. Yunck, J. R. Eyre, and R. N. Nagatani, "Initial results of radio occultation observations of Earth's atmosphere using the Global Positioning System," Science, vol. 271, no. 5252, pp. 1107-1110, Feb. 1996.

20. A. Rius, G. Ruffini, and A. Romeo, "Analysis of ionospheric electron-density distribution from GPS/MET occultations," IEEE Trans. Geosci. Remote Sens., vol. 36, no. 2, pp. 383-394, Mar. 1998.

21. R. A. Anthes, C. Rocken and Y. H. Kuo, "Application of COSMIC to meteorology and climate," Terrestrial, Atmospheric and Oceanic Sciences (TAO), vol. 11, no. 1, pp. 115-156, Mar. 2000.

22. G. A. Hajj, L. C. Lee, X. Pi, L. J. Romans, W. S. Schreiner. P. R. Straus and C. Wang, "COSMIC GPS ionospheric sensing and space weather," Terrestrial, Atmospheric and Oceanic Sciences (TAO), vol. 11, no. 1, pp. 235-272, Mar. 2000.

23. Y.-H. Kuo, S. Sokolovskiy, R. Anthes, and V. Vandenberghe, "Assimilation of GPS radio occultation data for numerical weather prediction," Terrestrial, Atmospheric and Oceanic Sciences (TAO), vol. 11, no. 1, pp. 157–186, Mar. 2000.

24. L.-C. Lee, R. Kursinski, and C. Rocken, Ed., Applications of Constellation Observing System for Meteorology, Ionosphere & Climate: Observing System for Meteorology Ionosphere and Climate, Springer, ISBN 9624301352, 2001.

25. Y.-A. Liou, A. G. Pavelyev, C.-Y. Huang, K. Igarashi, and K. Hocke, "Simultaneous observation of the vertical gradients of refractivity in the atmosphere and electron density in the lower ionosphere by radio occultation amplitude method," Geophys. Res. Lett., vol. 29, no. 19, pp. 43-1-43-4, doi: 10.1029/2002GL015155, 2002.

26. ——, ——, ——, ——, ——, and S.-K. Yan, "An analytic method for observing the gravity waves using radio occultation data," Geophys. Res. Lett., vol. 30, no. 20, pp. 2021, doi: 10.1029/2003GL017818, 2003.

27. ——, ——, J. Wickert, T. Schmidt, and A. A. Pavelyev, "Analysis of atmospheric and ionospheric structures using the GPS/MET and CHAMP radio occultation database: a methodological review," GPS Solutions, vol. 9, no. 2, 122-143, doi: 10.1007/s10291-005-0141-y, 2005.

28. C.-Z. F. Cheng, Y.-H. Kuo, R. A. Anthes, and L. Wu, "Satellite constellation monitors global and space weather," EOS Trans. Amer. Geophy. Union, vol. 87, no. 17, pp. 166-167, Apr. 2006.

29. Y.-A. Liou, A. G. Pavelyev, S.-F. Liu, A. A. Pavelyev, N. Yen, C.-Y. Huang, and C.-J. Fong, "FORMOSAT-3 GPS radio occultation mission: preliminary results," IEEE Trans. Geosci. Remote Sens., vol. 45, no. 11, doi: 10.1109/TGRS.2007.903365, Nov. 2007.

30. R. A. Anthes, P. A. Bernhardt, Y. Chen, L. Cucurull, K. F. Dymond, D. Ector, S, B. Healy, S.-P. Ho, D. C. Hunt, Y.-H. Kuo, H. Liu, K. Manning, C. McCormick, T. K. Mehan, W. J. Randel, C. Rocken, W. S. Schreiner, S. V. Sokolovskiy, S. Syndergaard, D. C. Thompson, K. E. Trenberth, T. K. Wee, N. L. Yen, and Z. Zeng, "The COSMIC/FORMOSAT-3 mission: early results," Bulletin of the American Meteorological Society (BAMS), doi: 10.1175/BAMS-89-3-313, Mar. 2008.

31. C.-J. Fong, C.-Y. Huang, C.-H. Chu, N. L. Yen, Y.-H. Kuo, Y.-A. Liou, and S. Chi., "Mission results from FORMOSAT-3/COSMIC constellation system," AIAA J. Spacecraft and Rockets, vol. 45, no. 6, doi: 10.2514/1.34427, Nov./Dec. 2008.

32. ——, N. Yen, V. Chu, E. Yang, A. Shiau, C.-Y. Huang, S. Chi, S.-S. Chen, Y.-A. Liou and, Y. H. Kuo, "FORMOSAT-3/COSMIC spacecraft constellation system, mission results, and prospect for follow-on mission," Terrestrial, Atmospheric and Oceanic Sciences (TAO), vol. 20, no. 1, Feb. 2009.

33. C.-Y. Huang, C. Z. Cheng, P. H. Lin, C.-J. Fong, J. Wicker, and C. C. Hsiao, "Radio occultation retrieval of atmospheric profiles in the FORMOSAT-3/COSMIC mission: current status," Terrestrial, Atmospheric and Oceanic Sciences (TAO), vol. 20, no. 1, Feb. 2009.

34. C.-H. Vicky Chu, N. Yen, C.-C. Hsiao, C.-J. Fong, S.-K. Eddy Yang, T.-Y. Liu, M. Lin, and J.-J. Miau, "Earth observations with orbiting thermometers – prospective FORMOSAT-3/COSMIC follow-on mission," Small Satellite Conference 2008 Proceedings, Logan, Utah, 11-14 Aug. 2008.

35. C.-J. Fong, N. Yen,.C.-H. Chu,.C.-C. Hsiao, Y.-C. Lin, S.-S. Chen, Y.-A. Liou, and S. Chi, "In quest of global radio occultation mission for meteorology beyond 2011," 2009 IEEE Aerospace Conference Proceedings, Big Sky, MT, 7-14 Mar. 2009. (to be published)

36. ——, ——, ——, ——, Y.-A. Liou, and S. Chi, "Space-based global weather monitoring system – FORMOSAT-3/COSMIC constellation and its follow-on mission," AIAA J. Spacecraft and Rockets, Submitted on 24 Sep. 2008, to be published.

37. Y.-H. Kuo, T.-K. Wee, S. Sokolovskiy, C. Rocken, W. Schreiner, D. Hunt, and R. A. Anthes, "Inversion and error estimation of GPS radio occultation data," Journal of the

Meteorological Society of Japan, vol. 82, no. 1B, pp. 507-531, doi:10.2151/jmsj.2004.507, 2004.

38. ——, H. Liu, Z. Ma, , and Y.-R. Guo, “The impact of FORMOSAT-3/COSMIC GPS radio occultation,” 4th Asian Space Conference and 2008 FORMOSAT-3/COSMIC International Workshop, Taipei, Taiwan, 1-3 Oct. 2008.

39. C. Rocken, Y.-H. Kuo, W. S. Schreiner, D. Hunt, S. Sokolovskiy, C. McCormick, “COSMIC system description,” Terrestrial, Atmospheric and Oceanic Sciences (TAO), vol. 11, no. 1, pp. 21-54, Mar. 2000.

40. B.-H. Wu, C.-J. Fong, C.-Y. Huang, Y.-A. Liou, N. Yen, and P. Chen, “FORMOSAT-3/COSMIC mission to global earth weather monitoring, operation, and TACC/CDAAC post-processing,” 86th AMS Annual Meeting,-14th conf. satellite meteorology and oceanography, Atlanta, GA, 29-2 Feb. 2006.

41. WMO Secretariat, Workshop on the “Redesign and Optimization of the Space Based Global Observing System, Outcome of the OPT-2 Workshop,” ETSAT/SUP3/Doc. 5(1), World Meteorological Organization, Geneva, Switzerland, 21-22 Jun. 2007.

42. M. Born and E. Wolf, Principles of Optics, 6th Ed., Oxford, United Kingdom: Pergamon Press, 1980.

43. S. Sokolovskiy, Y.-H. Kuo, C. Rocken, W.S. Schreiner, D. Hunt, and R.A. Anthes, “Monitoring the atmospheric boundary layer by GPS radio occultation signals recorded in the open-loop mode,” Geophysical Research Letters, vol.33, no. L12813, pp. 1-4, doi:10.1029/2006GL025955, 2006.

44. ——, “Modeling and inverting radio occultation signals in the moist troposphere,” Radio Sci., vol. 36, no. 3, pp. 441-458, 2001.

45. ——, “Tracking tropospheric radio occultation signals from low Earth orbit,” Radio Sci., vol. 36, no. 3, pp. 483-498, 2001.

46. D. D. Feng and M. Herman, "Remote sensing the Earth's atmosphere using the global positioning system (GPS)—The GPS/MET data analysis" J. Atmos. Ocean. Technol., vol. 16, no.8, pp. 989–1002, Aug. 1999.

47. M. D. Mortensen and P. Hoeg, "Inversion of GPS occultation measurements using Fresnel diffraction theory," Geophys. Res. Lett., vol. 25, no. 13, pp. 2441–2444, 1998.

48. M. E. Gorbunov, "Three-dimensional satellite refractive tomography of the atmosphere: Numerical simulation" Radio Sci., vol. 31, no. 1, pp. 95– 104, 1996.

49. —— and A. S. Gurvich, "Microlab-1 experiment: multipath effects in the lower troposphere," J. Geophys. Res., vol. 103, no. D12, pp. 13 819–13 826, 1998.

50. K. Igarashi, A. Pavelyev, J. Wickert, K. Hocke, and D. Pavelyev, "Application of radio holographic method for observation of altitude variations of the electron density in the mesosphere/lower thermosphere using GPS/MET radio occultation data," J. Atmos. Sol.-Terr. Phys., vol. 64, no. 8–11, pp. 959–969, May 2002.

51. A. G. Pavelyev, Y.-A. Liou, C. Reigber, J. Wickert, K. Igrashi, K. Hocke, and C. Y. Huang, "GPS radio holography as a tool for remote sensing of the atmosphere and mesosphere from space," GPS Solut., vol. 6, no. 1/2, pp. 100–108, doi: 10.1007/s10291-002-0025-3, 2002.

52. ——, T. Tsuda, K. Igarashi, Y.-A. Liou, and K. Hocke, "Wave structures in the electron density profile in the ionospheric D- and E-layers observed by radio holography analysis of the GPS/MET radio occultation data," J. Atmos. Sol.-Terr. Phys., vol. 65, no. 1, pp. 59–70, Jan. 2003.

53. A. S. Jensen, M. S. Lohmann, H.-H. Benzon, and A. S. Nielsen, "Full spectrum inversion of radio occultation signals," Radio Sci., vol. 38, no. 3, p. 1040, 2003.

54. M. E. Gorbunov, "Ionospheric correct and statistical optimization of radio occultation data," Radio Sci., vol. 37, no. 5, pp. 1084-1092, doi:10.1029/2000RS002370, Oct. 2002.

55. Y.-A. Liou and C.-Y. Huang, “Active limb sounding of atmospheric refractivity and dry temperature profiles by GPS/Met occultation,” Proc. COSPAR Colloquia Series, Taipei, Taiwan, vol. 12, pp. 325–328, Sep. 2002.

56. T.-C. Chiu, Y.-A. Liou, W.-H. Yeh, and C.Y. Huang, “NCURO Data-Retrieval Algorithm in FORMOSAT-3 GPS Radio-Occultation Mission,” IEEE Trans. Geosc. Remot. Sens., vol. 46, no. 11, pp. 3395-3405, Nov. 2008.

57. C.-J. Fong, W.-T. Shiau, C.-T. Lin, T.-C. Kuo, C.-H. Chu, S.-K. Yang, N. L. Yen, S.-S. Chen, Y.-H. Kuo, Y.-A. Liou, and S. Chi, “Constellation deployment for FORMOSAT-3/COSMIC mission,” IEEE Trans. Geosci. Remote Sens., vol. 46, no. 11, doi: 10.1109/TGRS.2008.2005202, Nov. 2008

58. W.-T. Shiau and R. Kuo, “FORMOSAT-3 constellation deployment plan,” National Space Organization, Hsin-Chu, Taiwan, Tech. Rep. NSPO-PLAN-0009_0000, Jun. 2006.

59. J. R. Wertz Ed., “Summary of orbit properties and terminology – Spacecraft Orbits,” in Spacecraft Attitude Determination and Control, Dordrecht, Netherlands, Kluwer Academic Publishers, ch. 3, sec. 3, Eq. (3-41d), p.68, 1978.

60. C.-J. Fong, N. Yen, V. Chu, S.S. Chen, and S. Chi, “Operations challenges from the FORMOSAT-3/COSMIC constellation for global Earth weather monitoring,” in IEEE 2007 Aerospace Conference Proc., Big Sky, MT, doi: 10.1109/AERO.2007.352986, pp. 1-14, 3-10 Mar. 2007.

61. – –, S.-K. Yang, C.-H. Chu, J.-J. Yeh, C.-T. Lin, T.-C. Kuo, T.-Y. Liu, N. L. Yen, S.-S. Chen, C.-Y. Huang, Y.-H. Kuo, Y.-A. Liou, and S. Chi, “FORMOSAT-3/COSMIC constellation spacecraft system performance: after one-year in orbit,” IEEE Trans. Geosci. Remote Sens., vol. 46, no. 11. doi: 10.1109/TGRS.2008.2005203, Nov. 2008

62. J. A. King, N. J. Beidleman, “Method and apparatus for deploying a satellite network,” U.S. Patent 5 199 672, 25 May 1990.

63. C. Hwang, T.-P. Tseng, T. Ling, D. Švehla, and B. Schreiner, “Precise orbit determination for the FORMOSAT-3/COSMIC satellite mission using GPS,” J. of Geod., doi 10.1007/s00190-008-0256-3, Aug. 2008.

64. ——, T.-J. Lin, T.-P. Tseng, and B. F. Chao, “Modeling orbit dynamics of FORMOSAT-3/COSMIC satellites for recovery of temporal gravity variations” IEEE Trans. Geosci. Remote Sens., vol. 46, no. 11, pp. 3412-3423, doi: 10.1109/TGRS.2008.2004789, Nov. 2008.

65. C.-J. Fong, C.-H. Chu, R. Lo, and N. L. Yen, “The FORMOSAT-3/COSMIC FM6 67-days-outage event,” S12-06, 4th Asian Space Conference and 2008 FORMOSAT-3/COSMIC Data Users Workshop, Taipei, Taiwan, Oct. 1-3, 2008.

66. ——, ——, S.-K. Yang, J.-J. Yeh, C.-T. Lin, T.-C. Kuo, R. Lo, T.-Y. Liu, and Nick Yen, “The FORMOSAT-3/COSMIC constellation spacecraft system performance: after two years in orbit” C22-04, 4th Asian Space Conference and 2008 FORMOSAT-3 / COSMIC Data Users Workshop, Taipei, Taiwan, 1-3 Oct. 2008.

67. C.-H. Chu, N. Yen, C.-C. Hsiao, C.-J. Fong, S.-K. Yang, T.-Y. Liu, M. Lin, and J.-J. Miau, “Earth observations with orbiting thermometers — prospective FORMOSAT-3/COSMIC follow-on mission,” 22nd Annual AIAA/USU Conference on Small Satellites, SSC008-II-02, Logan, Utah, 11-14 Aug. 2008.

Appendix Acronyms and Abbreviations

3D	Three-dimensional
ABL	Atmospheric Boundary Layer
ACE	Attitude Control Electronics
ACS	Attitude Control Subsystem
AFWA	Air Force Weather Agency
AIAA	American Institute of Aeronautics and Astronautics
ANT	Antenna
AOL	Argument of Latitude
ARM	Amplitude-Retrieval Method
ARS	Attitude Reference System
ATS-6	Applications Technology Satellite-6
BAMS	Bulletin of the American Meteorological Society
BCR	Battery Charge Regulator
BOL	Beginning of Life
BPM	Back-Propagation Method
C/A Code	Clear/Acquisition Code
Canada Met	Canadian Meteorological Centre
CCSDS	Consultative Committee for Space Data Systems
CDAAC	COSMIC Data Analysis and Archive Center
C&DH	Command and Data Handling
CG	Center of Gravity
CHAMP	Challenging Minisatellite Payload
COSMIC	Constellation Observing Systems for Meteorology, Ionosphere, and Climate mission

CPT	Comprehensive Performance Test
CSD	Common Spacecraft Database
CSS	Cosine Sun Sensors
CTM	Canonical Transformation Method
CWB	Central Weather Bureau
DC	Direct Current
dMdC	Derivative of Battery Molecular to Charge
E	Eccentricity
ECMWF	European Centre for Medium Range Forecasts
EDU	Engineering Development Unit
EHS	Earth Horizon Sensor
EOL	End of Life
EPS	Electrical Power Subsystem
ETE	End-to-End
F	Force
FB	Firmware Build
FBK	Fairbanks
FC	Flight Computer
FCDAS	Fairbanks Command and Data Acquisition Station
FDC	Failure Detection & Correction
FDF	Flight Dynamics Facility
FM	Flight Model
FO	Follow-on
FORMOSAT-3	FORMOSA SATellite mission no.3
FPGA	Field Programmable Gate Array
FSIM	Full-Spectrum-Inversion Method

FSW	Flight Software Subsystem
GEOS-3	Geodetic and Earth Orbiting Satellite 3
GHe	Gas-Helium
GLONASS	Global Navigation Satellite System
GNSS	Global Navigation Satellite Systems
GOM	Geometrical Optics Method
GOX	GPS Occultation Receiver
GPS	Global Positioning System
GPS-ARC	GPS Scientific Application Research Center
GPS/MET	GPS/Meteorology
GPSR	Global Positioning System Receiver
GRACE	Gravity Recovery and Climate Experiment
I	Inclination
IEEE	Institute of Electrical and Electronics Engineers
IGS	International GPS Service
IOP	Intensive Operation Period
IOX	Ionospheric Occultation Experiment
Isp	Specific Impulse
I&T	Integration and Test
JMA	Japan Meteorological Agency
JPL	Jet Propulsion Laboratory
K	Kelvin
KOMPSAT	Korean Multi-Purpose Satellite
LEO	Low-Earth-Orbit
LTS	Local Tracking Stations
L&EO	Launch and Early Orbit

MB	Maga Byte
MEOP	Maximum Expected Operating Pressure
Météo-France	French National Meteorological Service
MIU	Mission Interface Unit
MOI	Moment of Inertia
NSF	National Science Foundation
N	Refractivity
N_2H_4	Hydrazine
NASA	National Aeronautics and Space Administration
NCAR	National Center for Atmospheric Research
NCEP	National Centers for Environmental Prediction
NCKU	National Cheng-Kung University
NCTU	National Chao-Tung University
NCU	National Central University
NCURO	National Central University Radio Occultation
NDM	Navigation Data Messages
NESDIS	National Environmental Satellite, Data, and Information Service
NOAA	National Oceanic and Atmospheric Administration
NORAD	North American Aerospace Defense Command
NSC	National Science Council
NSF	National Science Foundation
NSPO	National Space Organization
NRL	Naval Research Laboratory
NRT	Near Real Time
NTU	National Taiwan University
NWP	Numerical Weather Prediction

OASYS	Orbit Analysis System
OCC	Occultation
OL	Open Loop
Orbital	Orbital Sciences Corporation
OSC	Orbital Sciences Corporation
P	Pressure
P Code	Precision Code
PCM	Power Control Module
PGA	Pin Grid Array
PID	Proportional-Integral-Derivative
PL	Payload
PLL	Phase Lock Loop
POD	Precision Orbit Determination
PVT	Position/Velocity/Time
PW	Precipitable Water
RAAN	Right Ascension Ascending Node
RCS	Reaction Control Subsystem
RF	Radio Frequency
RFS	Radio Frequency Subsystem
RHM	Radio Holographic Method
RO	Radio Occultation
ROC	Republic of China
ROM	Radio Optics Method
RTS	Remote Tracking Stations
SAA	South Atlantic Anomaly
SAC-C	Satellite de Aplicaciones Cientificas-C

SAD	Solar Array Drive
S/C	Spacecraft
SDRAM	Synchronous Dynamic Random Access Memory
SI	International System of Units
SMA	Semi-Major Axis
SNR	Signal-to-Noise Ratio
SOC	State of Charge
SOCC	Satellite Operations Control Center
SOH	State-of-Health
SSM	Sliding Spectral Method
SSR	Solid State Recorder
STOL	Satellite Test and Operations Language
T	Temperature
TACC	Taiwan Analysis Center for COSMIC
TanDEM-X	TerraSAR-X add-on for Digital Elevation Measuremen
TAO	Terrestrial, Atmospheric and Oceanic Sciences
TBB	Tri-Band Beacon
TBR	To Be Resolved
TCS	Thermal Control Subsyste
TEC	Total Electron Contents
TIP	Tiny Ionospheric Photometer
TRO	Tromso
TT&C	Tracking, Telemetry and Command
UCAR	University Corporation for Atmospheric Research
UKMO	UK Meteorological Office
USA	United States of America

USN	United Service Network
WMO	World Meteorological Organization

Autobiography

Chen-Joe Fong (方振洲) received the B.S.E.E., M.S.E.E. and Ph. D. degrees in Electrophysics, Electro-optical engineering, and Department of Photonics and Institute of Electro-Optical Engineering from the National Chiao Tung University (NCTU), Hsinchu, Taiwan, in 1983, 1985 and 2009, respectively. He is the FORMOSAT-3 follow-on program Satellite Technical Manager and research fellow with the Systems Engineering Division, National Space Organization (NSPO), Hsinchu. For the FORMOSAT-3/COSMIC mission, he is a program Systems Engineering Manager and also a Spacecraft Lead which responsible for the anomaly resolution team during mission operation phase. He has been with NSPO since 1993 and later acted as the Satellite Integration and Test (I&T) Project Manager of ROCSAT-1 program and the I&T Division Director. From 1987 to 1993, he was with the Center for Measurement Standards as a Microwave Lab Head and Systems Engineer in the Center for Aviation and Space Technology, Industrial Technology Research Institute, for the ROCSAT-1 program. His current research interests include incoherent time domain pump fiber Raman amplifier, optical soliton, GPS radio occultation, systems engineering, satellite test bed, spacecraft simulator, and mission simulation. Dr. Fong is a member of the Institute of Electrical and Electronics Engineers, the American Institute of Aeronautics and Astronautics, the Optical Society of America, the Optical Engineering Society of the Republic of China, the Aeronautical and Astronautical Society of the Republic of China, and Phi Tau Phi Scholastic Honor Society of the Republic of China.

PUBLICATION LIST of
CHEN-JOE FONG (方振洲)
(FORMOSAT-3 RELATED)

JOURNAL PAPERS/PERIODICALS:

1. C.-J. Fong, N. L. Yen, C.-H. Chu, C.-C. Hsiao, Y.-A. Liou, and S. Chi, "Space-based Global Weather Monitoring System – FORMOSAT-3/COSMIC Constellation and its Follow-On Mission," AIAA J. Spacecraft and Rockets, Submitted on 24 September 2008, Accepted on 7 January 2009.
2. C.-J. Fong, C.-Y. Huang, C.-H. Chu, N. L. Yen, Y.-H. Kuo, Y.-A. Liou, and S. Chi., "Mission Results from FORMOSAT-3/COSMIC Constellation System," AIAA J. Spacecraft and Rockets, vol. 45, no. 6, pp 1293-1302. doi: 10.2514/1.34427, Nov./Dec. 2008.
3. C.-J. Fong, W.-T. Shiau, C.-T. Lin, T.-C. Kuo, C.-H. Chu, S.-K. Yang, N. L. Yen, S. S. Chen, Y.-H. Kuo, Y.-A. Liou, and S. Chi, "Constellation Deployment for FORMOSAT-3/COSMIC Mission," IEEE Trans. Geosci. Remote Sens., vol. 46, no. 11, pp.3367-3379. doi: 10.1109/TGRS.2008.2005202, Nov. 2008.
4. C.-J. Fong, S.-K. Yang, C.-H. Chu, J.-J. Yeh, C.-T. Lin, T.-C. Kuo, T.-Y. Liu, N. L. Yen, S.-S. Chen, C.-Y. Huang, Y.-H. Kuo, Y.-A. Liou, and S. Chi, "FORMOSAT-3/COSMIC Constellation Spacecraft System Performance: After One-Year in Orbit," IEEE Trans. Geosci. Remote Sens., vol. 46, no. 11, doi: 10.1109/TGRS.2008.2005203, Nov. 2008.
5. C.-Y. Huang, C. Z. Cheng, P. H. Lin, C.-J. Fong, J. Wicker, and C. C. Hsiao, "Radio Occultation Retrieval of Atmospheric Profiles in the FORMOSAT-3/COSMIC Mission: Early Results," Terrestrial, Atmospheric and Oceanic Sciences (TAO), vol. 20, no. 1, doi: 10.3319/TAO.2008.04.24.01(F3C), Feb. 2009.
6. C.-J. Fong, N. Yen, V. Chu, E. Yang, A. Shiau, C.-Y. Huang, S. Chi, S.-S. Chen, Y.-A. Liou and, Y. H. Kuo, "FORMOSAT-3/COSMIC Spacecraft Constellation System,

Mission Results, and Prospect for Follow-on Mission," Terrestrial, Atmospheric and Oceanic Sciences (TAO), vol. 20, no. 1, doi:10.3319/TAO.2008.01.03.01(F3C), Feb. 2009.

7. Y.-A. Liou, A. G. Pavelyev, S.-F. Liu, A. A. Pavelyev, N. L. Yen, C.-Y. Huang, and C.-J. Fong, "FORMOSAT-3 GPS Radio Occultation Mission: Preliminary Results," IEEE Trans. Geosci. Remote Sens., vol. 45, no. 10, doi:10.1109/TGRS.2007.903365, Oct. 2007.

CONFERENCE/WORKSHOP PAPERS:

1. Yuei-An Liou, An-Ming Wu, Wolfgang Rack, Hsin-Yin Lin, Nick L. Yen, and Chen-Joe Fong, "Observations of polar region by Formosat-2 and Formosat-3 space missions," AOGS 2009.
2. C.-J. Fong, N. Yen,.C.-H. Chu,.C.-C. Hsiao, Y.-C. Lin, S.-S. Chen, Y.-A. Liou, and S. Chi, "In Quest of Global Radio Occultation Mission for Meteorology Beyond 2011," 2009 IEEE Aerospace Conference Proceedings, Big Sky, MT, 7-14 March 2009.
3. N. Yen, C.-J. Fong, V. Chu, C.-C. Hsiao, J.-J. Miao, and Y.-A. Liou, "International Collaboration of Global Radio Occultation Mission for Meteorology Beyond 2011," 13th Conference on Integrated Observing and Assimilation Systems for Atmosphere, Oceans, and Land Surface (IOAS-AOLS), and 89th AMS Annual Meeting, Phoenix, Arizona, 13 Jan. 2008.
4. C. Z. Cheng, C.-Y. Huang, K. Wang, P.-H. Lin, C.-J. Fong, J. Wickert, and C.-C. Hsiao, "Radio Occultation Retrieval of Atmospheric Profiles in the Profiles in the FORMOSAT-3/COSMIC Mission: Early Results," C11-07, 4th Asian Space Conference and 2008 FORMOSAT-3 / COSMIC Data Users Workshop, Taipei, Taiwan, 1-3 Oct. 2008.

5. V. Chu, N. Yen, C.-J. Fong, E. Yang, M. Lin, T.-Y. Liu, and C.-C. Hsiao, "THUNDERSAT – A Successor of FORMOSAT-3/COSMIC," C12-03, 4th Asian Space Conference and 2008 FORMOSAT-3/COSMIC Data Users Workshop, Taipei, Taiwan, 1-3 Oct. 2008.
6. C.-J. Fong, C.-H. Chu, S.-K. Yang, J.-J. Yeh, C.-T. Lin, T.-C. Kuo, R. Lo, T.-Y. Liu, Nick Yen, "The FORMOSAT-3/COSMIC Constellation Spacecraft System Performance After Two Years in Orbit," C22-04, 4th Asian Space Conference and 2008 FORMOSAT-3 / COSMIC Data Users Workshop, Taipei, Taiwan, 1-3 Oct. 2008.
7. C.-J. Fong, C.-H. Chu, R. Lo, and N. L. Yen, "The FORMOSAT-3/COSMIC FM6 67-Days-Outage Event," S12-06, 4th Asian Space Conference and 2008 FORMOSAT-3/COSMIC Data Users Workshop, Taipei, Taiwan, 1-3 Oct. 2008.
8. C.-J. Fong, N. L. Yen, V. Chu, C.-C. Hsiao, S.-S. Chen, J.-J. Miau, Y.-A. Liou, and S. Chi, "Space-based Global Weather Monitoring System – FORMOSAT-3/COSMIC Constellation and its Follow-on Mission," AIAA 2008-7671, AIAA Space 2008 Conference & Exposition, San Diego, California, 9-11 Sep. 2008.
9. C.-H. Vicky Chu, N. Yen, C.-C. Hsiao, C.-J. Fong, S.-K. Eddy Yang, T.-Y. Liu, M. Lin, and J.-J. Miau, "Earth Observations with Orbiting Thermometers – Prospective FORMOSAT-3/COSMIC Follow-On Mission," Small Satellite Conference 2008 Proceedings, Logan, Utah, 11-14 Aug. 2008.
10. N. Yen and C.-J. Fong, "FORMOSAT-3/COSMIC GPS Radio Occultation Constellation Mission Results and its Follow-on Mission for Global Climate Monitoring," AOGS 2008, Busan, Korea, 16-20 Jun. 2008.
11. C.-J. Fong, N. Yen, V. Chu, E. Yang, C.-Y. Huang, S. S. Chen, Y.-A. Liou, and S. Chi, "Constellation Challenges and Contributions of Taiwan Weather Monitoring Satellites," 2008 IEEE Aerospace Conference Proceedings, Big Sky, Montana, 1-8 Mar. 2008.

12. N. Yen, V. Chu, C.-J. Fong, T.-Y. Liu, S.-S. Chen, Y.-A. Liou, and B. Kuo, "A Remarkable Radio Occultation Constellation Program – The Most Accurate and Stable Space-Borne Thermometers," AMS 2008 - 12th Conference on IOAS-AOLS, New Orleans, LA, 20-24 Jan. 2008
13. Y.-A Liou, C.-J. Fong, S. K. Yan, N. Yen, V. Chu, B. F. Chao, A.-M. Wu, and S. Chi, "contributions of TAIWAN FORMOSAT-3 satellite missions to the global community," 4th Japan-Taiwan Workshop on Mechanical and Aerospace Engineering, Hakone, Japan, 29-30 Oct. 2007
14. N. Yen, C.-H. V. Chu, C.-J. Fong, T.-Y. Liu, S.-S. Chen, B. F. Chao and Y.-A. Liou, "The Rising of a Remarkable Radio Occultation Constellation Program," Second FORMOSAT-3/COSMIC Data Users Workshop, Boulder, Colorado, 22-24 Oct. 2007.
15. C.-Y. Huang, C. Z. Cheng, P. H. Lin, C.-J. Fong, J. Wicker, C. C. Hsiao, K. Wang, "Radio Occultation Retrieval of Atmospheric Profiles in the FORMOSAT-3/COSMIC Mission: Current Status," Second FORMOSAT-3/COSMIC Data Users Workshop, Boulder, Colorado, 22-24 Oct. 2007.
16. C.-J. Fong, C. Y. Huang, V. Chu, A. Shiau, E. Yang, N. Yen, S. S. Chao, D. Hawes,.-H. Kuo, Y.-A. Liou, Y and S. Chi, "Mission Results from FORMOSAT-3/COSMIC Constellation System," AIAA 2007-6086, AIAA SPACE 2007 Conference & Exposition, Long Beach, CA., 18-20 Sep. 2007.
17. C.-H. Vicky Chu, S.-K. Yang, C.-J. Fong, N. Yen, T.-Y. Liu, W.-J. Chen, D. Hawes, Y.-A. Liou, Y.-H. Kuo, "The Most Accurate and Stable Space-Borne Thermometers – FORMOSAT-3/COSMIC Constellation", SSC07-VII-1, 21st Annual AIAA/USU Conference on Small Satellites, Logan, Utah, 13-16 Aug. 2007.
18. N. Yen, C.-J. Fong and Y.-A. Liou, "FORMOSAT-3/COSMIC GPS Radio Occultation Constellation Mission Results and the Future Plan for Global Climate Monitoring," AOGS 2007 (Asia Oceania Geosciences Society), Bangkok, Tailand, 30-4 Jul. 2007.

19. C.-J. Fong, N. Yen, S. K. Yang, S.S. Chen, and S. Chi, "GPS Radio Occultation and Mission Results from FORMOSAT-3/COSMIC Spacecraft Constellation," 3rd International Conference on Recent Advances in Spacecraft Technologies, Istanbul, Turkey, doi: 10.1109/RAST.2007.4284093, 14-16 Jun. 2007.

20. N. Yen, C.-J. Fong, C.-Y. Huang, J.-S. Chern, Y.-A. Liou, B. Chao, "The Growing Global Attention on the FORMOSAT-3/COSMIC Constellation: Mission Overview and Future Prospects," 2007 First AOPOD: Atmosphere Occultation & Precision Orbit Determination workshop, Jeju Island, Korea, 28-30 May 2007.

21. C.-J. Fong, V. Chu, E. Yang, N. Yen, C.-Y. Huang, J.-S. Chern, Y.-A. Liou, B. Chao, "FORMOSAT-3/COSMIC Constellation Spacecraft System Performance: After One-Year in Orbit," 2007 First AOPOD: Atmosphere Occultation & Precision Orbit Determination workshop, Jeju Island, Korea, 28-30 May 2007.

22. J.-S. Chern, C.-Y. Huang, Y.-A. Liou, N. Yen, C.-J. Fong, B. Chao, "FORMOSAT-3/COSMIC Measurement of Neutral Atmosphere: Results, Data Quality Statistics, and Status," 2007 First AOPOD: Atmosphere Occultation & Precision Orbit Determination workshop, Jeju Island, Korea, 28-30 May 2007.

23. Y. A. Liou, C. Y. Huang, A. G. Pavelyev, C. S. Wang, P. L. Tseng, W.H.Yeh, T.C. Chiu, N.Yen, C.-J. Fong, V. Chu, T. K. Yeh, C.S. Chern, S. K. Yan, S. Kar, B. Chao, "Advancement of ground and space borne GPS observation processing techniques for meteorology in Taiwan," 2007 First AOPOD: Atmosphere Occultation & Precision Orbit Determination workshop, Jeju Island, Korea, 28-30 May 2007.

24. N. Yen, L. Wu, and C.-J. Fong, "FORMOSAT-3/COSMIC radio occultation constellation mission and the future plan for global climate monitoring", AGU 2007 Joint Assembly, Acapulco, Mexico, 22-25 May 2007.

25. C. C. Haiao, N. Yen, L. Wu, C. Huang, C.-J. Fong, B. W. Reinisch, and C. S. Lin, "A Comparison of Ionosphere Profile Observed by FORMOSAT-3/COSMIC and Ionosonde Radar," AGU 2007 Joint Assembly, Acapulco, Mexico, 22-25 May 2007.
26. N. Yen, C.-J. Fong, and S. S. Chen, "The Growing Global Attention on the FORMOSAT-3/COSMIC Constellation," Taiwan Geosciences Assembly and 2007 International FORMOSAT-3/COSMIC Workshop, Acer Aspire Park, Longtan, Taoyuan, Taiwan, 15-18 May 2007.
27. C.-J. Fong, V. Chu, E. Yang, T. Tsai, and N. Yen, "FORMOSAT-3/COSMIC Constellation Mission Prospects and System Performance," Taiwan Geosciences Assembly and 2007 International FORMOSAT-3/COSMIC Workshop, Acer Aspire Park, Longtan, Taoyuan, Taiwan, 15-18 May 2007.
28. C.-Y. Huang, Y.-A. Liou, N. Yen, and C.-J. Fong, "FORMOSAT-3/COSMIC Measurement of Neutral Atmosphere," Taiwan Geosciences Assembly and 2007 International FORMOSAT-3/COSMIC Workshop, Acer Aspire Park, Longtan, Taoyuan, Taiwan, 15-18 May 2007.
29. C.-J. Fong, N. Yen, V. Chu, S.S. Chen, and S. Chi, "Operations Challenges from the FORMOSAT-3/COSMIC Constellation for Global Earth Weather Monitoring," 2007 IEEE Aerospace Conference Proceedings, Big Sky, Montana, 3-10 Mar. 2007.
30. A. Shiau, C.-J. Fong, V. Chu, T. Lin, T. C. Kuo and N. Yen, "FORMOSAT-3/COSMIC Orbit Raising and Constellation Deployment," FORMOSAT-3/COSMIC Workshop 2006 – Early Results and IOP Campaign, Taipei, Taiwan, 28-1 Nov. 2006.
31. E. Yang, V. Chu, V. Chang, A. Shiau, V. Huang, T. Tsai, C.-J. Fong, and R. Lo, "Operations Solutions to Spacecraft Anomalies and Technical Difficulties," FORMOSAT-3/COSMIC Workshop 2006 – Early Results and IOP Campaign, Taipei, Taiwan, 28-1 Nov. 2006.

32. C.-J. Fong, T. Tsai, E. Yang, R. Lo, J. Yeh, C.-R. Chen, M.-S. Chang, T. Lin, M. Yeh, T.-C. Kuo, C.-Y. H, C.-H. Lin, C.-C. Hsiao, V. Chu, and N. Yen, "System Evaluation and On-Orbit Performance of the FORMOSAT-3/COSMIC Constellation Mission," FORMOSAT-3/COSMIC Workshop 2006 – Early Results and IOP Campaign, Taipei, Taiwan, 28-1 Nov. 2006.

33. N. Yen, C.-J. Fong, V. Chu, A. Hsiao, T. Tsai, and C.Y. Huang, "FORMOSAT-3/COSMIC Mission to Global Earth Weather Monitoring: Early Orbit, Orbit Transfer and Mission Operation Overview," FORMOSAT-3/COSMIC Data Users Workshop, Boulder, CO, 16-18 Oct. 2006.

34. B. H. Wu, C.-J. Fong, C.Y. Huang, Y.A. Liou, N. Yen, and P. Chen, "FORMOSAT-3/COSMIC mission to global earth weather monitoring, operation, and TACC/CDAAC post-processing," 86th AMS Annual Meeting,- 14th conf. satellite meteorology and oceanography, Atlanta, GA, 29 -2 Jan. 2006.

35. C. -J. Fong, B. H. Wu, N. Yen and P. Chen, "Application of FORMOSAT-3/COSMIC Mission to Global Earth Monitoring," AIAA-2005-6774, Space 2005, Long Beach, California, 30-1 Aug. 2005.

中文文章：

1. 顏隆政、林瑤章、福衛三號計畫團隊 (陳紹興、方振洲、傅載豪、朱崇惠、楊善國、徐銘煌、劉代瑜、彭鴻霖、及黃文莊)， "科技服務類-秀姑巒山獎 - 福爾摩沙衛星三號星系計畫的科技成效與成就，" 國研科技，2008 年 10 月，pp54-60，國研院。

2. 陳正一、顏隆政、方振洲、朱崇惠， "世界新氣象－福爾摩沙衛星三號介紹，" 中國航空太空學會會刊，第 35 卷第 2 期，2007 年 2 月。

3. 顏隆政、陳維鈞、方振洲， "世界上最精準及最穩定的太空大氣溫度計，" 國研科技，國研科技 專題企劃 福爾摩沙衛星三號星系初期之科學應用及研究成果，2007 年 1 月 7 日，國研院。[http://www.narl.org.tw/tw/topic/topic.php?topic_id=22]